EUROPEAN ORGANIZATION FOR NUCLEAR RESEARCH

CERN-EP/2001-021
February 28, 2001

A Combination of Preliminary Electroweak Measurements and Constraints on the Standard Model

The LEP Collaborations* ALEPH, DELPHI, L3, OPAL, the LEP Electroweak Working Group† and the SLD Heavy Flavour and Electroweak Groups‡

Prepared from Contributions of the LEP and SLD experiments to the 2000 Summer conferences.

Abstract

This note presents a combination of published and preliminary electroweak results from the four LEP collaborations and the SLD collaboration which were prepared for the 2000 summer conferences. Averages from Z resonance results are derived for hadronic and leptonic cross sections, the leptonic forward-backward asymmetries, the τ polarisation asymmetries, the $b\overline{b}$ and $c\overline{c}$ partial widths and forward-backward asymmetries and the $q\overline{q}$ charge asymmetry. Above the Z resonance, averages are derived for di–fermion cross sections and asymmetries, W–pair, Z–pair and single–W production cross section, electroweak gauge boson couplings and W mass and decay branching ratios. The major changes with respect to results presented in summer 1999 are final Z lineshape results from LEP, updates to the W mass and gauge-boson couplings from LEP, and $A_{\rm LR}$ from SLD. The results are compared with precise electroweak measurements from other experiments. The parameters of the Standard Model are evaluated, first using the combined LEP electroweak measurements, and then using the full set of electroweak results.

*The LEP Collaborations each take responsibility for the preliminary results of their own.

†The members of the LEP Electroweak Working Group who contributed significantly to this note are : D. Abbaneo, J. Alcaraz, P. Antilogus, S. Arcelli, P. Bambade, E. Barberio, G. Bella, A. Blondel, S. Blyth, D. Bourilkov, R. Chierici, R. Clare, P. de Jong, G. Duckeck, A. Ealet, M. Elsing, F. Fiedler, P. Garcia-Abia, A. Gurtu, M.W. Grünewald, J.B. Hansen, R. Hawkings, J. Holt, S. Jezequel, R.W.L. Jones, N. Kjaer, M. Kobel, E. Lançon, W. Lohmann, C. Mariotti, M. Martinez, F. Matorras, C. Matteuzzi, S. Mele, E. Migliore, M.N. Minard, K. Mönig, A. Olshevski, C. Parkes, U. Parzefall, Ch. Paus, M. Pepe-Altarelli, B. Pietrzyk, G. Quast, P. Renton, H. Rick, S. Riemann, J.M. Roney, K. Sachs, C. Sbarra, A. Schmidt-Kaerst, S. Spagnolo, A. Straessner, R. Ströhmer D. Strom, R. Tenchini, F. Terranova, F. Teubert, M.A. Thomson, E. Tournefier, M. Verzocchi, H. Voss, C.P. Ward, St. Wynhoff.

‡T. Abe, N. de Groot, M. Iwasaki, P.C. Rowson, D. Su, M. Swartz.

1 Introduction

The four LEP experiments and SLD have previously presented [1] parameters derived from the Z resonance using published and preliminary results based on data recorded until the end of 1995 for the LEP experiments and 1998 for SLD. Since 1996 LEP has run at energies above the W-pair production threshold. In 1999 the delivered luminosity was significantly higher than in previous years, and thus the knowledge of the properties of the W boson has been significantly improved. To allow a quick assessment, a box highlighting the updates is given at the beginning of each section.

LEP-I (1990-1995) Z-pole measurements are the hadronic and leptonic cross sections, the leptonic forward-backward asymmetries, the τ polarisation asymmetries, the $\mathrm{b\overline{b}}$ and $\mathrm{c\overline{c}}$ partial widths and forward-backward asymmetries and the $\mathrm{q\overline{q}}$ charge asymmetry. The measurements of the left-right cross section asymmetry, the $\mathrm{b\overline{b}}$ and $\mathrm{c\overline{c}}$ partial widths and left-right-forward-backward asymmetries for b and c quarks from SLD are treated consistently with the LEP data. Many technical aspects of their combination are described in References 2, 3 and references therein.

The LEP-II (1996-2000) measurements are di–fermion cross sections and asymmetries; W–pair, Z–pair and single–W production cross sections, electroweak gauge boson couplings. W boson properties, like mass, width and decay branching ratios are also measured.

Several measurements included in the combinations are still preliminary.

This note is organised as follows:

Section 2 Z Line Shape and Leptonic Forward-Backward Asymmetries;

Section 3 τ Polarisation;

Section 4 A_{LR} Measurement at SLD;

Section 5 Heavy Flavour Analyses;

Section 6 Inclusive Hadronic Charge Asymmetry;

Section 7 $\mathrm{f\overline{f}}$ Production at Energies above the Z;

Section 8 W Boson Properties, including m_{W}, Branching Ratios, W–pair Production Cross Section;

Section 9 Single–W Production Cross Section;

Section 10 ZZ Production Cross Section;

Section 11 Electroweak Gauge Boson Couplings;

Section 12 Interpretation of the Results, Including the Combination of Results from LEP, SLD, Neutrino Interaction Experiments and from CDF and DØ;

Section 13 Prospects for the Future.

2 Results from the Z Peak Data

Updates with respect to last summer:
All experiments have updated their results, and all are now final. Recent theoretical developments have been included in the results and fits.

2.1 Z Lineshape and Lepton Forward-Backward Asymmetries

The results presented here are based on the full LEP-I data set. This includes the data taken during the energy scans in 1990 and 1991 in the range[1] $|\sqrt{s} - m_{\rm Z}| < 3$ GeV, the data collected at the Z peak in 1992 and 1994 and the precise energy scans in 1993 and 1995 ($|\sqrt{s} - m_{\rm Z}| < 1.8$ GeV). The total event statistics are given in Table 1. Details of the individual analyses can be found in References 4–7.

$\rm q\overline{q}$					
year	A	D	L	O	all
'90/91	433	357	416	454	1660
'92	633	697	678	733	2741
'93	630	682	646	649	2607
'94	1640	1310	1359	1601	5910
'95	735	659	526	659	2579
total	4071	3705	3625	4096	15497

$\ell^+\ell^-$					
year	A	D	L	O	all
'90/91	53	36	39	58	186
'92	77	70	59	88	294
'93	78	75	64	79	296
'94	202	137	127	191	657
'95	90	66	54	81	291
total	500	384	343	497	1724

Table 1: The $\rm q\overline{q}$ and $\ell^+\ell^-$ event statistics, in units of 10^3, used for the analysis of the Z line shape and lepton forward-backward asymmetries by the experiments ALEPH (A), DELPHI (D), L3 (L) and OPAL (O).

For the averaging of results the LEP experiments provide a standard set of 9 parameters describing the information contained in hadronic and leptonic cross sections and leptonic forward-backward asymmetries. These parameters are convenient for fitting and averaging since they have small correlations. They are:

- The mass and total width of the Z boson, where the definition is based on the Breit-Wigner denominator $(s - m_{\rm Z}^2 + is\Gamma_{\rm Z}/m_{\rm Z})$ with s-dependent width [8].
- The hadronic pole cross section of Z exchange:

$$\sigma_{\rm h}^0 \equiv \frac{12\pi}{m_{\rm Z}^2}\frac{\Gamma_{\rm ee}\Gamma_{\rm had}}{\Gamma_{\rm Z}^2}\,. \tag{1}$$

  Here $\Gamma_{\rm ee}$ and $\Gamma_{\rm had}$ are the partial widths of the Z for decays into electrons and hadrons.

- The ratios:

$$R_{\rm e} \equiv \Gamma_{\rm had}/\Gamma_{\rm ee}, \quad R_\mu \equiv \Gamma_{\rm had}/\Gamma_{\mu\mu} \text{ and } R_\tau \equiv \Gamma_{\rm had}/\Gamma_{\tau\tau}. \tag{2}$$

  Here $\Gamma_{\mu\mu}$ and $\Gamma_{\tau\tau}$ are the partial widths of the Z for the decays $\rm Z \to \mu^+\mu^-$ and $\rm Z \to \tau^+\tau^-$. Due to the mass of the τ lepton, a difference of 0.2% is expected between the values for $R_{\rm e}$ and R_μ, and the value for R_τ, even under the assumption of lepton universality [9].

[1] In this note $\hbar = c = 1$.

- The pole asymmetries, $A_{\rm FB}^{0,\,\rm e}$, $A_{\rm FB}^{0,\,\mu}$ and $A_{\rm FB}^{0,\,\tau}$, for the processes $\rm e^+e^- \to e^+e^-$, $\rm e^+e^- \to \mu^+\mu^-$ and $\rm e^+e^- \to \tau^+\tau^-$. In terms of the real parts of the effective vector and axial-vector neutral current couplings of fermions, $g_{V\rm f}$ and $g_{A\rm f}$, the pole asymmetries are expressed as

$$A_{\rm FB}^{0,\,\rm f} \equiv \frac{3}{4}\mathcal{A}_{\rm e}\mathcal{A}_{\rm f} \tag{3}$$

with

$$\mathcal{A}_{\rm f} \equiv \frac{2g_{V\rm f}g_{A\rm f}}{g_{V\rm f}^2+g_{A\rm f}^2} = 2\frac{g_{V\rm f}/g_{A\rm f}}{1+(g_{V\rm f}/g_{A\rm f})^2}\,. \tag{4}$$

The imaginary parts of the vector and axial-vector coupling constants as well as real and imaginary parts of the photon vacuum polarisation are taken into account explicitly in the fitting formulae and are fixed to their Standard Model values. The fitting procedure takes into account the effects of initial-state radiation [8] to $\mathcal{O}(\alpha^3)$ [10–12], as well as the t-channel and the s-t interference contributions in the case of $\rm e^+e^-$ final states.

The set of 9 parameters does not describe hadron and lepton-pair production completely, because it does not include the interference of the s-channel Z exchange with the s-channel γ exchange. For the results presented in this section and used in the rest of the note, the γ-exchange contributions and the hadronic γZ interference terms are fixed to their Standard Model values. The leptonic γZ interference terms are expressed in terms of the effective couplings.

The four sets of 9 parameters provided by the LEP experiments are presented in Table 2. For performing the average over these four sets of nine parameters, the overall covariance matrix is constructed from the covariance matrices of the individual LEP experiments and common systematic errors [2]. The common systematic errors include theoretical errors as well as errors arising from the uncertainty in the LEP beam energy. The beam energy uncertainty contributes an uncertainty of ±1.7 MeV to $m_{\rm Z}$ and ±1.2 MeV to $\Gamma_{\rm Z}$. In addition, the uncertainty in the centre-of-mass energy spread of about ±1 MeV contributes ±0.2 MeV to $\Gamma_{\rm Z}$. The theoretical error on calculations of the small-angle Bhabha cross section is $\pm0.054\,\%$ [13] for OPAL and $\pm0.061\,\%$ [14] for all other experiments, and results in the largest common systematic uncertainty on $\sigma_{\rm h}^0$. QED radiation, dominated by photon radiation from the initial state electrons, contributes a common uncertainty of $\pm0.02\,\%$ on $\sigma_{\rm h}^0$, of ±0.3 MeV on $m_{\rm Z}$ and of ±0.2 MeV on $\Gamma_{\rm Z}$. The contribution of t-channel diagrams and the s-t interference in $\rm Z \to e^+e^-$ leads to an additional theoretical uncertainty estimated to be ±0.24 on $R_{\rm e}$ and ±0.0014 on $A_{\rm FB}^{0,\,\rm e}$, which are fully anti–correlated. Uncertainties from the model-independent parameterisation of the energy dependence of the cross section are almost negligible, if the definitions of Reference [15] are applied. Through unavoidable Standard Model remnants, dominated by the need to fix the γ-Z interference contribution in the $\rm q\overline{q}$ channel, there is some small dependence of ±0.2 MeV of $m_{\rm Z}$ on the Higgs mass, $m_{\rm H}$ (in the range 100 GeV to 1000 GeV) and the value of the electromagnetic coupling constant. Such "parametric" errors are negligible for the other pseudo-observables. The combined parameter set and its correlation matrix are given in Table 3.

If lepton universality is assumed, the set of 9 parameters is reduced to a set of 5 parameters. R_ℓ is defined as $R_\ell \equiv \Gamma_{\rm had}/\Gamma_{\ell\ell}$, where $\Gamma_{\ell\ell}$ refers to the partial Z width for the decay into a pair of massless charged leptons. The data of each of the four LEP experiments are consistent with lepton universality (the difference in χ^2 over the difference in d.o.f. with and without the assumption of lepton universality is 3/4, 6/4, 5/4 and 3/4 for ALEPH, DELPHI, L3 and OPAL, respectively). The lower part of Table 3 gives the combined result and the corresponding correlation matrix. Figure 1 shows, for each lepton species and for the combination assuming lepton universality, the resulting 68% probability contours in the R_ℓ-$A_{\rm FB}^{0,\,\ell}$ plane. Good agreement is observed.

		correlations								
		$m_{\rm Z}$	$\Gamma_{\rm Z}$	$\sigma^0_{\rm h}$	$R_{\rm e}$	R_μ	R_τ	$A^{0,{\rm e}}_{\rm FB}$	$A^{0,\mu}_{\rm FB}$	$A^{0,\tau}_{\rm FB}$
χ^2/N_{df} = 169/176					ALEPH					
$m_{\rm Z}$ [GeV]	91.1891 ± 0.0031	1.00								
$\Gamma_{\rm Z}$ [GeV]	2.4959 ± 0.0043	.038	1.00							
$\sigma^0_{\rm h}$ [nb]	41.558 ± 0.057	−.091	−.383	1.00						
$R_{\rm e}$	20.690 ± 0.075	.102	.004	.134	1.00					
R_μ	20.801 ± 0.056	−.003	.012	.167	.083	1.00				
R_τ	20.708 ± 0.062	−.003	.004	.152	.067	.093	1.00			
$A^{0,{\rm e}}_{\rm FB}$	0.0184 ± 0.0034	−.047	.000	−.003	−.388	.000	.000	1.00		
$A^{0,\mu}_{\rm FB}$	0.0172 ± 0.0024	.072	.002	.002	.019	.013	.000	−.008	1.00	
$A^{0,\tau}_{\rm FB}$	0.0170 ± 0.0028	.061	.002	.002	.017	.000	.011	−.007	.016	1.00
$\chi^2/N_{\rm df}$ = 177/168					DELPHI					
$m_{\rm Z}$ [GeV]	91.1864 ± 0.0028	1.00								
$\Gamma_{\rm Z}$ [GeV]	2.4876 ± 0.0041	.047	1.00							
$\sigma^0_{\rm h}$ [nb]	41.578 ± 0.069	−.070	−.270	1.00						
$R_{\rm e}$	20.88 ± 0.12	.063	.000	.120	1.00					
R_μ	20.650 ± 0.076	−.003	−.007	.191	.054	1.00				
R_τ	20.84 ± 0.13	.001	−.001	.113	.033	.051	1.00			
$A^{0,{\rm e}}_{\rm FB}$	0.0171 ± 0.0049	.057	.001	−.006	−.106	.000	−.001	1.00		
$A^{0,\mu}_{\rm FB}$	0.0165 ± 0.0025	.064	.006	−.002	.025	.008	.000	−.016	1.00	
$A^{0,\tau}_{\rm FB}$	0.0241 ± 0.0037	.043	.003	−.002	.015	.000	.012	−.015	.014	1.00
$\chi^2/N_{\rm df}$ = 158/166					L3					
$m_{\rm Z}$ [GeV]	91.1897 ± 0.0030	1.00								
$\Gamma_{\rm Z}$ [GeV]	2.5025 ± 0.0041	.065	1.00							
$\sigma^0_{\rm h}$ [nb]	41.535 ± 0.054	.009	−.343	1.00						
$R_{\rm e}$	20.815 ± 0.089	.108	−.007	.075	1.00					
R_μ	20.861 ± 0.097	−.001	.002	.077	.030	1.00				
R_τ	20.79 ± 0.13	.002	.005	.053	.024	.020	1.00			
$A^{0,{\rm e}}_{\rm FB}$	0.0107 ± 0.0058	−.045	.055	−.006	−.146	−.001	−.003	1.00		
$A^{0,\mu}_{\rm FB}$	0.0188 ± 0.0033	.052	.004	.005	.017	.005	.000	.011	1.00	
$A^{0,\tau}_{\rm FB}$	0.0260 ± 0.0047	.034	.004	.003	.012	.000	.007	−.008	.006	1.00
$\chi^2/N_{\rm df}$ = 155/194					OPAL					
$m_{\rm Z}$ [GeV]	91.1858 ± 0.0030	1.00								
$\Gamma_{\rm Z}$ [GeV]	2.4948 ± 0.0041	.049	1.00							
$\sigma^0_{\rm h}$ [nb]	41.501 ± 0.055	.031	−.352	1.00						
$R_{\rm e}$	20.901 ± 0.084	.108	.011	.155	1.00					
R_μ	20.811 ± 0.058	.001	.020	.222	.093	1.00				
R_τ	20.832 ± 0.091	.001	.013	.137	.039	.051	1.00			
$A^{0,{\rm e}}_{\rm FB}$	0.0089 ± 0.0045	−.053	−.005	.011	−.222	−.001	.005	1.00		
$A^{0,\mu}_{\rm FB}$	0.0159 ± 0.0023	.077	−.002	.011	.031	.018	.004	−.012	1.00	
$A^{0,\tau}_{\rm FB}$	0.0145 ± 0.0030	.059	−.003	.003	.015	−.010	.007	−.010	.013	1.00

Table 2: Line Shape and asymmetry parameters from fits to the data of the four LEP experiments and their correlation coefficients.

For completeness the partial decay widths of the Z boson are listed in Table 4, although they are more correlated than the ratios given in Table 3. The leptonic pole cross-section, σ^0_ℓ, defined as

$$\sigma^0_\ell \equiv \frac{12\pi}{m^2_{\rm Z}} \frac{\Gamma^2_{\ell\ell}}{\Gamma^2_{\rm Z}} \,,$$

in analogy to $\sigma^0_{\rm h}$, is shown in the last line of the Table. Because QCD final state corrections appear

quadratically in the denominator via Γ_Z, σ^0_ℓ has a higher sensitivity to α_s than σ^0_h or R_ℓ, where the dependence on QCD corrections is only linear.

without lepton universality		correlations								
χ^2/N_{df} = 32.6/27		m_Z	Γ_Z	σ^0_h	R_e	R_μ	R_τ	$A^{0,e}_{FB}$	$A^{0,\mu}_{FB}$	$A^{0,\tau}_{FB}$
m_Z [GeV]	91.1876± 0.0021	1.00								
Γ_Z [GeV]	2.4952 ± 0.0023	−.024	1.00							
σ^0_h [nb]	41.541 ± 0.037	−.044	−.297	1.00						
R_e	20.804 ± 0.050	.078	−.011	.105	1.00					
R_μ	20.785 ± 0.033	.000	.008	.131	.069	1.00				
R_τ	20.764 ± 0.045	.002	.006	.092	.046	.069	1.00			
$A^{0,e}_{FB}$	0.0145 ± 0.0025	−.014	.007	.001	−.371	.001	.003	1.00		
$A^{0,\mu}_{FB}$	0.0169 ± 0.0013	.046	.002	.003	.020	.012	.001	−.024	1.00	
$A^{0,\tau}_{FB}$	0.0188 ± 0.0017	.035	.001	.002	.013	−.003	.009	−.020	.046	1.00

with lepton universality

χ^2/N_{df} = 36.5/31		m_Z	Γ_Z	σ^0_h	R_ℓ	$A^{0,\ell}_{FB}$
m_Z [GeV]	91.1875± 0.0021	1.00				
Γ_Z [GeV]	2.4952 ± 0.0023	−.023	1.00			
σ^0_h [nb]	41.540 ± 0.037	−.045	−.297	1.00		
R_ℓ	20.767 ± 0.025	.033	.004	.183	1.00	
$A^{0,\ell}_{FB}$	0.0171 ± 0.0010	.055	.003	.006	−.056	1.00

Table 3: Average line shape and asymmetry parameters from the data of the four LEP experiments, without and with the assumption of lepton universality.

without lepton universality		correlations			
Γ_{had} [MeV]	1745.8 ±2.7	1.00			
Γ_{ee} [MeV]	83.92±0.12	−0.29	1.00		
$\Gamma_{\mu\mu}$ [MeV]	83.99±0.18	0.66	−0.20	1.00	
$\Gamma_{\tau\tau}$ [MeV]	84.08±0.22	0.54	−0.17	0.39	1.00

with lepton universality

Γ_{inv} [MeV]	499.0 ±1.5	1.00			
Γ_{had} [MeV]	1744.4 ±2.0	−0.29	1.00		
$\Gamma_{\ell\ell}$ [MeV]	83.984±0.086	0.49	0.39	1.00	
$\Gamma_{inv}/\Gamma_{\ell\ell}$	5.942 ±0.016				
σ^0_ℓ [nb]	2.0003±0.0027				

Table 4: Partial decay widths of the Z boson, derived from the results of the 9-parameter averages in Table 3. In the case of lepton universality, $\Gamma_{\ell\ell}$ refers to the partial Z width for the decay into a pair of massless charged leptons.

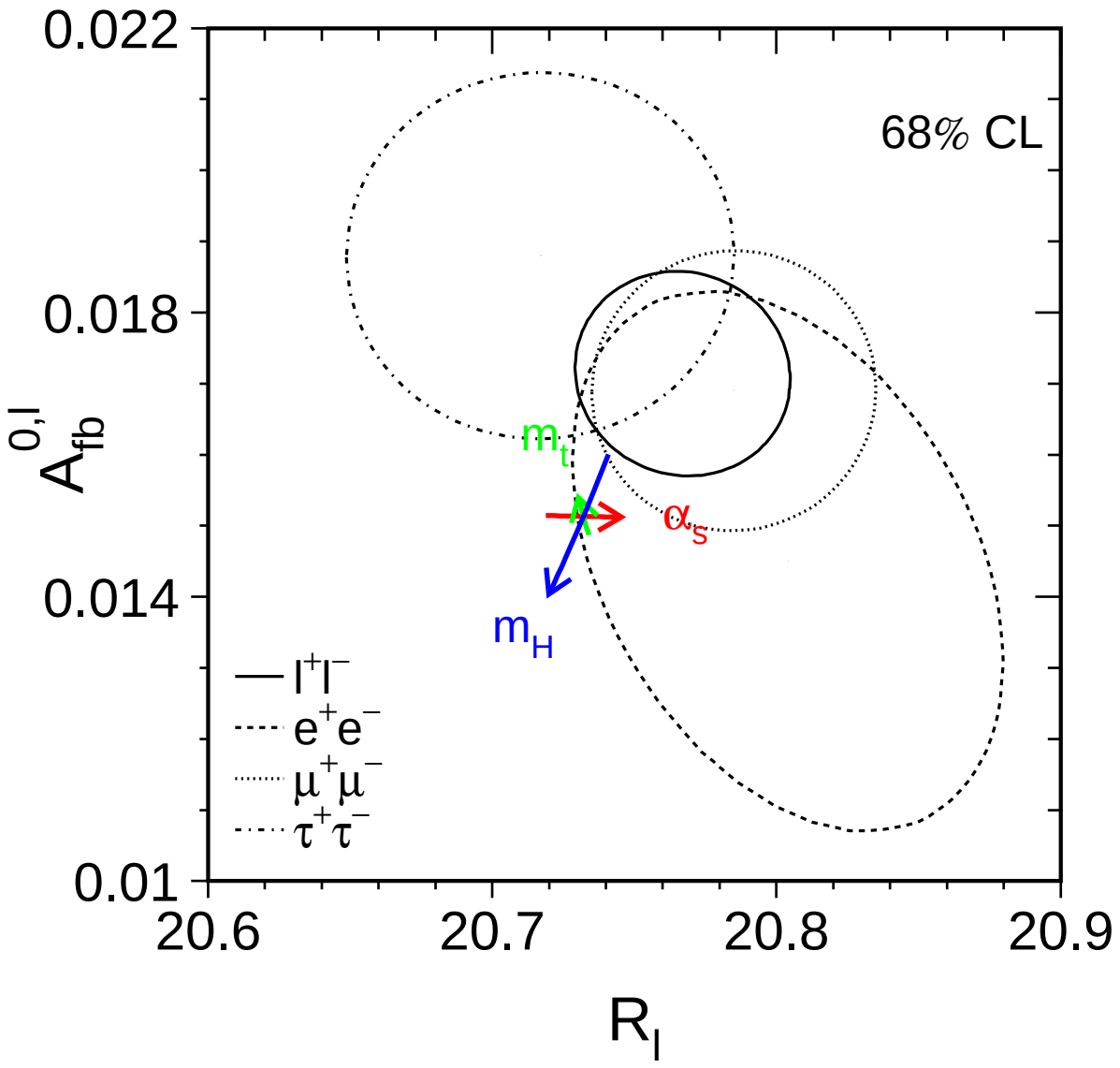

Figure 1: Contours of 68% probability in the R_ℓ-$A_{\rm FB}^{0,\ell}$ plane. For better comparison the results for the τ lepton are corrected to correspond to the massless case. The Standard Model prediction for $m_{\rm Z} = 91.1875$ GeV, $m_{\rm t} = 174.3$ GeV, $m_{\rm H} = 300$ GeV, and $\alpha_{\rm s}(m_{\rm Z}^2) = 0.119$ is also shown. The lines with arrows correspond to the variation of the Standard Model prediction when $m_{\rm t}$, $m_{\rm H}$ and $\alpha_{\rm s}(m_{\rm Z}^2)$ are varied in the intervals $m_{\rm t} = 174.3 \pm 5.1$ GeV, $m_{\rm H} = 300^{+700}_{-187}$ GeV, and $\alpha_{\rm s}(m_{\rm Z}^2) = 0.119 \pm 0.002$, respectively. The arrows point in the direction of increasing values of $m_{\rm t}$, $m_{\rm H}$ and $\alpha_{\rm s}$.

3 The τ Polarisation

Updates with respect to last summer:
DELPHI have finalised their results.
OPAL have updated their results.

The longitudinal τ polarisation $\mathcal{P}_\tau$ of τ pairs produced in Z decays is defined as

$$\mathcal{P}_\tau \equiv \frac{\sigma_{\mathrm{R}} - \sigma_{\mathrm{L}}}{\sigma_{\mathrm{R}} + \sigma_{\mathrm{L}}}, \tag{5}$$

where σ_{R} and σ_{L} are the τ-pair cross sections for the production of a right-handed and left-handed τ^-, respectively. The distribution of $\mathcal{P}_\tau$ as a function of the polar scattering angle θ between the e^- and the τ^-, at $\sqrt{s} = m_{\mathrm{Z}}$, is given by

$$\mathcal{P}_\tau(\cos\theta) = -\frac{\mathcal{A}_\tau(1+\cos^2\theta) + 2\mathcal{A}_{\mathrm{e}}\cos\theta}{1+\cos^2\theta + 2\mathcal{A}_\tau\mathcal{A}_{\mathrm{e}}\cos\theta}, \tag{6}$$

with $\mathcal{A}_{\mathrm{e}}$ and $\mathcal{A}_\tau$ as defined in Equation (4). Equation (6) is valid for pure Z exchange. The effects of γ exchange, γ-Z interference and electromagnetic radiative corrections in the initial and final states are taken into account in the experimental analyses. In particular, these corrections account for the $\sqrt{s}$ dependence of the τ polarisation, which is important because the off-peak data are included in the event samples for all experiments. When averaged over all production angles $\mathcal{P}_\tau$ is a measurement of $\mathcal{A}_\tau$. As a function of $\cos\theta$, $\mathcal{P}_\tau(\cos\theta)$ provides nearly independent determinations of both $\mathcal{A}_\tau$ and $\mathcal{A}_{\mathrm{e}}$, thus allowing a test of the universality of the couplings of the Z to e and τ.

Each experiment makes separate $\mathcal{P}_\tau$ measurements using the five τ decay modes $\mathrm{e}\nu\overline{\nu}$, $\mu\nu\overline{\nu}$, $\pi\nu$, $\rho\nu$ and $a_1\nu$ [16–19]. The $\rho\nu$ and $\pi\nu$ are the most sensitive channels, contributing weights of about 40% each in the average. DELPHI and L3 have also used an inclusive hadronic analysis. The combination is made using the results from each experiment already averaged over the τ decay modes.

3.1 Results

Tables 5 and 6 show the most recent results for $\mathcal{A}_\tau$ and $\mathcal{A}_{\mathrm{e}}$ obtained by the four LEP collaborations [16–19] and their combination. Common systematic errors arise from uncertainties in the decay radiation in the $\pi\nu$ and $\rho\nu$ channels, and in the modelling of the a_1 decays [20]. These errors need further investigation and might need to be taken into account for the final results (see Reference 18). For the current combination the systematic errors on $\mathcal{A}_\tau$ and $\mathcal{A}_{\mathrm{e}}$ are treated as uncorrelated between the experiments. The statistical correlation between the extracted values of $\mathcal{A}_\tau$ and $\mathcal{A}_{\mathrm{e}}$ is small ($\leq 5\%$), and is neglected.

The average values for $\mathcal{A}_\tau$ and $\mathcal{A}_{\mathrm{e}}$:

$$\mathcal{A}_\tau = 0.1439 \pm 0.0042 \tag{7}$$
$$\mathcal{A}_{\mathrm{e}} = 0.1498 \pm 0.0048, \tag{8}$$

are compatible, in agreement with lepton universality. Assuming e-τ universality, the values for $\mathcal{A}_\tau$ and $\mathcal{A}_{\mathrm{e}}$ can be combined. This combination is performed neglecting any possible common systematic error between $\mathcal{A}_\tau$ and $\mathcal{A}_{\mathrm{e}}$ within a given experiment, as these errors are also estimated to be small. The combined result of $\mathcal{A}_\tau$ and $\mathcal{A}_{\mathrm{e}}$ is:

$$\mathcal{A}_\ell = 0.1464 \pm 0.0032. \tag{9}$$

Experiment		$\mathcal{A}_\tau$
ALEPH	(90 - 95), prel.	$0.1452 \pm 0.0052 \pm 0.0032$
DELPHI	(90 - 95), final	$0.1359 \pm 0.0079 \pm 0.0055$
L3	(90 - 95), final	$0.1476 \pm 0.0088 \pm 0.0062$
OPAL	(90 - 95), prel.	$0.1456 \pm 0.0075 \pm 0.0057$
LEP Average		0.1439 ± 0.0042

Table 5: LEP results for $\mathcal{A}_\tau$. The χ^2/d.o.f. for the average is 0.9/3. The first error is statistical and the second systematic. In the LEP average, statistical and systematic errors are combined in quadrature. The systematic component of the error is ± 0.0023.

Experiment		$\mathcal{A}_\mathrm{e}$
ALEPH	(90 - 95), prel.	$0.1505 \pm 0.0069 \pm 0.0010$
DELPHI	(90 - 95), final	$0.1382 \pm 0.0116 \pm 0.0005$
L3	(90 - 95), final	$0.1678 \pm 0.0127 \pm 0.0030$
OPAL	(90 - 95), prel.	$0.1456 \pm 0.0103 \pm 0.0034$
LEP Average		0.1498 ± 0.0048

Table 6: LEP results for $\mathcal{A}_\mathrm{e}$. The χ^2/d.o.f. for the average is 3.1/3. The first error is statistical and the second systematic. In the LEP average, statistical and systematic errors are combined in quadrature. The systematic component of the error is ± 0.0010.

4 Measurement of $A_{\rm LR}$ at SLC

Updates with respect to last summer:
SLD have final results for $A_{\rm LR}$ and the leptonic left-right forward-backward asymmetries.

The measurement of the left-right cross section asymmetry ($A_{\rm LR}$) by SLD [21] at the SLC provides a systematically precise, statistics-dominated determination of the coupling $\mathcal{A}_{\rm e}$, and is presently the most precise single measurement, with the smallest systematic error, of this quantity. In principle the analysis is straightforward: one counts the numbers of Z bosons produced by left and right longitudinally polarised electrons, forms an asymmetry, and then divides by the luminosity-weighted e^- beam polarisation magnitude (the e^+ beam is not polarised):

$$A_{\rm LR} = \frac{N_{\rm L} - N_{\rm R}}{N_{\rm L} + N_{\rm R}} \frac{1}{P_{\rm e}}. \tag{10}$$

Since the advent of high polarisation "strained lattice" GaAs photocathodes (1994), the average electron polarisation at the interaction point has been in the range 73% to 77%. The method requires no detailed final state event identification (e^+e^- final state events are removed, as are non-Z backgrounds) and is insensitive to all acceptance and efficiency effects. The small total systematic error of 0.64% is dominated by the 0.50% systematic error in the determination of the e^- polarisation. The statistical error on $A_{\rm LR}$ is about 1.3%.

The precision Compton polarimeter detects beam electrons that have been scattered by photons from a circularly polarised laser. Two additional polarimeters that are sensitive to the Compton-scattered photons and which are operated in the absence of positron beam, have verified the precision polarimeter result and are used to set a calibration uncertainty of 0.4%. In 1998, a dedicated experiment was performed in order to directly test the expectation that accidental polarisation of the positron beam was negligible; the e^+ polarisation was found to be consistent with zero (-0.02 ± 0.07)%.

The $A_{\rm LR}$ analysis includes several very small corrections. The polarimeter result is corrected for higher order QED and accelerator related effects, a total of (-0.22 ± 0.15)% for 1997/98 data. The event asymmetry is corrected for backgrounds and accelerator asymmetries, a total of $(+0.15\pm0.07)$%, for 1997/98 data.

The translation of the $A_{\rm LR}$ result to a "pole" value is a (-2.5 ± 0.4)% effect, where the uncertainty arises from the precision of the centre-of-mass energy determination. This small error due to the beam energy measurement is slightly larger than seen previously (it was closer to 0.3%) and reflects the results of a scan of the Z peak used to calibrate the energy spectrometers to $m_{\rm Z}$ from LEP data, which was performed for the first time during the most recent SLC run. The pole value, $A^0_{\rm LR}$, is equivalent to a measurement of $\mathcal{A}_{\rm e}$.

The 2000 result is included in a running average of all of the SLD $A_{\rm LR}$ measurements (1992, 1993, 1994/1995, 1996, 1997 and 1998). This updated result for $A^0_{\rm LR}$ ($\mathcal{A}_{\rm e}$) is 0.1514 ± 0.0022. In addition, the left-right forward-backward asymmetries for leptonic final states are measured [22]. From these, the parameters $\mathcal{A}_{\rm e}$, $\mathcal{A}_\mu$ and $\mathcal{A}_\tau$ can be determined. The results are $\mathcal{A}_{\rm e} = 0.1544\pm0.0060$, $\mathcal{A}_\mu = 0.142\pm0.015$ and $\mathcal{A}_\tau = 0.136 \pm 0.015$. The lepton-based result for $\mathcal{A}_{\rm e}$ can be combined with the $A^0_{\rm LR}$ result to yield $\mathcal{A}_{\rm e} = 0.1516 \pm 0.0021$, including small correlations in the systematic errors. The correlation of this measurement with $\mathcal{A}_\mu$ and $\mathcal{A}_\tau$ is indicated in Table 7.

Assuming lepton universality, the $A_{\rm LR}$ result and the results on the leptonic left-right forward-backward asymmetries can be combined, while accounting for small correlated systematic errors,

yielding

$$\mathcal{A}_\ell = 0.1513 \pm 0.0021. \tag{11}$$

	$\mathcal{A}_\mathrm{e}$	$\mathcal{A}_\mu$	$\mathcal{A}_\tau$
$\mathcal{A}_\mathrm{e}$	1.000		
$\mathcal{A}_\mu$	0.038	1.000	
$\mathcal{A}_\tau$	0.033	0.007	1.000

Table 7: Correlation coefficients between $\mathcal{A}_\mathrm{e}$, $\mathcal{A}_\mu$ and $\mathcal{A}_\tau$

5 Results from b and c Quarks

Updates with respect to last summer:
DELPHI has presented new measurements of $A_{\rm FB}^{\rm b\bar{b}}$ and $A_{\rm FB}^{\rm c\bar{c}}$.
SLD has presented updated measurements of $R_{\rm b}$, $R_{\rm c}$, $\mathcal{A}_{\rm b}$ with leptons and vertex charge and $\mathcal{A}_{\rm c}$ with leptons and D-mesons.
ALEPH has presented a new measurement of BR($\rm b \to \ell$) and BR($\rm b \to c \to \bar{\ell}$) and L3 has published their measurement of $R_{\rm b}$ and BR($\rm b \to \ell$).

The relevant quantities in the heavy quark sector at LEP/SLD which are currently determined by the combination procedure are:

- The ratios of the b and c quark partial widths of the Z to its total hadronic partial width: $R_{\rm b}^0 \equiv \Gamma_{\rm b\bar{b}}/\Gamma_{\rm had}$ and $R_{\rm c}^0 \equiv \Gamma_{\rm c\bar{c}}/\Gamma_{\rm had}$.
- The forward-backward asymmetries, $A_{\rm FB}^{\rm b\bar{b}}$ and $A_{\rm FB}^{\rm c\bar{c}}$.
- The final state coupling parameters $\mathcal{A}_{\rm b}$, $\mathcal{A}_{\rm c}$ obtained from the left-right-forward-backward asymmetry at SLD.
- The semileptonic branching ratios, BR($\rm b \to \ell$), BR($\rm b \to c \to \bar{\ell}$) and BR($\rm c \to \ell$), and the average time-integrated $\rm B^0\overline{B^0}$ mixing parameter, $\overline{\chi}$. These are often determined at the same time or with similar methods as the asymmetries. Including them in the combination greatly reduces the errors. For example the measurements of $\overline{\chi}$ act as an effective measurement of the charge tagging efficiency, so that all errors coming from the mixture of different lepton sources in $\rm b\overline{b}$ events cancel in the asymmetries.
- The probability that a c quark produces a $\rm D^+$, $\rm D_s$, $\rm D^{*+}$ meson[2] or a charmed baryon. The probability that a c quark fragments into a $\rm D^0$ is calculated from the constraint that the probabilities for the weakly decaying charmed hadrons add up to one.

A full description of the averaging procedure is published in [3]; the main motivations for the procedure are outlined here. Several analyses measure more than one parameter simultaneously, for example the asymmetry measurements with leptons or D mesons. Some of the measurements of electroweak parameters depend explicitly on the values of other parameters, for example $R_{\rm b}$ depends on $R_{\rm c}$. The common tagging and analysis techniques lead to common sources of systematic uncertainty, in particular for the double-tag measurements of $R_{\rm b}$. The starting point for the combination is to ensure that all the analyses use a common set of assumptions for input parameters which give rise to systematic uncertainties. The input parameters are updated and extended [1, 23] to accommodate new analyses and more recent measurements. The correlations and interdependences of the input measurements are then taken into account in a χ^2 minimisation which results in the combined electroweak parameters and their correlation matrix.

In a first fit the asymmetry measurements on peak, above peak and below peak are corrected to three common centre-of-mass energies and are then combined at each energy point. The results of this fit, including the SLD results, are given in Appendix A. The dependence of the average asymmetries on centre-of-mass energy agrees with the prediction of the Standard Model. A second fit is made to derive the pole asymmetries $A_{\rm FB}^{0,\rm q}$ from the measured quark asymmetries, in which all the off-peak

[2] Actually the product $\rm P(c \to D^{*+}) \times BR(D^{*+} \to \pi^+ D^0)$ is fitted because this quantity is needed and measured by the LEP experiments.

asymmetry measurements are corrected to the peak energy before combining. This fit determines a total of 14 parameters: the two partial widths, two LEP asymmetries, two coupling parameters from SLD, three semileptonic branching ratios, the average mixing parameter and the probabilities for c quark to fragment into a D^+, a D_s, a D^{*+}, or a charmed baryon. If the SLD measurements are excluded from the fit there are 12 parameters to be determined.

5.1 Summary of Measurements and Averaging Procedure

All measurements are presented by the LEP and SLD collaborations in a consistent manner for the purpose of combination. The tables prepared by the experiments include a detailed breakdown of the systematic error of each measurement and its dependence on other electroweak parameters. Where necessary, the experiments apply small corrections to their results in order to use agreed values and ranges for the input parameters to calculate systematic errors. The measurements, corrected where necessary, are summarised in Appendix A in Tables 44–63, where the statistical and systematic errors are quoted separately. The correlated systematic entries are from physics sources shared with one or more other results in the table and are derived from the full breakdown of common systematic uncertainties. The uncorrelated systematic entries come from the remaining sources.

5.1.1 Averaging Procedure

A χ^2 minimisation procedure is used to derive the values of the heavy-flavour electroweak parameters as published in Reference 3. The full statistical and systematic covariance matrix for all measurements is calculated. This correlation matrix takes into account correlations between different measurements of one experiment and between different experiments. The explicit dependence of each measurement on the other parameters is also accounted for.

Since c-quark events form the main background in the R_b analyses, in the lifetime R_b analyses, the value of R_b depends on the value of R_c. If R_b and R_c are measured in the same analysis, this is reflected in the correlation matrix for the results. However the analyses do not determine R_b and R_c simultaneously but instead measure R_b for an assumed value of R_c. In this case the dependence is parameterised as

$$R_b \;=\; R_b^{\rm meas} + a(R_c)\frac{(R_c - R_c^{\rm used})}{R_c}. \qquad (12)$$

In this expression, $R_b^{\rm meas}$ is the result of the analysis assuming a value of $R_c = R_c^{\rm used}$. The values of $R_c^{\rm used}$ and the coefficients $a(R_c)$ are given in Table 44 where appropriate. The dependence of all other measurements on other electroweak parameters is treated in the same way, with coefficients $a(x)$ describing the dependence on parameter x.

5.1.2 Partial Width Measurements

The measurements of R_b and R_c fall into two categories. In the first, called a single-tag measurement, a method to select b or c events is devised, and the number of tagged events is counted. This number must then be corrected for backgrounds from other flavours and for the tagging efficiency to calculate the true fraction of hadronic Z decays of that flavour. The dominant systematic errors come from understanding the branching ratios and detection efficiencies which give the overall tagging efficiency.

For the second technique, called a double-tag measurement, each event is divided into two hemispheres. With N_t being the number of tagged hemispheres, N_{tt} the number of events with both hemispheres tagged and $N_{\rm had}$ the total number of hadronic Z decays one has

$$\frac{N_t}{2N_{\rm had}} = \varepsilon_{\rm b}R_{\rm b} + \varepsilon_{\rm c}R_{\rm c} + \varepsilon_{\rm uds}(1 - R_{\rm b} - R_{\rm c}), \tag{13}$$

$$\frac{N_{tt}}{N_{\rm had}} = \mathcal{C}_{\rm b}\varepsilon_{\rm b}^2R_{\rm b} + \mathcal{C}_{\rm c}\varepsilon_{\rm c}^2R_{\rm c} + \mathcal{C}_{\rm uds}\varepsilon_{\rm uds}^2(1 - R_{\rm b} - R_{\rm c}), \tag{14}$$

where $\varepsilon_{\rm b}$, $\varepsilon_{\rm c}$ and $\varepsilon_{\rm uds}$ are the tagging efficiencies per hemisphere for b, c and light-quark events, and $\mathcal{C}_{\rm q} \neq 1$ accounts for the fact that the tagging efficiencies between the hemispheres may be correlated. In the case of $R_{\rm b}$ one has $\varepsilon_{\rm b} \gg \varepsilon_{\rm c} \gg \varepsilon_{\rm uds}$, $\mathcal{C}_{\rm b} \approx 1$. The correlations for the other flavours can be neglected. These equations can be solved to give $R_{\rm b}$ and $\varepsilon_{\rm b}$. Neglecting the c and uds backgrounds and the correlations they are approximately given by

$$\varepsilon_{\rm b} \approx 2N_{tt}/N_t, \tag{15}$$

$$R_{\rm b} \approx N_t^2/(4N_{tt}N_{\rm had}). \tag{16}$$

The double-tagging method has the advantage that the b tagging efficiency is derived from the data, reducing the systematic error. The residual background of other flavours in the sample, and the evaluation of the correlation between the tagging efficiencies in the two hemispheres of the event are the main sources of systematic uncertainty in such an analysis.

This method can be enhanced by including more tags. All additional efficiencies can be determined from the data, reducing the statistical uncertainties without adding new systematic uncertainties.

Small corrections must be applied to the results to obtain the partial width ratios $R_{\rm b}^0$ and $R_{\rm c}^0$ from the cross section ratios $R_{\rm b}$ and $R_{\rm c}$. These corrections depend slightly on the invariant mass cutoff of the simulations used by the experiments, so that they are applied by the collaborations before the combination.

The partial width measurements included are:

- Lifetime (and lepton) double tag measurements for $R_{\rm b}$ from ALEPH [24], DELPHI [25], L3 [26], OPAL [27] and SLD [28]. These are the most precise determinations of $R_{\rm b}$. Since they completely dominate the combined result, no other $R_{\rm b}$ measurements are used at present. The basic features of the double-tag technique are discussed above. In the ALEPH, DELPHI, OPAL and SLD measurements the charm rejection is enhanced by using the invariant mass information. DELPHI, OPAL and SLD also add kinematic information from the particles at the secondary vertex. The ALEPH and DELPHI measurements make use of several different tags; this improves the statistical accuracy and reduces the systematic errors due to hemisphere correlations and charm contamination, compared with the simple single/double tag.
- Analyses with $\rm D/D^{*\pm}$ mesons to measure $R_{\rm c}$ from ALEPH, DELPHI and OPAL. All measurements are constructed in such a way that no assumptions on the energy dependence of charm fragmentation are necessary. The available measurements can be divided into four groups:
  - inclusive/exclusive double tag (ALEPH [29], DELPHI [30, 31], OPAL [32]): In a first step $\rm D^{*\pm}$ mesons are reconstructed in several decay channels and their production rate is measured, which depends on the product $R_{\rm c} \times {\rm P(c \to D^{*+}) \times BR(D^{*+} \to \pi^+ D^0)}$. This sample of $\rm c\overline{c}$ (and $\rm b\overline{b}$) events is then used to measure $\rm P(c \to D^{*+}) \times BR(D^{*+} \to \pi^+ D^0)$ using a slow pion tag in the opposite hemisphere. In the ALEPH measurement $R_{\rm c}$ is unfolded internally in the analysis so that no explicit $\rm P(c \to D^{*+}) \times BR(D^{*+} \to \pi^+ D^0)$ is available.

  - exclusive double tag (ALEPH [29]): This analysis uses exclusively reconstructed D^{*+}, D^0 and D^+ mesons in different decay channels. It has lower statistics but better purity than the inclusive analyses.
  - reconstruction of all weakly decaying charmed states (ALEPH [33], DELPHI [31], OPAL [34]): These analyses make the assumption that the production rates of D^0, D^+, D_s and Λ_c in $c\overline{c}$ events add up to one with small corrections due to unmeasured charms strange baryons. This is a single tag measurement, relying only on knowing the decay branching ratios of the charm hadrons. These analyses are also used to measure the c hadron production ratios which are needed for the R_b analyses.

- A lifetime plus mass double tag from SLD to measure R_c [28]. This analysis uses the same tagging algorithm as the SLD R_b analysis, but with the neural net tuned to tag charm. Although the charm tag has a purity of about 84%, most of the background is from b which can be measured with high precision from the b/c mixed tag rate.

- A measurement of R_c using single leptons assuming $BR(c \to \ell)$ from ALEPH [29].

To avoid effects from non linearities in the fit, for the inclusive/exclusive single/double tag and for the charm-counting analyses, the products $R_c P(c \to D^{*+}) \times BR(D^{*+} \to \pi^+ D^0)$, $R_c f_{D^0}$, $R_c f_{D^+}$, $R_c f_{D_s}$ and $R_c f_{\Lambda_c}$that are actually measured in the analyses are directly used as inputs to the fit. The measurements of the production rates of weakly decaying charmed hadrons, especially $R_c f_{D_s}$ and $R_c f_{\Lambda_c}$ have a substantial error due to the branching ratio of the decay mode used. Since this error is a relative one there is a potential bias towards lower measurements. To avoid this bias, for the production rates of weakly decaying charmed hadrons the logarithm of the production rates instead of the rates themselves are input to the fit. For $R_c f_{D^0}$ and $R_c f_{D^+}$ the difference between the results using the logarithm or the value itself is negligible. For $R_c f_{D_s}$ and $R_c f_{\Lambda_c}$ the difference in the R_c-result is about one tenth of a standard deviation.

5.1.3 Asymmetry Measurements

All b and c asymmetries given by the experiments are corrected to full acceptance.

The QCD corrections to the forward-backward asymmetries depend strongly on the experimental analyses. For this reason the numbers given by the collaborations are also corrected for QCD effects. A detailed description of the procedure can be found in [35] with updates reported in [1]

For the 12- and 14-parameter fits described above, the LEP peak and off-peak asymmetries are corrected to $\sqrt{s} = 91.26$ GeV using the predicted dependence from ZFITTER [36]. The slope of the asymmetry around m_Z depends only on the axial coupling and the charge of the initial and final state fermions and is thus independent of the value of the asymmetry itself.

After calculating the overall averages, the quark pole asymmetries, $A_{FB}^{0,q}$, are derived by applying the corrections described below. To relate the pole asymmetries to the measured ones a few corrections that are summarised in Table 8 have to be applied. These corrections are due to the energy shift from 91.26 GeV to m_Z, initial state radiation, γ exchange and γ-Z interference. A very small correction due to the nonzero value of the b quark mass is included in the correction called γ-Z interference. All corrections are calculated using ZFITTER.

The SLD left-right-forward-backward asymmetries are also corrected for all radiative effects and are directly presented in terms of $\mathcal{A}_b$ and $\mathcal{A}_c$.

Source	$\delta A_{\rm FB}^{\rm b}$	$\delta A_{\rm FB}^{\rm c}$
$\sqrt{s} = m_{\rm Z}$	-0.0013	-0.0034
QED corrections	$+0.0041$	$+0.0104$
γ, γ-Z, mass	-0.0003	-0.0008
Total	$+0.0025$	$+0.0062$

Table 8: Corrections to be applied to the quark asymmetries as $A_{\rm FB}^0 = A_{\rm FB}^{\rm meas} + \delta A_{\rm FB}$.

The measurements used are:

- Measurements of $A_{\rm FB}^{\rm b\bar{b}}$ and $A_{\rm FB}^{\rm c\bar{c}}$ using leptons from ALEPH [37], DELPHI [38], L3 [39] and OPAL [40]. These analyses measure either $A_{\rm FB}^{\rm b\bar{b}}$ only from a high p_t lepton sample or they obtain $A_{\rm FB}^{\rm b\bar{b}}$ and $A_{\rm FB}^{\rm c\bar{c}}$ from a fit to the lepton spectra. In the case of OPAL the lepton information is combined with hadronic variables in a neural net. DELPHI uses in addition lifetime information and jet-charge in the hemisphere opposite to the lepton to separate the different lepton sources. Some asymmetry analyses also measure $\overline{\chi}$.
- Measurements of $A_{\rm FB}^{\rm b\bar{b}}$ based on lifetime tagged events with a hemisphere charge measurement from ALEPH [41], DELPHI [42], L3 [43] and OPAL [44]. These measurements contribute roughly the same weight to the combined result as the lepton fits.
- Analyses with D mesons to measure $A_{\rm FB}^{\rm c\bar{c}}$ from ALEPH [45] or $A_{\rm FB}^{\rm c\bar{c}}$ and $A_{\rm FB}^{\rm b\bar{b}}$ from DELPHI [46] and OPAL [47].
- Measurements of $\mathcal{A}_{\rm b}$ and $\mathcal{A}_{\rm c}$ from SLD. These results include measurements using lepton [48,49], D meson [50] and vertex mass plus hemisphere charge [51] tags, which have similar sources of systematic errors as the LEP asymmetry measurements. SLD also uses vertex mass for bottom or charm tag in conjunction with a kaon tag or a vertex charge tag for both $\mathcal{A}_{\rm b}$ and $\mathcal{A}_{\rm c}$ measurements [52–54].

5.1.4 Other Measurements

The measurements of the charmed hadron fractions $\mathrm{P(c \to D^{*+}) \times BR(D^{*+} \to \pi^+ D^0)}$, $f(\mathrm{D^+})$, $f(\mathrm{D_s})$ and $f(\mathrm{c_{baryon}})$ are included in the $R_{\rm c}$ measurements and are described there.

ALEPH [55], DELPHI [56], L3 [26, 57] and OPAL [58] measure $\mathrm{BR(b \to \ell)}$, $\mathrm{BR(b \to c \to \bar{\ell})}$ and $\overline{\chi}$ or a subset of them from a sample of leptons opposite to a b-tagged hemisphere and from a double lepton sample. DELPHI [30] and OPAL [59] measure $\mathrm{BR(c \to \ell)}$ from a sample opposite to a high energy $\mathrm{D^{*\pm}}$.

5.2 Results

5.2.1 Results of the 12-Parameter Fit to the LEP Data

Using the full averaging procedure gives the following combined results for the electroweak parameters:

$$R_{\rm b}^0 \quad = \quad 0.21648 \pm 0.00075 \tag{17}$$

$$
\begin{aligned}
R_{\mathrm{c}}^{0} &= 0.1674 \pm 0.0047 \\
A_{\mathrm{FB}}^{0,\mathrm{b}} &= 0.0989 \pm 0.0020 \\
A_{\mathrm{FB}}^{0,\mathrm{c}} &= 0.0688 \pm 0.0035\,,
\end{aligned}
$$

where all corrections to the asymmetries and partial widths are applied. The χ^2/d.o.f. is $49/(89-12)$. The corresponding correlation matrix is given in Table 9.

	R_{b}^{0}	R_{c}^{0}	$A_{\mathrm{FB}}^{0,\mathrm{b}}$	$A_{\mathrm{FB}}^{0,\mathrm{c}}$
R_{b}^{0}	1.00	−0.15	−0.03	0.01
R_{c}^{0}	−0.15	1.00	0.07	−0.01
$A_{\mathrm{FB}}^{0,\mathrm{b}}$	−0.03	0.07	1.00	0.11
$A_{\mathrm{FB}}^{0,\mathrm{c}}$	0.01	−0.01	0.11	1.00

Table 9: The correlation matrix for the four electroweak parameters from the 12-parameter fit.

5.2.2 Results of the 14-Parameter Fit to LEP and SLD Data

Including the SLD results for R_{b}, R_{c}, $\mathcal{A}_{\mathrm{b}}$ and $\mathcal{A}_{\mathrm{c}}$ into the fit the following results are obtained:

$$
\begin{aligned}
R_{\mathrm{b}}^{0} &= 0.21653 \pm 0.00069 \\
R_{\mathrm{c}}^{0} &= 0.1709 \pm 0.0034 \\
A_{\mathrm{FB}}^{0,\mathrm{b}} &= 0.0990 \pm 0.0020 \\
A_{\mathrm{FB}}^{0,\mathrm{c}} &= 0.0689 \pm 0.0035 \\
\mathcal{A}_{\mathrm{b}} &= 0.922 \pm 0.023 \\
\mathcal{A}_{\mathrm{c}} &= 0.631 \pm 0.026\,,
\end{aligned}
\tag{18}
$$

with a χ^2/d.o.f. of $54/(98-14)$. The corresponding correlation matrix is given in Table 10 and the largest errors for the electroweak parameters are listed in Table 11.

In deriving these results the parameters $\mathcal{A}_{\mathrm{b}}$ and $\mathcal{A}_{\mathrm{c}}$ are treated as independent of the forward-backward asymmetries $A_{\mathrm{FB}}^{0,\mathrm{b}}$ and $A_{\mathrm{FB}}^{0,\mathrm{c}}$. In Figure 2 the results for R_{b}^{0} and R_{c}^{0} are shown compared with the Standard Model expectation.

	R_{b}^{0}	R_{c}^{0}	$A_{\mathrm{FB}}^{0,\mathrm{b}}$	$A_{\mathrm{FB}}^{0,\mathrm{c}}$	$\mathcal{A}_{\mathrm{b}}$	$\mathcal{A}_{\mathrm{c}}$
R_{b}^{0}	1.00	−0.13	−0.02	0.01	−0.04	0.02
R_{c}^{0}	−0.13	1.00	0.05	−0.01	0.02	−0.02
$A_{\mathrm{FB}}^{0,\mathrm{b}}$	−0.02	0.05	1.00	0.10	0.02	0.00
$A_{\mathrm{FB}}^{0,\mathrm{c}}$	0.01	−0.01	0.10	1.00	0.00	0.01
$\mathcal{A}_{\mathrm{b}}$	−0.04	0.02	0.02	0.00	1.00	0.14
$\mathcal{A}_{\mathrm{c}}$	0.02	−0.02	0.00	0.01	0.14	1.00

Table 10: The correlation matrix for the six electroweak parameters from the 14-parameter fit.

The 14 parameter fit yields the $\mathrm{b} \to \ell$ branching ratio:

$$
\mathrm{BR}(\mathrm{b} \to \ell) \;=\; 0.1057 \pm 0.0019. \tag{19}
$$

	R_b^0 (10^{-3})	R_c^0 (10^{-3})	$A_{FB}^{0,b}$ (10^{-3})	$A_{FB}^{0,c}$ (10^{-3})	$\mathcal{A}_b$ (10^{-2})	$\mathcal{A}_c$ (10^{-2})
statistics	0.43	2.6	1.7	3.0	1.6	2.0
internal systematics	0.31	1.8	0.7	1.4	1.6	1.6
QCD effects	0.19	0.1	0.2	0.1	0.6	0.3
BR(D $\to$ neut.)	0.14	0.1	0	0	0	0
D decay multiplicity	0.12	0.2	0	0	0	0
BR($D^+ \to K^-\pi^+\pi^+$)	0.10	0.3	0.1	0	0	0
BR($D_s \to \phi\pi^+$)	0.02	0.7	0.1	0	0	0
BR($\Lambda_c \to$p $K^-\pi^+$)	0.06	0.6	0	0.1	0	0
D lifetimes	0.06	0.1	0	0.1	0	0
gluon splitting	0.26	0.6	0	0.2	0.1	0.1
c fragmentation	0.10	0.3	0.1	0.2	0.1	0.1
light quarks	0.07	0.3	0.5	0.1	0	0
total	0.69	3.4	2.0	3.5	2.3	2.6

Table 11: The dominant error sources for the electroweak parameters from the 14-parameter fit.

The largest error sources on this quantity are the dependences on the semileptonic decay models $b \to \ell$, $c \to \ell$ with

$$\begin{aligned} \Delta BR(b \to \ell)|_{(b\to\ell)\text{model}} &= 0.0008, \\ \Delta BR(b \to \ell)|_{(c\to\ell)\text{model}} &= 0.0005. \end{aligned}$$

Extensive studies are made to understand the size of these errors. If all the asymmetry measurements are excluded from the fit a consistent result is obtained with modelling errors of 0.0010 and 0.0006. The reduction of the modelling uncertainty is due to the inclusion of asymmetry measurements using different methods. Those using leptons depend on the semileptonic decay models while those using a lifetime tag and jet charge or D mesons do not. The mutual consistency of the asymmetry measurements effectively constrains the semileptonic decay models, and reduces the uncertainty in the semileptonic branching ratio.

The result of the full fit to the LEP+SLC results including the off-peak asymmetries and the non-electroweak parameters can be found in Appendix A. Results for the non-electroweak parameters are independent of the treatment of the off-peak asymmetries and the SLD data.

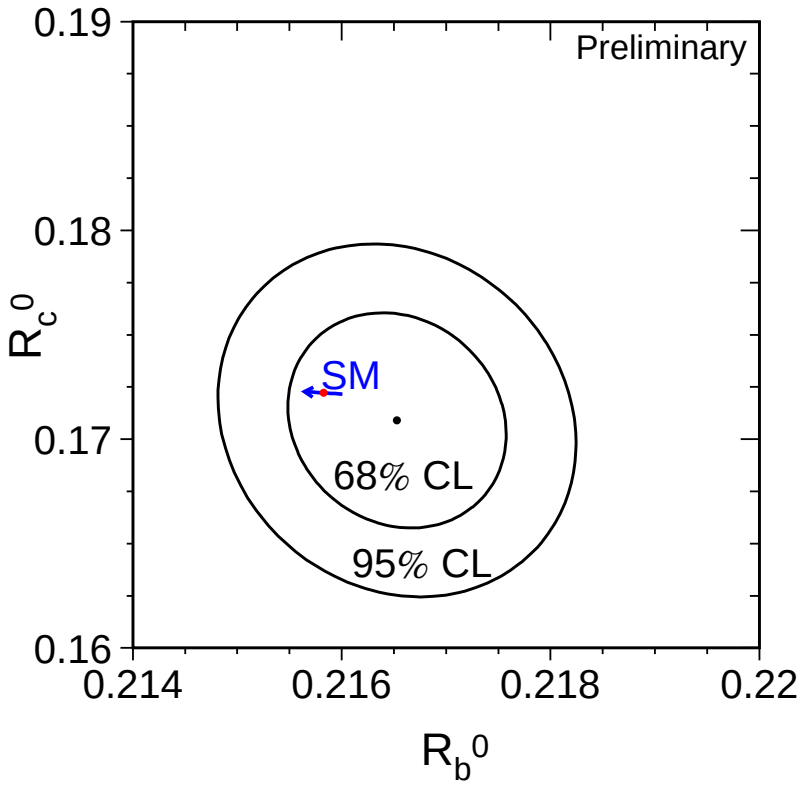

Figure 2: Contours in the R_b^0-R_c^0 plane derived from the LEP+SLD data, corresponding to 68% and 95% confidence levels assuming Gaussian systematic errors. The Standard Model prediction for $m_t = 174.3 \pm 5.1$ GeV is also shown. The arrow points in the direction of increasing values of m_t.

6 The Hadronic Charge Asymmetry $\langle Q_{\rm FB} \rangle$

Updates with respect to last summer:
L3 have published their result.

The LEP experiments ALEPH [60–62], DELPHI [63, 64], L3 [43] and OPAL [65, 66] have provided measurements of the hadronic charge asymmetry based on the mean difference in jet charges measured in the forward and backward event hemispheres, $\langle Q_{\rm FB} \rangle$. DELPHI have also provided a related measurement of the total charge asymmetry by making a charge assignment on an event-by-event basis and performing a likelihood fit [63]. The experimental values quoted for the average forward-backward charge difference, $\langle Q_{\rm FB} \rangle$, cannot be directly compared as some of them include detector dependent effects such as acceptances and efficiencies. Therefore the effective electroweak mixing angle, $\sin^2\theta^{\rm lept}_{\rm eff}$, as defined in Section 12.4, is used as a means of combining the experimental results summarised in Table 12.

Experiment		$\sin^2\theta^{\rm lept}_{\rm eff}$
ALEPH	(90-94), final	$0.2322 \pm 0.0008 \pm 0.0011$
DELPHI	(91-94), prel.	$0.2311 \pm 0.0010 \pm 0.0014$
L3	(91-95), final	$0.2327 \pm 0.0012 \pm 0.0013$
OPAL	(91-94), prel.	$0.2326 \pm 0.0012 \pm 0.0013$
LEP Average		0.2321 ± 0.0010

Table 12: Summary of the determination of $\sin^2\theta^{\rm lept}_{\rm eff}$ from inclusive hadronic charge asymmetries at LEP. For each experiment, the first error is statistical and the second systematic. The latter is dominated by fragmentation and decay modelling uncertainties.

The dominant source of systematic error arises from the modelling of the charge flow in the fragmentation process for each flavour. All experiments measure the required charge properties for $Z \to b\overline{b}$ events from the data. ALEPH also determines the charm charge properties from the data. The fragmentation model implemented in the JETSET Monte Carlo program [67] is used by all experiments as reference; the one of the HERWIG Monte Carlo program [68] is used for comparison. The JETSET fragmentation parameters are varied to estimate the systematic errors. The central values chosen by the experiments for these parameters are, however, not the same. The smaller of the two fragmentation errors in any pair of results is treated as common to both. The present average of $\sin^2\theta^{\rm lept}_{\rm eff}$ from $\langle Q_{\rm FB} \rangle$ and its associated error are not very sensitive to the treatment of common uncertainties. The ambiguities due to QCD corrections may cause changes in the derived value of $\sin^2\theta^{\rm lept}_{\rm eff}$. These are, however, well below the fragmentation uncertainties and experimental errors. The effect of fully correlating the estimated systematic uncertainties from this source between the experiments has a negligible effect upon the average and its error.

There is also some correlation between these results and those for $A^{b\bar{b}}_{\rm FB}$ using jet charges. The dominant source of correlation is again through uncertainties in the fragmentation and decay models used. The typical correlation between the derived values of $\sin^2\theta^{\rm lept}_{\rm eff}$ from the $\langle Q_{\rm FB} \rangle$ and the $A^{b\bar{b}}_{\rm FB}$ jet charge measurements is estimated to be about 20% to 25%. This leads to only a small change in the relative weights for the $A^{b\bar{b}}_{\rm FB}$ and $\langle Q_{\rm FB} \rangle$ results when averaging their $\sin^2\theta^{\rm lept}_{\rm eff}$ values (Section 12.4). Furthermore, the jet charge method contributes at most half of the weight of the $A^{b\bar{b}}_{\rm FB}$ measurement. Thus, the correlation between $\langle Q_{\rm FB} \rangle$ and $A^{b\bar{b}}_{\rm FB}$ from jet charge will have little impact on the overall Standard Model fit, and is neglected at present.

7 Averages for $f\bar{f}$ Production at LEP-II

Updates with respect to last summer:
Results are updated with data taken in 1999 and 2000.

Since the start of the LEP-II program LEP has delivered collisions at energies from ~ 130 GeV to ~ 209 GeV. The four LEP experiments have made measurements on the $e^+e^- \to f\bar{f}$ process over this range of energies, and preliminary combinations of these data are discussed in this note.

For the combination presented here, only data taken up to the end of June 2000 are considered. The nominal and actual centre-of-mass energies to which the LEP data are averaged for each year are given in Table 13.

A number of measurements on the process $e^+e^- \to f\bar{f}$ exist and are combined.

- preliminary averages of cross section and forward-backward asymmetry measurements
- a preliminary average of the differential cross section measurements, $\frac{d\sigma}{d\cos\theta}$, for the channels $e^+e^- \to \mu^+\mu^-$ and $e^+e^- \to \tau^+\tau^-$
- heavy flavour results R_b, R_c, $A_{FB}^{b\bar{b}}$ and $A_{FB}^{c\bar{c}}$

Complete results of the combinations are available on the web page [69] and are discussed in [70].

The combined results are interpreted in terms of contact interactions, the exchange of Z′ bosons, and contours of the S-Matrix parameters $j_{b,c}^{tot}$ and $j_{b,c}^{fb}$, that describe γ-Z interference, are derived. The interpretations are discussed fully in [70].

7.1 Cross Sections and Asymmetry Measurements

Cross section results are combined for the $e^+e^- \to q\bar{q}$, $e^+e^- \to \mu^+\mu^-$ and $e^+e^- \to \tau^+\tau^-$ channels, forward-backward asymmetry measurements are combined for the $\mu^+\mu^-$ and $\tau^+\tau^-$ final states. The averages are made for the samples of events with high $\sqrt{s'}$.

As before [71], the averaged results are given for two signal definitions:

- **Definition 1:** $\sqrt{s'}$ is taken to be the mass of the s-channel propagator, with the $f\bar{f}$ signal being defined by the cut $\sqrt{s'/s} > 0.85$. ISR-FSR photon interference is subtracted to render the propagator mass unambiguous.

- **Definition 2:** For dilepton events, $\sqrt{s'}$ is taken to be the bare invariant mass of the outgoing difermion pair. For hadronic events, it is taken to be the mass of the s-channel propagator. In both cases, ISR-FSR photon interference is included and the signal is defined by the cut $\sqrt{s'/s} > 0.85$. When calculating the contribution to the hadronic cross section due to ISR-FSR interference, since the propagator mass is ill-defined, it is replaced by the bare $q\bar{q}$ mass.

Events containing additional fermion pairs from radiative processes are considered to be signal, providing that the primary pair passes the cut on $\sqrt{s'/s}$ and that the secondary pair has a mass below 70 GeV/c^2.

Year	Nominal Energy GeV	Actual Energy GeV	Luminosity pb^{-1}
1995	130	130.2	~ 3
	136	136.2	~ 3
	133*	133.2	~ 6
1996	161	161.3	~ 10
	172	172.1	~ 10
	167*	166.6	~ 20
1997	130	130.2	~ 2
	136	136.2	~ 2
	183	182.7	~ 50
1998	189	188.6	~ 170
1999	192	191.6	~ 30
	196	195.5	~ 80
	200	199.5	~ 80
	202	201.6	~ 40
2000	205	204.9	~ 60
	207	206.7	~ 30
	206*	205.5	~ 90

Table 13: The nominal and actual centre-of-mass energies for data collected during LEP-II operation in each year. The approximate average luminosity analysed per experiment at each energy is also shown. Values marked with a * are average energies for 1995, 1996 and 2000 used for heavy flavour results. The data taken at nominal energies of 130 and 136 in 1995 and 1997 are combined by most experiments.

The data are split into 3 sets: data taken at energies from 130–189 GeV, data taken during 1999, and data taken in 2000. Averages are performed separately for each of these data sets. Within each subset correlations between experiments and energies and channels are considered.

Tables 14 and 15 show the preliminary combined results for the 1995–1999 data corresponding to the signal definition 1 and the difference in the results if definition 2 is used. The results for the averages of the 130–189 GeV data are identical to those given in [72]. Results for the more preliminary data taken during 2000 are not given in numerical form but are shown in Figure 3 which show the LEP averaged cross sections and asymmetries (based on definition 1), respectively, as a function of the centre-of-mass energy, together with the SM predictions.

The χ^2 per degree of freedom for the average of the 1999 data is 52.5/60. The correlations are rather small, with the largest components at any given pair of energies being between the hadronic cross sections.

There is good agreement between the SM expectations and the measurements of the individual experiments and the combined averages. The cross sections for hadronic final states at most of the energy points are somewhat above the SM expectations. Taking into account the correlations between the data points and also assigning a theory error of $\pm 0.2\%$ [73] to the SM predictions, the difference of the cross section from the SM expectations averaged over all energies is approximately a 2.5 standard deviation excess. It is concluded that there is no significant evidence in the results of the combinations for physics beyond the SM in the process $e^+e^- \to f\bar{f}$.

$\sqrt{s}$ (GeV)	Quantity	Value	SM	Δ
130	$\sigma(q\overline{q})$ [pb]	81.938±2.220	82.803	-0.251
	$\sigma(\mu^+\mu^-)$ [pb]	8.592±0.682	8.439	-0.331
	$\sigma(\tau^+\tau^-)$ [pb]	9.082±0.931	8.435	-0.108
	$A_{fb}(\mu^+\mu^-)$	0.692±0.060	0.705	0.012
	$A_{fb}(\tau^+\tau^-)$	0.663±0.076	0.704	0.012
136	$\sigma(q\overline{q})$ [pb]	66.570±1.967	66.596	-0.224
	$\sigma(\mu^+\mu^-)$ [pb]	8.231±0.678	7.281	-0.280
	$\sigma(\tau^+\tau^-)$ [pb]	7.123±0.821	7.279	-0.091
	$A_{fb}(\mu^+\mu^-)$	0.704±0.060	0.684	0.013
	$A_{fb}(\tau^+\tau^-)$	0.752±0.088	0.683	0.014

Table 14: Preliminary combined LEP results for $e^+e^- \to f\overline{f}$ for centre-of-mass energies below the W–pair production threshold. All the results correspond to the signal definition 1. The Standard Model predictions are from ZFITTER v6.10 [74]. The difference, Δ, in the averages for the measurements for definition 2 relative to definition 1 are also indicated. The quoted uncertainties do not include the theoretical uncertainties on the corrections discussed in [70]

7.2 Differential cross sections

The LEP experiments have measured the differential cross section, $\frac{d\sigma}{d\cos\theta}$, for the $e^+e^- \to \mu^+\mu^-$ and $e^+e^- \to \tau^+\tau^-$ channels. This section discusses a procedure to combine these measurements and presents preliminary results.

Using a Monte Carlo simulation it is found that a χ^2 fit to the measured differential cross sections, using the expected error on the differential cross sections, computed from the expected cross sections and the expected numbers of events in each experiment, provided a very good approximation to the exact likelihood method based on Poisson statistics. Further details are given in [70].

Data are binned in 10 bins of $\cos\theta$. The scattering angle, θ, is the angle of the negative lepton with respect to the incoming electron direction in the lab coordinate system. The outer acceptances of the most forward and most backward bins for which the four experiments have presented their data are different. This is accounted for as a correction to a common signal definition. The signal definition used corresponds to definition 1 of Section 7.1.

Correlated small systematic errors between different experiments, channels and energies, arising from uncertainties on the overall normalisation are considered.

The data are subdivided into two energy ranges, 183 and 189 GeV and 192–202 GeV, and averages are made for each energy point within each of these subsets. The results of the averages are shown in Figures 4 and 5.

The correlations between bins in the average are less that 2% of the total error on the averages in each bin. The overall agreement between the averaged data and the predictions is good, with a χ^2 of 114 for 120 degrees of freedom. At 202 GeV the cross section in the most backward bin, $-1.00 < \cos\theta < -0.8$, for both muon and tau final states is above the predictions. For the muons the excess in data corresponds to 3.3 standard deviations. For the taus the excess is 2.3 standard deviations, however, for this measurement the individual experiments are somewhat inconsistent, having a chi-squared with respect to the average of 10.5 for 2 degrees of freedom.

$\sqrt{s}$ (GeV)	Quantity	Value	SM	Δ
161	$\sigma(q\overline{q})$ [pb]	36.909±1.071	35.247	-0.143
	$\sigma(\mu^+\mu^-)$ [pb]	4.586±0.364	4.613	-0.178
	$\sigma(\tau^+\tau^-)$ [pb]	5.692±0.545	4.613	-0.061
	$A_{fb}(\mu^+\mu^-)$	0.535±0.067	0.609	0.017
	$A_{fb}(\tau^+\tau^-)$	0.646±0.077	0.609	0.016
172	$\sigma(q\overline{q})$ [pb]	29.172±0.987	28.738	-0.124
	$\sigma(\mu^+\mu^-)$ [pb]	3.556±0.317	3.952	-0.157
	$\sigma(\tau^+\tau^-)$ [pb]	4.026±0.450	3.951	-0.054
	$A_{fb}(\mu^+\mu^-)$	0.672±0.077	0.591	0.018
	$A_{fb}(\tau^+\tau^-)$	0.342±0.094	0.591	0.017
183	$\sigma(q\overline{q})$ [pb]	24.567±0.421	24.200	-0.109
	$\sigma(\mu^+\mu^-)$ [pb]	3.484±0.147	3.446	-0.139
	$\sigma(\tau^+\tau^-)$ [pb]	3.398±0.174	3.446	-0.050
	$A_{fb}(\mu^+\mu^-)$	0.558±0.035	0.576	0.018
	$A_{fb}(\tau^+\tau^-)$	0.608±0.045	0.576	0.018
189	$\sigma(q\overline{q})$ [pb]	22.420±0.248	22.156	-0.101
	$\sigma(\mu^+\mu^-)$ [pb]	3.109±0.077	3.207	-0.131
	$\sigma(\tau^+\tau^-)$ [pb]	3.140±0.100	3.207	-0.048
	$A_{fb}(\mu^+\mu^-)$	0.565±0.021	0.569	0.019
	$A_{fb}(\tau^+\tau^-)$	0.584±0.028	0.569	0.018
192	$\sigma(q\overline{q})$ [pb]	22.292±0.514	21.237	–0.098
	$\sigma(\mu^+\mu^-)$ [pb]	2.941±0.175	3.097	–0.127
	$\sigma(\tau^+\tau^-)$ [pb]	2.863±0.216	3.097	–0.047
	$A_{FB}(\mu^+\mu^-)$	0.540±0.052	0.566	0.019
	$A_{FB}(\tau^+\tau^-)$	0.610±0.071	0.566	0.019
196	$\sigma(q\overline{q})$ [pb]	20.730±0.330	20.127	–0.094
	$\sigma(\mu^+\mu^-)$ [pb]	2.965±0.106	2.962	–0.123
	$\sigma(\tau^+\tau^-)$ [pb]	3.015±0.139	2.962	–0.045
	$A_{FB}(\mu^+\mu^-)$	0.579±0.031	0.562	0.019
	$A_{FB}(\tau^+\tau^-)$	0.489±0.045	0.562	0.019
200	$\sigma(q\overline{q})$ [pb]	19.376±0.306	19.085	–0.090
	$\sigma(\mu^+\mu^-)$ [pb]	3.038±0.104	2.834	–0.118
	$\sigma(\tau^+\tau^-)$ [pb]	2.995±0.135	2.833	–0.044
	$A_{FB}(\mu^+\mu^-)$	0.518±0.031	0.558	0.019
	$A_{FB}(\tau^+\tau^-)$	0.546±0.043	0.558	0.019
202	$\sigma(q\overline{q})$ [pb]	19.291±0.425	18.572	–0.088
	$\sigma(\mu^+\mu^-)$ [pb]	2.621±0.139	2.770	–0.116
	$\sigma(\tau^+\tau^-)$ [pb]	2.806±0.183	2.769	–0.043
	$A_{FB}(\mu^+\mu^-)$	0.543±0.048	0.556	0.020
	$A_{FB}(\tau^+\tau^-)$	0.580±0.060	0.556	0.019

Table 15: Preliminary combined LEP results for $e^+e^- \to f\overline{f}$ for centre-of-mass energies above the W–pair production threshold. All the results correspond to the signal definition 1. The Standard Model predictions are from ZFITTER v6.10 [74]. The difference, Δ, in the averages for the measurements for definition 2 relative to definition 1 are also indicated. The quoted uncertainties do not include the theoretical uncertainties on the corrections discussed in [70]

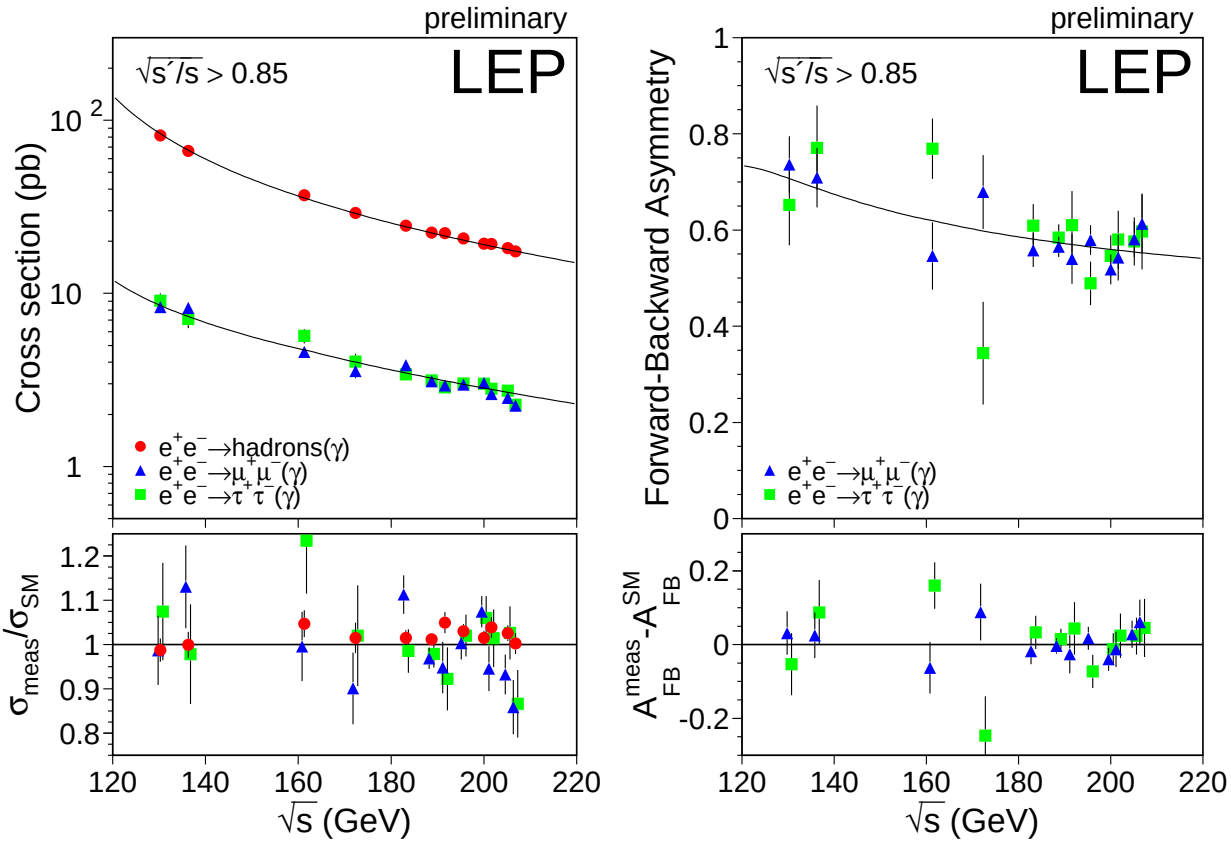

Figure 3: Preliminary combined LEP results on the cross sections for $q\bar{q}$, $\mu^+\mu^-$ and $\tau^+\tau^-$ final states, and forward-backward asymmetries for $\mu^+\mu^-$ and $\tau^+\tau^-$ final states as a function of centre-of-mass energy. The values at 130–189 GeV are taken from [72]. The prediction of the Standard Model, computed with ZFITTER [74], are shown as curves. The lower plots shows the ratio of the data divided by the predictions for the cross sections, and the difference between the measurements and the predictions for the asymmetries. For better visibility, the $\mu^+\mu^-$ and $\tau^+\tau^-$ data points are slightly shifted apart from their nominal centre-of-mass value.

7.3 Heavy Flavour Measurements

A combination of measurements of the ratios[3], R_b and R_c and the forward-backward asymmetries, $A_{FB}^{b\bar{b}}$ and $A_{FB}^{c\bar{c}}$, from the LEP collaborations at centre-of-mass energies in the range of 130 to 209 GeV is performed.

A common signal definition is defined for all the measurements, requiring:

- an effective centre-of-mass energy $\sqrt{s'} > 0.85\sqrt{s}$
- the inclusion of ISR and FSR photon interference contribution and
- extrapolation to full angular acceptance.

Systematic errors are divided into three categories: uncorrelated errors, errors correlated between the measurements of each experiment, and errors common to all experiments.

[3]Unlike at LEP-I, R_q is defined as $\frac{\sigma_{q\bar{q}}}{\sigma_{had}}$.

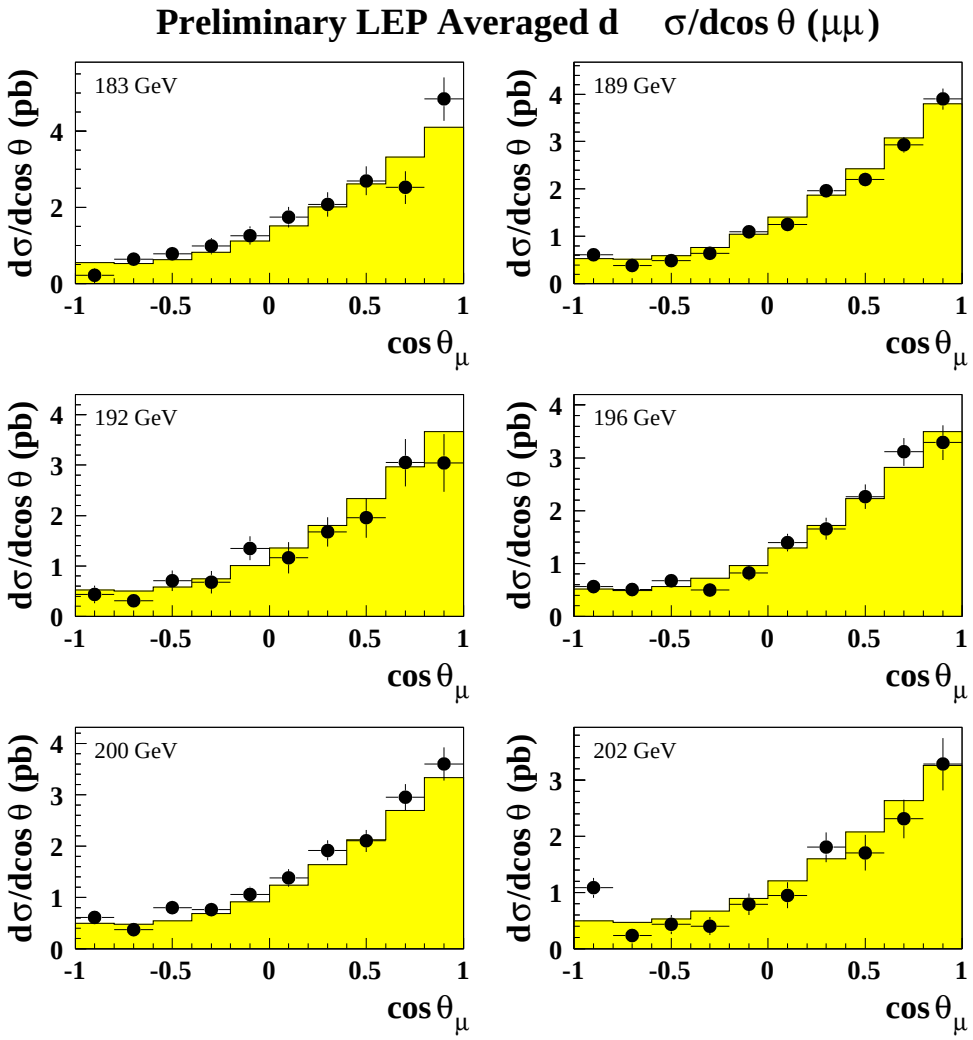

Figure 4: LEP averaged differential cross sections for $e^+e^- \to \mu^+\mu^-$ at energies of 183-202 GeV. The Standard Model Predictions shown as solid histograms are computed with ZFITTER [74]

The results of the combination are presented in Table 16 and Figure 6. Because of the large correlation (-0.36) with R_c at 183 GeV and 189 GeV, the errors on the corresponding measurements of R_b receive an additional contribution which is absent at the other energy points. For other energies where there is no measurement of R_c, the Standard Model value of R_c is used in extracting R_b. The error that this introduces on R_b is assumed to be negligible. The results are consistent with the Standard Model predictions of ZFITTER.

7.4 Interpretation

The combined cross sections, asymmetries and results on heavy flavour production are interpreted in a variety of models. The cross section and asymmetry results are used to place limits on the mass of a possible additional heavy neutral boson, Z′. Limits on contact interactions between leptons and on contact interaction between electrons and b and c quarks are obtained. Heavy flavour results are also used within the S-Matrix formalism to give information on the γ-Z interference for heavy quarks.

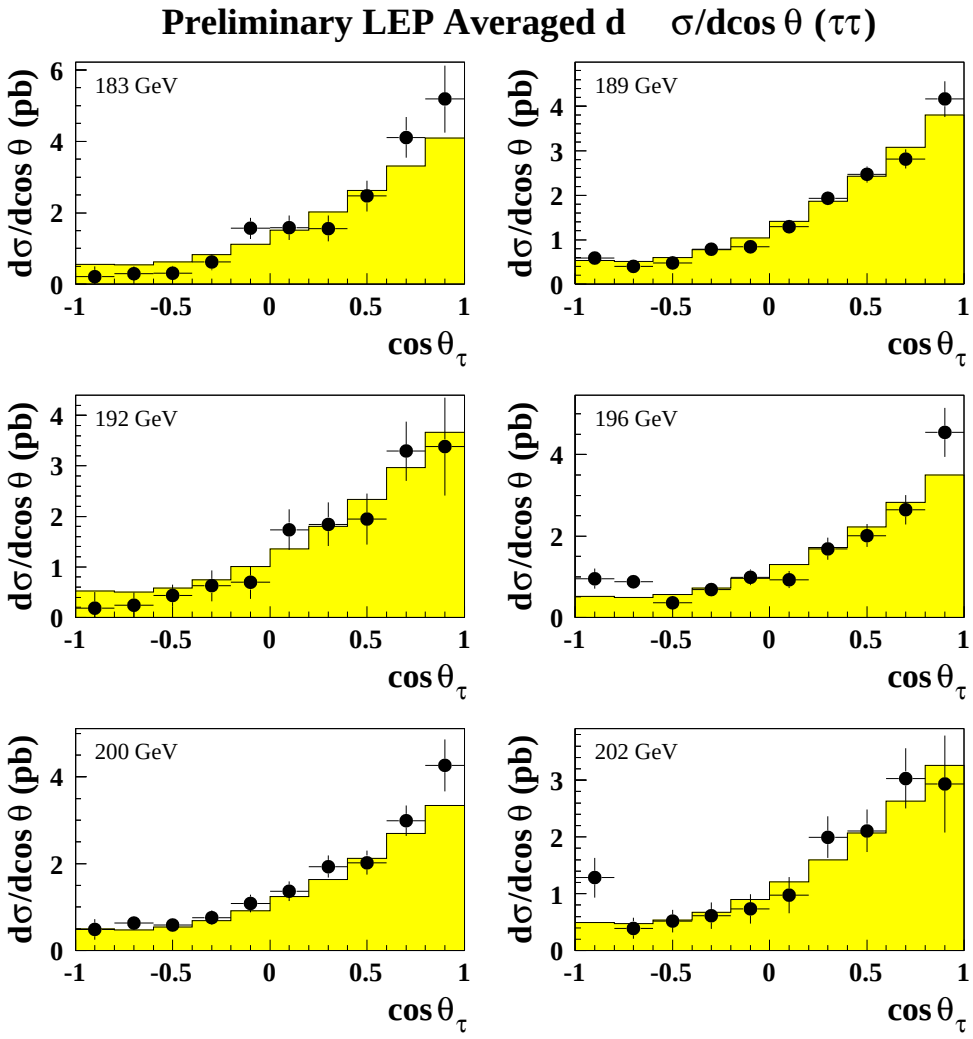

Figure 5: LEP averaged differential cross sections for $e^+e^- \to \tau^+\tau^-$ at energies of 183-202 GeV. The Standard Model Predictions shown as solid histograms are computed with ZFITTER [74]

7.5 Models with Z′ Bosons

The combined hadronic and leptonic cross sections and the leptonic forward-backward asymmetries are used to fit the data to models including an additional heavy neutral boson, Z′ within a variety of models [77].

Fits are made to the mass of a Z′, $M_{Z'}$, for 4 different models referred to as χ, ψ, η and L-R and for the Sequential Standard Model [78], which proposes the existence of a Z′ with exactly the same coupling to fermions as the standard Z. LEP-II data alone does not significantly constrain the mixing angle between the Z and Z′ fields, $\Theta_{ZZ'}$. However results from a single experiment where LEP-I data is used in the fit show that the mixing is consistent with zero (see for example [79]). So for these fits $\Theta_{ZZ'}$ is fixed to zero.

No evidence is found for the existence of a Z′ boson in any of the models. 95% confidence level lower limits on $M_{Z'}$ are obtained, by integrating the likelihood function[4]. The lower limits on the Z′

[4]To be able to obtain confidence limits from the likelihood function it is necessary to convert the likelihood to a

$\sqrt{s}$ (GeV)	R_b	R_c	A_{FB}^{bb}	$A_{FB}^{c\bar{c}}$
133	0.1809 ±0.0133	-	0.357 ±0.251	0.580 ±0.314
	(0.1853)	-	(0.487)	(0.681)
167	0.1479 ±0.0127	-	0.618 ±0.254	0.921 ±0.344
	(0.1708)	-	(0.561)	(0.671)
183	0.1616 ±0.0101	0.270 ±0.043	0.527 ±0.155	0.662 ±0.209
	(0.1671)	(0.250)	(0.578)	(0.656)
189	0.1559 ±0.0066	0.241 ±0.024	0.500 ±0.096	0.462 ±0.197
	(0.1660)	(0.252)	(0.583)	(0.649)
192	0.1688 ±0.0187	-	0.371 ±0.302	-
	(0.1655)	-	(0.585)	-
196	0.1577 ±0.0109	-	0.721 ±0.194	-
	(0.1648)	-	(0.587)	-
200	0.1621 ±0.0111	-	0.741 ±0.206	-
	(0.1642)	-	(0.590)	-
202	0.1873 ±0.0177	-	0.591 ±0.284	-
	(0.1638)	-	(0.591)	-
206	0.1696 ±0.0182	-	0.881 ±0.221	-
	(0.1633)	-	(0.593)	-

Table 16: Results of the global fit, compared to the Standard Model predictions for the signal definition, computed with ZFITTER [75] in parentheses. Quoted errors represent the statistical and systematic errors added in quadrature.

mass are shown in Table 17.

Model	χ	ψ	η	L-R	SSM
$M_{Z'}^{limit}$ (GeV/c^2)	630	510	400	950	2260

Table 17: 95% confidence level lower limits on the Z′ mass and χ, ψ, η, L-R and SSM models.

7.6 Contact Interactions between Leptons

Following reference [80], contact interactions are parameterised by an effective Lagrangian, $\mathcal{L}_{\rm eff}$, which is added to the Standard Model Lagrangian and has the form:

$$\mathcal{L}_{\rm eff} = \frac{g^2}{(1+\delta)\Lambda^2} \sum_{i,j=L,R} \eta_{ij} \overline{e}_i \gamma_\mu e_i \overline{f}_j \gamma^\mu f_j,$$

where $g^2/4\pi$ is taken to be 1 by convention, $\delta = 1(0)$ for $f = e$ ($f \neq e$), $\eta_{ij} = \pm 1$ or 0, Λ is the scale of the contact interactions, e_i and f_j are left or right-handed spinors. By assuming different helicity coupling between the initial state and final state currents, a set of different models can be defined from this Lagrangian [81], with either constructive (+) or destructive (−) interference between the Standard Model process and the contact interactions. The models and corresponding choices of η_{ij}

probability density function; this is done in a Bayesian approach by multiplying by a prior probability function. Simply integrating the likelihood is equivalent to multiplying by a uniform prior probability function.

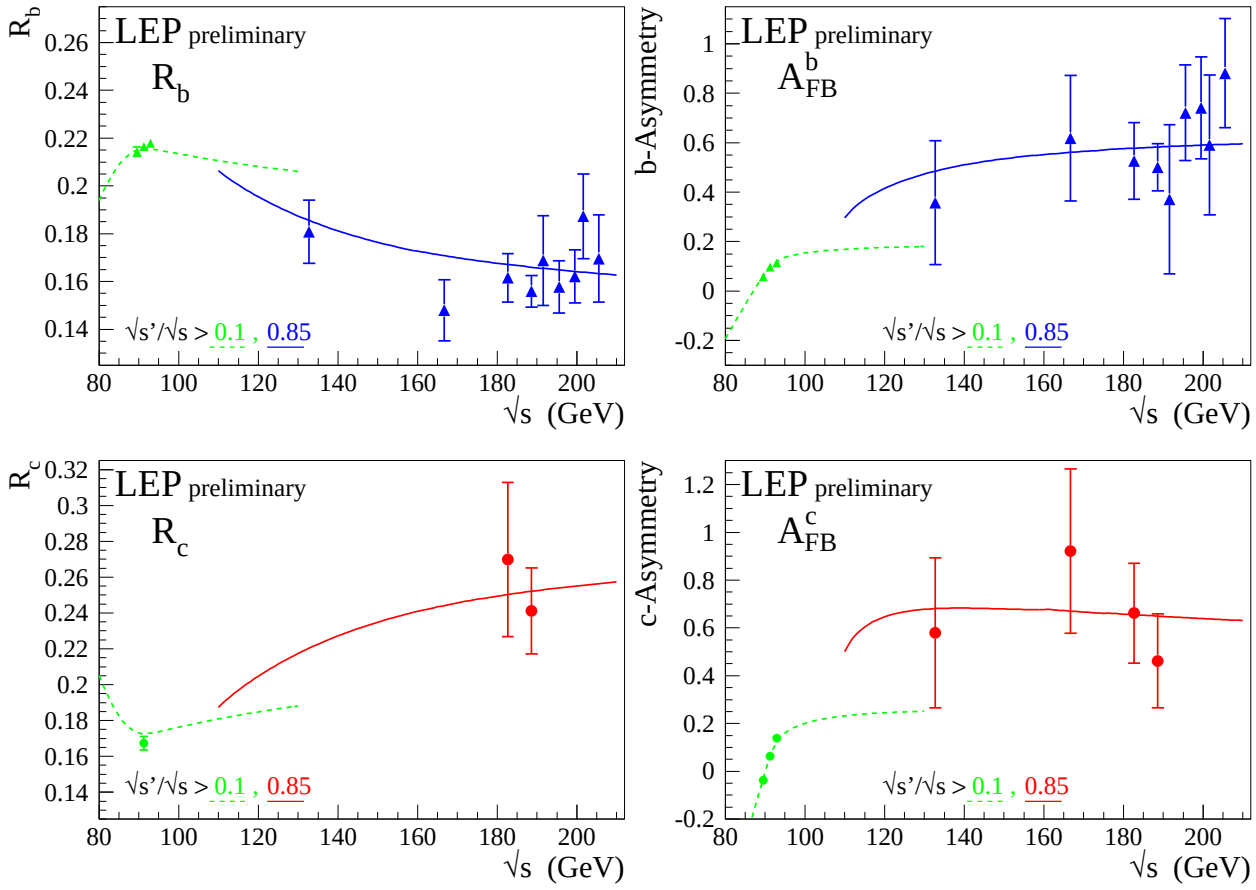

Figure 6: Preliminary combined LEP measurements of R_b, R_c and $A_{FB}^{b\bar{b}}$ and $A_{FB}^{c\bar{c}}$. Solid lines represent the Standard Model prediction for the signal definition and dotted lines the inclusive prediction. The theoretical predictions are computed with ZFITTER [75]. The LEP-I measurements are taken from [1, 76].

are given in Table 18. The models LL, RR, VV, AA, LR, RL, V0, A0 are considered here since these models lead to large deviations in the $e^+e^- \to \mu^+\mu^-$ and $e^+e^- \to \tau^+\tau^-$ channels. The total hadronic cross section on its own is not particularly sensitive to contact interactions involving quarks. For the purpose of fitting contact interaction models to the data, a new parameter $\epsilon = 1/\Lambda^2$ is defined; $\epsilon = 0$ in the limit that there are no contact interactions. This parameter is allowed to take both positive and negative values in the fits.

The averaged measurements of the cross sections and forward-backward asymmetries for $e^+e^- \to \mu^+\mu^-$ and $e^+e^- \to \tau^+\tau^-$ from all energies from 130 to 207 GeV are used. Theoretical uncertainties on the SM predictions of $\pm 0.5\%$ [82] on the cross sections and ± 0.005 on the forward-backward asymmetries, fully correlated between all energies, are assumed.

The values of ϵ extracted for each model are all compatible with the Standard Model expectation $\epsilon = 0$, at the two standard deviation level. These errors on ϵ are typically a factor of two smaller than those obtained from a single LEP experiment with the same data set. The fitted values of ϵ are converted into 95% confidence level lower limits on Λ. The limits are obtained by integrating the likelihood function over the physically allowed values, $\epsilon \geq 0$ for each Λ^+ limit and $\epsilon \leq 0$ for Λ^- limits. The fitted values of ϵ and the extracted limits are shown in Table 19. Figure 7 shows the limits obtained on the scale Λ for the different models assuming universality between contact interactions

Model	η_{LL}	η_{RR}	η_{LR}	η_{RL}
$LL^{\pm}$	±1	0	0	0
$RR^{\pm}$	0	±1	0	0
$VV^{\pm}$	±1	±1	±1	±1
$AA^{\pm}$	±1	±1	∓1	∓1
$LR^{\pm}$	0	0	±1	0
$RL^{\pm}$	0	0	0	±1
$V0^{\pm}$	±1	±1	0	0
$A0^{\pm}$	0	0	±1	±1

Table 18: Choices of η_{ij} for different contact interaction models

.

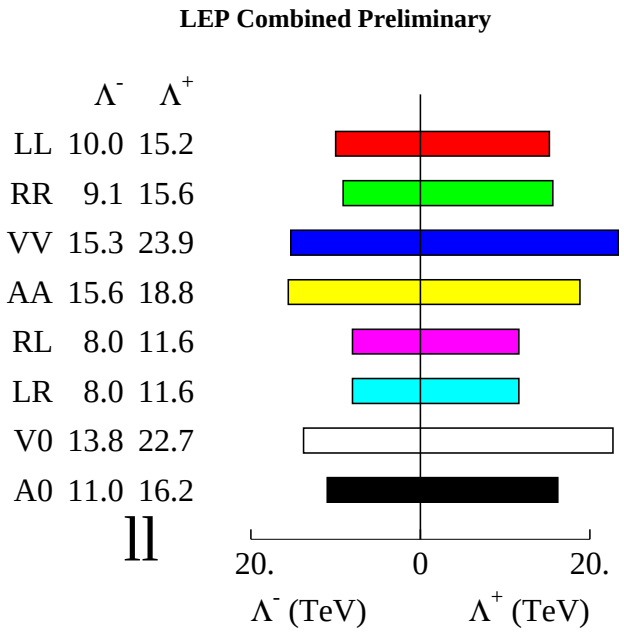

Figure 7: The limits on Λ for $e^+e^- \to \ell^+\ell^-$ assuming universality in the contact interactions between $e^+e^- \to \mu^+\mu^-$ and $e^+e^- \to \tau^+\tau^-$.

for $e^+e^- \to \mu^+\mu^-$ and $e^+e^- \to \tau^+\tau^-$.

7.7 Contact Interactions from Heavy Flavour Averages

Limits on contact interactions between electrons and b and c quarks are obtained. These results are of particular interest since they are inaccessible to $p\bar{p}$ or ep colliders. The formalism for describing contact interactions including heavy flavours is identical to that described above for leptons.

All heavy flavour LEP-II combined results from 133 to 205 GeV listed in Table 16 are used as inputs. For the purpose of fitting contact interaction models to the data, R_b and R_c are converted to cross sections $\sigma_{b\overline{b}}$ and $\sigma_{c\overline{c}}$ using the averaged $q\overline{q}$ cross section of section 7.1 corresponding to signal

$e^+e^- \to \mu^+\mu^-$			
Model	ϵ (TeV^{-2})	Λ^-(TeV)	Λ^+(TeV)
LL	$-0.0066^{+0.0039}_{-0.0042}$	8.2	14.3
RR	$-0.0069^{+0.0045}_{-0.0054}$	8.0	13.4
VV	$-0.0023^{+0.0017}_{-0.0018}$	13.7	21.6
AA	$-0.0033^{+0.0032}_{-0.0012}$	13.1	19.2
RL	$-0.0052^{+0.0067}_{-0.0074}$	7.2	10.1
LR	$-0.0052^{+0.0067}_{-0.0074}$	7.2	10.1
V0	$-0.0036^{+0.0024}_{-0.0022}$	11.9	20.6
A0	$-0.0027^{+0.0035}_{-0.0033}$	10.8	14.4

$e^+e^- \to \tau^+\tau^-$			
Model	ϵ (TeV^{-2})	Λ^-(TeV)	Λ^+(TeV)
LL	$-0.0005^{+0.0057}_{-0.0055}$	9.5	9.8
RR	$-0.0005^{+0.0060}_{-0.0063}$	8.7	9.5
VV	$-0.0008^{+0.0023}_{-0.0036}$	14.4	16.1
AA	$-0.0008^{+0.0033}_{-0.0016}$	13.4	12.2
RL	$-0.0052^{+0.0093}_{-0.0102}$	6.5	8.8
LR	$-0.0052^{+0.0093}_{-0.0102}$	6.5	8.8
V0	$-0.0003^{+0.0029}_{-0.0029}$	12.9	13.7
A0	$-0.0026^{+0.0049}_{-0.0050}$	9.5	12.4

$e^+e^- \to l^+l^-$			
Model	ϵ (TeV^{-2})	Λ^-(TeV)	Λ^+(TeV)
LL	$-0.0046^{+0.0038}_{-0.0036}$	10.0	15.2
RR	$-0.0046^{+0.0038}_{-0.0044}$	9.1	15.6
VV	$-0.0019^{+0.0024}_{-0.0012}$	15.3	23.9
AA	$-0.0013^{+0.0018}_{-0.0015}$	15.6	18.8
RL	$-0.0052^{+0.0054}_{-0.0060}$	8.0	11.6
LR	$-0.0052^{+0.0054}_{-0.0060}$	8.0	11.6
V0	$-0.0023^{+0.0018}_{-0.0020}$	13.8	22.7
A0	$-0.0027^{+0.0028}_{-0.0028}$	11.0	16.2

Table 19: Fitted values of ϵ and 95% confidence limits on the scale, Λ, for constructive (+) and destructive interference (−) with the Standard Model, for the contact interaction models discussed in the text. Results are given for $e^+e^- \to \mu^+\mu^-$, $e^+e^- \to \tau^+\tau^-$ and $e^+e^- \to \ell^+\ell^-$, assuming universality in the contact interactions between $e^+e^- \to \mu^+\mu^-$ and $e^+e^- \to \tau^+\tau^-$.

definition 2. In the calculation of errors, the correlations between R_b, R_c and $\sigma_{q\overline{q}}$ are assumed to be negligible.

The fitted values of $\epsilon = \frac{1}{\Lambda^2}$ and their 68% confidence level uncertainties together with the 95% confidence level lower limits on Λ are shown in Table 20. Figure 8 shows the limits obtained on the scale, Λ, of models with different helicity combinations involved in the interactions.

$e^+e^- \to b\bar{b}$			
Model	ϵ (TeV^{-2})	Λ^- (TeV)	Λ^+ (TeV)
LL	$-0.0025^{+0.0049}_{-0.0052}$	9.1	11.1
RR	$-0.1890^{+0.1290}_{-0.0151}$	2.2	7.2
VV	$-0.0020^{+0.0041}_{-0.0043}$	10.0	12.4
AA	$-0.0018^{+0.0032}_{-0.0034}$	11.2	14.0
RL	$0.0190^{+0.1299}_{-0.0201}$	7.3	2.4
LR	$-0.0428^{+0.0408}_{-0.0367}$	3.2	5.7
V0	$-0.0018^{+0.0035}_{-0.0037}$	10.8	12.9
A0	$0.0266^{+0.0234}_{-0.0255}$	6.4	4.1

$e^+e^- \to c\bar{c}$			
Model	ϵ (TeV^{-2})	Λ^- (TeV)	Λ^+ (TeV)
LL	$0.0127^{+0.5957}_{-0.0264}$	5.2	1.6
RR	$0.0466^{+0.3781}_{-0.0576}$	4.5	1.5
VV	$-0.0008^{+0.0109}_{-0.0103}$	7.3	6.6
AA	$0.0046^{+0.0168}_{-0.0151}$	6.4	5.1
RL	$0.0127^{+0.0845}_{-0.0845}$	2.8	2.6
LR	$0.0874^{+0.1049}_{-0.1127}$	3.5	2.1
V0	$0.0036^{+0.0181}_{-0.0135}$	6.7	1.4
A0	$0.0499^{+0.0691}_{-0.0691}$	3.9	2.6

Table 20: Fitted values of ϵ and 95% confidence limits on the scale, Λ, for constructive (+) and destructive interference (−) with the Standard Model, for the contact interaction models discussed in the text. From combined $b\bar{b}$ and $c\bar{c}$ results with centre-of-mass energies from 133 to 205 GeV.

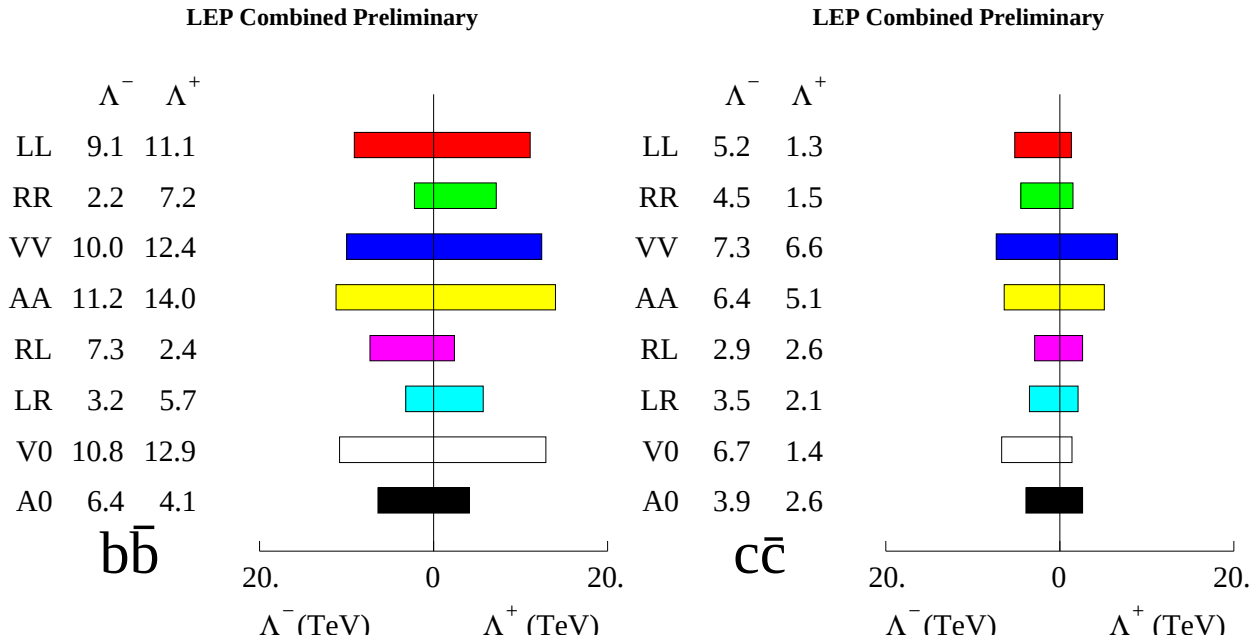

Figure 8: 95% CL limits on the scale of contact interactions in $e^+e^- \to b\bar{b}$ and $e^+e^- \to c\bar{c}$ using Heavy Flavour LEP combined results from 133 to 205 GeV.

7.8 S-Matrix Parameters for Heavy Flavour Production

The S-Matrix formalism [83] parameterises the cross sections and forward-backward asymmetries for two-fermion production in terms of the exchange of a massless (γ) and a massive vector boson (Z):

$$\sigma_{\rm tot}^{0,f}(s) = \frac{4}{3}\pi\alpha^2 + \left[\frac{g_f^{\rm tot}}{s} + \frac{j_f^{\rm tot}(s-\overline{m}_{\rm Z}^2) + r_f^{\rm tot}s}{(s-\overline{m}_{\rm Z}^2)^2 + \overline{m}_{\rm Z}^2\overline{\Gamma}_{\rm Z}^2}\right]$$

$$\sigma_{\rm fb}^{0,f}(s) = \frac{4}{3}\pi\alpha^2 + \left[\frac{g_f^{\rm fb}}{s} + \frac{j_f^{\rm fb}(s-\overline{m}_{\rm Z}^2) + r_f^{\rm fb}s}{(s-\overline{m}_{\rm Z}^2)^2 + \overline{m}_{\rm Z}^2\overline{\Gamma}_{\rm Z}^2}\right]$$

$$A_{\rm fb}^{0,f}(s) = \frac{3}{4}\frac{\sigma_{\rm fb}^{0,f}(s)}{\sigma_{\rm tot}^{0,f}(s)}$$

The mass, $\overline{m}_{\rm Z}$, and width, $\overline{\Gamma}_{\rm Z}$, used in the S-Matrix fits are slightly different from the usual mass $m_{\rm Z}$, and width $\Gamma_{\rm Z}$ which are defined using an s-dependent width term in the Breit-Wigner resonance of the Z:

$$\begin{aligned}\overline{m}_{\rm Z} &\sim m_{\rm Z} - 34.1{\rm Mev}\\ \overline{\Gamma}_{\rm Z} &\sim \Gamma_{\rm Z} - 0.9{\rm Mev}\end{aligned}$$

The parameters g, r and j parameterise the cross sections and forward-backward asymmetries arising from the exchange of the γ (g) and the Z (r) and the interference of the two (j). Values for these parameters can be obtained for each fermion species and also for a combination of all $\rm q\overline{q}$ final states, f = had. Values of the g, r and j parameters and $\overline{\Gamma}_{\rm Z}$ are computed in the Standard Model for comparison with the results of the fits.

S-Matrix fits have already been performed using the hadronic and leptonic cross section and leptonic forward-backward asymmetry data from LEP-I and LEP-II for energies up to 172 GeV [71], providing constraints on $r_{\rm had}^{\rm tot}$ and $j_{\rm had}^{\rm tot}$, the parameters describing charged lepton production and $\overline{m}_{\rm Z}$ and $\overline{\Gamma}_{\rm Z}$. The results of these existing fits and the full error matrix are used to constrain these parameters in the fit performed here.

LEP-I and SLD heavy flavour averages [84], $R_{\rm b}$, $R_{\rm c}$, $A_{\rm FB}^{\rm b\bar{b}}$ and $A_{\rm FB}^{\rm c\bar{c}}$ are used to constrain the S-Matrix parameters $r_{\rm b,c}^{\rm tot}$ and $r_{\rm b,c}^{\rm fb}$ that describe the heavy quark couplings to the Z. By including the combined LEP-II heavy flavour measurements from 133 to 205 GeV listed in Table 16 values of the parameters $j_{\rm b,c}^{\rm tot}$ and $j_{\rm b,c}^{\rm fb}$ that describe γ-Z interference in heavy quark production are obtained. Contours for these parameters are given at the end of this section.

The LEP-II average values of $R_{\rm b}$ and $R_{\rm c}$ from Section 7.3 for centre-of-mass energies from 130 up to 166 GeV are used directly in the fit. These are largely uncorrelated with the measured total cross sections, therefore, the correlations between the existing S-Matrix fits parameters and these measurements are neglected. The measurements are fitted using the ratio of the predicted b and c cross sections and the total hadronic cross section.

For energies of 183 GeV and above, the flavour tagged measurements are more precise than those from 133–166 GeV. The uncertainties on $j_{\rm had}^{\rm tot}$ from the existing fits introduces a sizeable uncertainty on the prediction of $R_{\rm b}$ and $R_{\rm c}$. For these energies the measurements of $R_{\rm b}$ and $R_{\rm c}$ are first converted into cross sections for $\rm b\overline{b}$ and $\rm c\overline{c}$ production by multiplying by the the total hadronic cross sections

from section 7.1. The full error matrix of the quantities and the correlations with the lower energy R_b and R_c values are computed. Correlations between the existing S-Matrix fit results and the total hadronic cross sections from 183 GeV and above are neglected. For this reason the highest energy hadronic cross sections are not used to improve the fits to the inclusive hadronic S-Matrix parameters.

The forward-backward asymmetries for b and c quark production are fitted directly to predictions of the asymmetries at all energies.

Predictions of the S-Matrix formalism are made using the SMATASY [85] program. The couplings to the photon are fixed to the expectation from the Standard Model.

In summary, the following parameters are obtained from the fit:

- The mass and total width of the Z boson, the S-Matrix parameters $r_{\mathrm{had}}^{\mathrm{tot}}$ and $j_{\mathrm{had}}^{\mathrm{tot}}$ for the total hadronic cross section, and the parameters $r_{\mathrm{l}}^{\mathrm{tot}}$, $j_{\mathrm{l}}^{\mathrm{tot}}$, $r_{\mathrm{l}}^{\mathrm{fb}}$, and $j_{\mathrm{l}}^{\mathrm{fb}}$ for leptons[5].
- The S-Matrix parameters $r_{\mathrm{b,c}}^{\mathrm{tot}}$ and $r_{\mathrm{b,c}}^{\mathrm{fb}}$ that describe the total $\mathrm{b\overline{b}}$ and $\mathrm{c\overline{c}}$ cross sections and asymmetries due to Z boson exchange.
- The four parameters $j_{\mathrm{b,c}}^{\mathrm{tot}}$ and $j_{\mathrm{b,c}}^{\mathrm{fb}}$ that describe the the effect of γ-Z interference on the energy dependence of the bottom and charm cross sections and asymmetries.

The following data are used:

- The results of the existing S-Matrix fits [71], derived from LEP-I data and including total hadronic cross sections up to 172 GeV.
- LEP-I and SLD heavy flavour averages [84].
- LEP-II heavy flavour averages R_b and R_c for energies up to and including 172 GeV from Table 16.
- Values of the flavour tagged b and c cross sections σ_b and σ_c derived from measurements of R_b and R_c and the total hadronic cross section for energies of 183 GeV and above, from section 7.1 and Table 16.
- LEP-II heavy flavour averages $A_{\mathrm{FB}}^{\mathrm{b\bar{b}}}$ and $A_{\mathrm{FB}}^{\mathrm{c\bar{c}}}$ for all LEP-II energies from Table 16.

The results for the S-Matrix parameters $j_{\mathrm{b,c}}^{\mathrm{tot}}$ and $j_{\mathrm{b,c}}^{\mathrm{fb}}$ are shown in Figure 9 for both bottom and charm quark production. Good agreement is observed with the Standard Model prediction [85] for γ-Z interference in heavy quark production.

[5] Lepton universality is assumed.

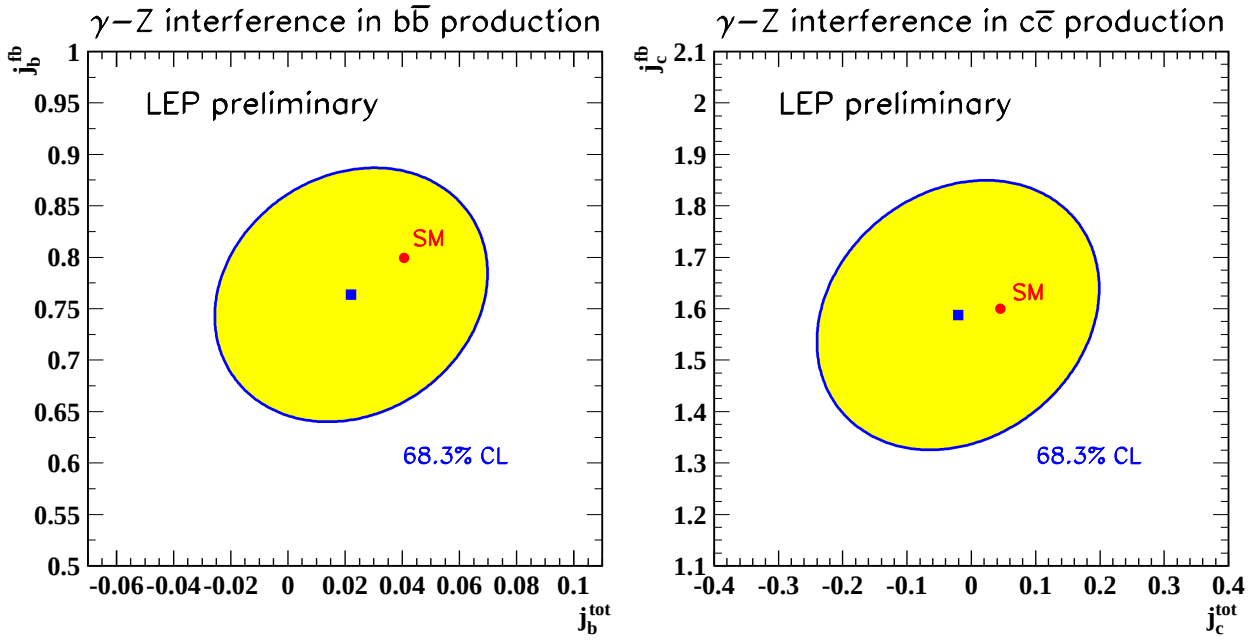

Figure 9: Preliminary combined LEP results on the S-Matrix parameters describing γ-Z interference in $b\bar{b}$ and $c\bar{c}$ production. The expectations of the SM are also shown.

8 Measurement of W Boson Properties at LEP-II

Updates with respect to last summer:
There are new results on the WW cross section and on the W mass. The W decay branching ratios are updated.

In the year 2000 LEP ran at centre-of-mass energies larger than 200 GeV, with a maximum of 209 GeV (see Table 13). The collected data are divided in two ranges of $\sqrt{s}$, below and above 205.5 GeV. The two data sets have mean centre-of-mass energies of 204.9 and 206.7 GeV and the respective integrated luminosities used for the analyses considered in this note are 60 and 30 pb^{-1}. The same centre-of-mass energy binning is also applied for the measurement of the Z–pair cross section. All data recorded from 1996 to 1999 over a range of centre-of-mass energies, $\sqrt{s} = 161 - 202$ GeV are used to extract the W boson mass and width.

8.1 W–pair Production Cross Section

All experiments have published final results on the W–pair (CC03) production cross section for centre-of-mass energies up to 189 GeV [86–89][6]. ALEPH [91], DELPHI [92] and L3 [93] preliminary results at $\sqrt{s} = 192$–202 GeV are unchanged with respect to combination of results prepared for the year 2000 winter conferences. OPAL has updated its preliminary results at $\sqrt{s} = 200$ and 202 GeV [94] to include the full luminosity collected in 1999, whereas the results at $\sqrt{s} = 192$ and 196 GeV [95] are unchanged since the winter conferences. All experiments have contributed preliminary results [94, 96–98] based on the analysis of year 2000 data.

Results from different experiments are combined using the method described in [99] and taking into account, when relevant, the correlations between the systematic uncertainties, which arise mainly from the use of the same Monte Carlo programs to predict background cross sections and to simulate the hadronisation processes.

The results from each experiments for the W–pair production cross section, assuming Standard Model values for the W decay branching ratios, are shown in Table 21, together with the LEP combination. In the averaging procedure the QCD component of the systematic errors [7] from each individual measurement is taken to be fully correlated between experiments. This common error ranges between 0.07 and 0.10 pb. These results supersede the ones presented in [100] for $\sqrt{s} = 189$, 200 and 202 GeV.

Figure 10 shows the total W–pair cross section measured as a function of the LEP centre-of-mass energy. The experimental points are compared with new calculations (RacoonWW [101] and YFSWW3 [102]) based on the double pole approximation (DPA) [103] for $m_{\mathrm{W}} = 80.35$ GeV. These two codes have been extensively compared and agree at a level better than 0.2% at the LEP-II energies. The theoretical uncertainty of the DPA decreases from 0.7% at 170 GeV to a level of 0.4% at centre-of-mass energies larger than 200 GeV[8]. This theoretical uncertainty is represented by the grey band in Figure 10. An error of 50 MeV on the W mass translates into a 0.1% error on the cross section predictions at 200 GeV. The DPA is only valid away from the production threshold, therefore below

[6] In the combination the preliminary results of the L3 collaboration [90] are still used, as the final results only became available shortly before the ICHEP conference.

[7] The QCD component of the systematic error, includes for example uncertainties on the 4–jet rate, on the fragmentation modelling and estimates of possible effects of colour reconnection and Bose-Einstein correlations.

[8] The theoretical uncertainty $\Delta\sigma/\sigma$ on the W–pair production cross section calculated in the DPA can be parametrised as $\Delta\sigma/\sigma = 0.4 \oplus 0.072 \cdot t_1 \cdot t_2$, where $t_1 = (200 - 2m_{\mathrm{W}})/(\sqrt{s} - 2m_{\mathrm{W}})$ and $t_2 = (1 - (\frac{2 \cdot m_{\mathrm{W}}}{200})^2)/(1 - (\frac{2 \cdot m_{\mathrm{W}}}{\sqrt{s}})^2)$ [104].

170 GeV the experimental results are compared with the GENTLE [105] prediction, which is adjusted to reproduce the DPA results at higher energies. All results, up to the highest centre-of-mass energies, are in agreement with the theoretical predictions.

$\sqrt{s}$	Cross section (pb)					χ^2/d.o.f.
(GeV)	ALEPH	DELPHI	L3	OPAL	LEP	
161.33	$4.23 \pm 0.75^*$	$3.67 \pm 0.93^*$	$2.89 \pm 0.77^*$	$3.62 \pm 0.89^*$	3.69 ± 0.45	1.3/3
172.12	$11.7 \pm 1.3^*$	$11.58 \pm 1.4^*$	$12.27 \pm 1.4^*$	$12.3 \pm 1.3^*$	12.0 ± 0.7	0.22/3
182.67	$15.57 \pm 0.68^*$	$15.86 \pm 0.74^*$	$16.53 \pm 0.72^*$	$15.43 \pm 0.66^*$	15.83 ± 0.36	1.49/3
188.63	$15.71 \pm 0.38^*$	$15.83 \pm 0.43^*$	16.20 ± 0.46	$16.30 \pm 0.38^*$	16.00 ± 0.21	1.57/3
191.6	17.23 ± 0.91	16.90 ± 1.02	16.39 ± 0.93	16.60 ± 0.97	16.78 ± 0.48	0.47/3
195.5	17.00 ± 0.57	17.86 ± 0.63	16.67 ± 0.60	18.59 ± 0.74	17.39 ± 0.32	5.26/3
199.5	16.98 ± 0.56	17.35 ± 0.60	16.94 ± 0.62	16.32 ± 0.66	16.93 ± 0.31	1.39/3
201.6	16.16 ± 0.76	17.67 ± 0.84	16.95 ± 0.88	18.48 ± 0.91	17.20 ± 0.43	4.27/3
204.9	16.70 ± 0.64	18.81 ± 0.80	17.70 ± 0.86	15.84 ± 0.71	17.11 ± 0.38	8.79/3
206.7	17.01 ± 0.88	16.50 ± 1.05	17.20 ± 1.03	15.96 ± 0.96	16.68 ± 0.49	1.01/3

Table 21: W–pair production cross sections from the four LEP experiments and combined values for the seven of the recorded centre-of-mass energies. All results are preliminary with the exception of those indicated by *. A common systematic error of (0.07–0.10) pb is taken into account in the averaging procedure. Final results for the combined W–pair production cross section at lower centre-of-mass energies can be found in [1, 71, 106] .

8.2 W Decay Branching Fractions

From the cross sections for the individual W decay channels measured by the four experiments at all energies larger than 161 GeV, the W decay branching ratios ($\mathcal{B}(\mathrm{W} \to \mathrm{f}\overline{\mathrm{f}}')$) are determined, with and without the assumption of lepton universality. ALEPH [96] and OPAL [94] have updated their results to include the data collected in the year 2000 at centre-of-mass energies up to 208 GeV, whereas DELPHI [92] and L3 [93] have not updated their preliminary results prepared for the year 2000 winter conferences. The results from the single experiments are given in Table 22 together with the result of the LEP combination. Correlated errors between the different channels of individual experiments are taken into account in the averaging procedure, together with the QCD component of the systematic error which is assumed to be fully correlated among experiments.

The results of the fit which does not make use of the lepton universality assumption show a negative correlation of 21.0% (18.7%) between the $\mathrm{W} \to \tau\overline{\nu}_\tau$ and $\mathrm{W} \to \mathrm{e}\overline{\nu}_\mathrm{e}$ ($\mathrm{W} \to \mu\overline{\nu}_\mu$) branching ratios, while between the electron and muon decay channels there is a positive correlation of 4.4%. These branching ratios are all consistent within the errors and allow to test lepton universality in the decay of on–shell W bosons at the level of 3.3%. Assuming lepton universality, the measured hadronic branching ratio is $(67.78 \pm 0.32)\%$ and the leptonic one is $(10.74 \pm 0.10)\%$. These results are consistent with the Standard Model expectations. Statistical and systematic uncertainties give approximately equal contributions to the total errors on the branching ratios. The systematic error is divided equally in the two components which are correlated and uncorrelated between experiments.

Within the Standard Model, the branching fractions of the W boson depend on the six matrix elements $|\mathrm{V}_{\mathrm{qq}'}|$ of the Cabibbo-Kobayashi-Maskawa (CKM) quark mixing matrix not involving the top quark. In terms of these $|\mathrm{V}_{\mathrm{qq}'}|$ the leptonic branching ratio of the W boson, $\mathcal{B}(\mathrm{W} \to \ell\overline{\nu}_\ell)$, is given by

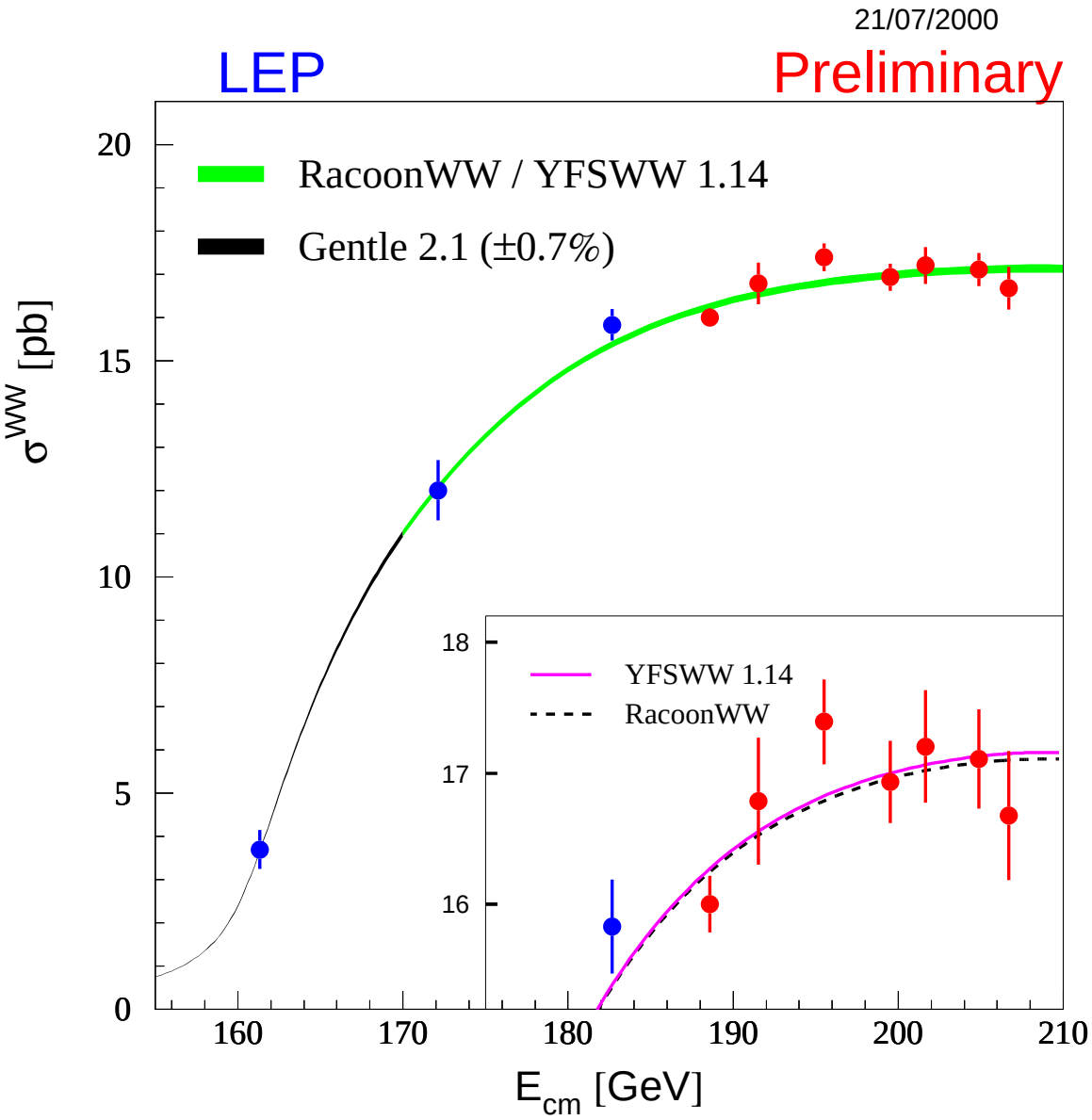

Figure 10: Measurements of the W–pair production cross section compared to the predictions of RacoonWW, and YFSWW3 and Gentle for $m_{\mathrm{W}} = 80.35$ GeV. The shaded area represent the uncertainty on the prediction which is ±0.7% for $\sqrt{s} < 170$ GeV and varies between ±0.4 and ±0.7% for $\sqrt{s} > 170$ GeV.

$$1/\mathcal{B}(\mathrm{W} \to \ell\overline{\nu}_\ell) \quad = \quad 3\{1 + [1 + \alpha_s({m_{\mathrm{W}}}^2)/\pi] \sum_{i=\mathrm{u,c},\ j=\mathrm{d,s,b}} |\mathrm{V}_{ij}|^2\}, \tag{20}$$

where $\alpha_s({m_{\mathrm{W}}}^2)$ is the strong coupling constant. Taking $\alpha_s({m_{\mathrm{W}}}^2) = (0.121 \pm 0.002)$, the measured leptonic branching ratio of the W yields

	Lepton non–universality			Lepton universality
Experiment	$W \to e\overline{\nu}_e$ (%)	$W \to \mu\overline{\nu}_\mu$ (%)	$W \to \tau\overline{\nu}_\tau$ (%)	W → hadrons (%)
ALEPH	11.19 ± 0.34	11.05 ± 0.32	10.53 ± 0.42	67.22 ± 0.53
DELPHI	10.33 ± 0.45	10.68 ± 0.34	11.28 ± 0.56	67.81 ± 0.61
L3	10.22 ± 0.36	9.87 ± 0.38	11.64 ± 0.51	68.47 ± 0.59
OPAL	10.52 ± 0.37	10.56 ± 0.35	11.15 ± 0.49	67.86 ± 0.62
LEP	10.62 ± 0.20	10.60 ± 0.18	11.07 ± 0.25	67.78 ± 0.32
χ^2/d.o.f.	11.1/9			13.2/9

Table 22: Summary of W branching ratios derived from W–pair production cross sections measurements up to 208 GeV centre-of-mass energy (DELPHI and L3 results are based only on data collected up to $\sqrt{s} = 202$ GeV). A common systematic error of (0.04–0.13)% is taken into account in the averaging procedure.

$$\sum_{i=\mathrm{u,c},\ j=\mathrm{d,s,b}} |\mathrm{V}_{ij}|^2 \quad = \quad 2.026 \ \pm \ 0.030\,(\mathrm{Br.}) \ \pm \ 0.001\,(\alpha_s), \tag{21}$$

where the first error is due to the uncertainty on the branching ratio measurement and the second to the uncertainty on α_s. Using the experimental knowledge of the sum $|\mathrm{V_{ud}}|^2+|\mathrm{V_{us}}|^2+|\mathrm{V_{ub}}|^2+|\mathrm{V_{cd}}|^2+|\mathrm{V_{cb}}|^2 = (1.0477 \pm 0.0074)$ [107], the above result can be interpreted as a measurement of $|\mathrm{V_{cs}}|$ which is the least well determined of these matrix elements:

$$|\mathrm{V_{cs}}| \quad = \quad 0.989 \ \pm \ 0.016. \tag{22}$$

The error includes the uncertainties on α_s and on the other $|\mathrm{V_{qq'}}|$ matrix elements but is dominated by the experimental error on the W branching fractions. The uncertainty in the sum of the other CKM matrix elements, which is dominated by the uncertainty on $|\mathrm{V}_{cd}|$, contributes a negligible uncertainty of 0.004 to this determination of $|\mathrm{V}_{cs}|$.

8.3 W Mass Measurement

The W boson mass results presented here are obtained from data recorded over a range of centre-of-mass energies, $\sqrt{s} = 161 - 202$ GeV during the 1996-1999 operation of the LEP collider. These data correspond to an integrated luminosity of approximately 460 pb^{-1} per experiment. No results from the year 2000 LEP running are included. The results on the W mass quoted below correspond to a mass definition based on a Breit-Wigner denominator with an s-dependent width, $|s - {m_\mathrm{W}}^2 + is\Gamma_\mathrm{W}/m_\mathrm{W}|$.

Since 1996 the LEP $\mathrm{e^+e^-}$ collider is operating above the threshold for $\mathrm{W^+W^-}$ pair production. Initially 10 pb^{-1} of data were recorded close to $\mathrm{W^+W^-}$ pair production threshold. At this energy the $\mathrm{W^+W^-}$ cross section is sensitive to the W boson mass, m_W. Table 23 summarises the W mass results from the four LEP collaborations based on these data [108–111].

Subsequently LEP has operated well above the $\mathrm{W^+W^-}$ threshold, delivering 450 pb^{-1} per experiment (excluding the operation in 2000). Above threshold, the $\mathrm{e^+e^-} \to \mathrm{W^+W^-}$ cross section has little

Threshold Cross Section	
Experiment	m_{W}/GeV
ALEPH [108]	80.14 ± 0.35
DELPHI [109]	80.40 ± 0.45
L3 [110]	$80.80^{+0.48}_{-0.42}$
OPAL [111]	$80.40^{+0.46}_{-0.43}$

Table 23: W mass measurements from the $\mathrm{W^+W^-}$ threshold cross section at $\sqrt{s} = 161$ GeV. The errors include statistical and systematic contributions.

sensitivity to m_{W}. For these data the W boson mass is measured using the method of direct reconstruction where the measured four-momenta of the reconstructed jets and leptons are used to reconstruct the invariant mass on an event-by-event basis. Table 24 summarises the W mass results from the four LEP experiments using the method of direct reconstruction. In addition to the combined numbers, each experiment presents mass measurements from $\mathrm{W^+W^-}\to\mathrm{q\overline{q}}\ell\overline{\nu}_\ell$ and $\mathrm{W^+W^-}\to\mathrm{q\overline{q}q\overline{q}}$ channels separately. The DELPHI, L3 and OPAL collaborations obtain results for the $\mathrm{q\overline{q}}\ell\overline{\nu}_\ell$ and $\mathrm{q\overline{q}q\overline{q}}$ channels using independent fits to data from each channel, taking into account correlated systematic errors. The $\mathrm{q\overline{q}}\ell\overline{\nu}_\ell$ and $\mathrm{q\overline{q}q\overline{q}}$ results quoted by the ALEPH collaboration are obtained from a simultaneous fit to all data which, in addition to other correlations, takes into account the correlated systematic uncertainties between the two channels. The large variation in the systematic uncertainties in the $\mathrm{W^+W^-}\to\mathrm{q\overline{q}q\overline{q}}$ channel are caused by differing estimates of the possible effects of colour reconnection (CR) and Bose-Einstein correlations (BEC), discussed below. The systematic errors in the $\mathrm{W^+W^-}\to\mathrm{q\overline{q}}\ell\overline{\nu}_\ell$ channel are dominated by uncertainties from hadronisation, with estimates ranging from 20-40 MeV.

	DIRECT RECONSTRUCTION		
	$\mathrm{W^+W^-}\to\mathrm{q\overline{q}}\ell\overline{\nu}_\ell$	$\mathrm{W^+W^-}\to\mathrm{q\overline{q}q\overline{q}}$	Combined
Experiment	m_{W}/GeV	m_{W}/GeV	m_{W}/GeV
ALEPH [112–114]	$80.435 \pm 0.063 \pm 0.048$	$80.467 \pm 0.064 \pm 0.057$	$80.449 \pm 0.045 \pm 0.047$
DELPHI [115–118]	$80.381 \pm 0.088 \pm 0.048$	$80.372 \pm 0.064 \pm 0.063$	$80.380 \pm 0.053 \pm 0.047$
L3 [119–122]]	$80.273 \pm 0.089 \pm 0.046$	$80.461 \pm 0.077 \pm 0.069$	$80.362 \pm 0.058 \pm 0.052$
OPAL [123–127]	$80.510 \pm 0.067 \pm 0.031$	$80.408 \pm 0.066 \pm 0.100$	$80.486 \pm 0.053 \pm 0.039$

Table 24: Preliminary W mass measurements from direct reconstruction ($\sqrt{s} = 172 - 202$ GeV). Results are given for the semileptonic, fully hadronic channels and the combined value. The errors are statistical and systematic respectively. The combined values of m_{W} from each collaboration take into account the correlated systematic uncertainties between the two channels and between the different years of data taking. The $\mathrm{W^+W^-}\to\mathrm{q\overline{q}}\ell\overline{\nu}_\ell$ results from the ALEPH and OPAL collaborations include mass information from the $\mathrm{W^+W^-} \to \ell^-\overline{\nu}_\ell\ell'^+\nu_{\ell'}$ channel.

8.3.1 Combination Procedure

A LEP combined W mass measurement is obtained from the results of the four experiments. To combine the measurements, a more detailed input than that given in Table 24 is required. Each experiment provides a W mass measurement for both $\mathrm{W^+W^-}\to\mathrm{q\overline{q}}\ell\overline{\nu}_\ell$ and $\mathrm{W^+W^-}\to\mathrm{q\overline{q}q\overline{q}}$ channels for each of the four years data taking (1996-1999), a total of 30 measurements (the L3 Collaboration provides results from the 1996 and 1997 data already combined). The subdivision into years enables a proper treatment of the correlated systematic uncertainty from the LEP beam energy and allows for the

possibility that the systematic uncertainties depend on the centre-of-mass energy and/or data-taking period. For each result a detailed breakdown of the sources of systematic uncertainty is provided and the correlations are specified. In the combination these inter-year, inter-channel and inter-experiment correlations are included. The main sources of correlated systematic errors are: colour reconnection, Bose-Einstein correlations, hadronisation, the LEP beam energy, and uncertainties from initial and final state radiation. The full correlation matrix for the LEP beam energy is employed [128].

The four LEP collaborations give different estimates of the systematic errors arising from final state interactions, ranging from 30-66 MeV for colour reconnection and from 20-67 MeV for Bose-Einstein correlations. These spreads could be due to different experimental sensitivities to these effects or, alternatively, they could be a reflection of the different models used to assess the uncertainties. This question is addressed using common Monte Carlo samples with and without CR effects. These are passed through the full detector simulations of each of the four experiments. Studies of these samples demonstrate that the four experiments are equally sensitive to colour reconnection effects, *i.e.* when looking at the same CR model similar biases are seen by all experiments. For this reason a common value of the CR systematic uncertainty is used in the combination. For Bose-Einstein Correlations, no similar test is made of the respective experimental sensitivities. However, in the absence of evidence that the experiments have different sensitivities to the effect, a common value of the systematic uncertainty from BEC is assumed. In the combination a common colour reconnection error of 50 MeV and a common Bose-Einstein systematic uncertainty of 25 MeV are used. These uncertainties are representative of the numbers estimated by the four LEP collaborations.

8.3.2 LEP Combined W Boson Mass

The combined W mass from direct reconstruction, taking into account all correlations including those between the $\mathrm{W^+W^-}\to\mathrm{q\overline{q}}\ell\overline{\nu}_\ell$ and $\mathrm{W^+W^-}\to\mathrm{q\overline{q}q\overline{q}}$ channels, years and experiments gives

$$m_{\mathrm{W}}(\mathit{direct}) = 80.428 \pm 0.030(\mathrm{stat.}) \pm 0.036(\mathrm{syst.})\ \mathrm{GeV},$$

with a χ^2/d.o.f. of 27.1/29, corresponding to a χ^2 probability of 57%. The weight of the fully hadronic channel in the combined fit is 0.27. The reduced weight is a consequence of the relatively large size of the current estimates of the systematic errors from CR and BEC. Table 25 gives a breakdown of the contribution to the total error of the systematic errors from different sources and the contribution to total error from statistics. The largest contribution to the systematic error comes from hadronisation uncertainties, which are treated as correlated between the two channels. In the absence of systematic effects the current LEP statistical precision on m_{W} would be 25 MeV. The statistical error contribution to the total error from the LEP combination is larger than this (30 MeV) due to the significantly reduced weight of the fully hadronic channel. Table 25 also shows the error breakdown for W mass measurements from the two channels separately (described in the following section).

In addition to the above results, the W boson mass is measured at LEP from the data recorded at threshold (10 pb^{-1}/experiment) for W pair production:

$$m_{\mathrm{W}}(\mathit{threshold}) = 80.40 \pm 0.20(\mathrm{stat.}) \pm 0.07(\mathrm{syst.}) \pm 0.03(\mathrm{LEP})\ \mathrm{GeV}.$$

When this is combined with the much more precise results obtained from direct reconstruction one obtains a W mass measurement of

$$m_{\mathrm{W}} = 80.427 \pm 0.046\ \mathrm{GeV}.$$

In combining the threshold and direct reconstruction measurements the only correlated systematic uncertainty is that from the LEP beam energy.

Source	Systematic Error on m_{W} (MeV)		
	$\mathrm{q\overline{q}}\ell\overline{\nu}_\ell$	$\mathrm{q\overline{q}q\overline{q}}$	Combined
ISR/FSR	8	10	8
Hadronisation	26	23	24
Detector Systematics	11	7	10
LEP Beam Energy	17	17	17
Colour Reconnection	–	50	13
Bose-Einstein Correlations	–	25	7
Other	5	5	4
Total Systematic	35	64	36
Statistical	38	34	30
Total	51	73	47

Table 25: Error decomposition for the combined W mass results. Detector systematics include uncertainties in the jet and lepton energy scales and resolution. The 'Other' category refers to errors, all of which are uncorrelated between experiments, arising from: Monte Carlo statistics, background, four-fermion treatment, fitting and event selection. The error decomposition in the $\mathrm{q\overline{q}}\ell\overline{\nu}_\ell$ and $\mathrm{q\overline{q}q\overline{q}}$ channels refers to the independent fits to the results from the two channels separately.

8.3.3 Consistency Checks

In addition to fitting for the combined W mass from the $\mathrm{W^+W^-}\rightarrow\mathrm{q\overline{q}}\ell\overline{\nu}_\ell$ and $\mathrm{W^+W^-}\rightarrow\mathrm{q\overline{q}q\overline{q}}$ channels, the difference between the W boson mass measurements obtained from the fully hadronic and semileptonic channels, $\Delta m_{\mathrm{W}}(\mathrm{q\overline{q}q\overline{q}} - \mathrm{q\overline{q}}\ell\overline{\nu}_\ell)$, can be determined. A significant non-zero value for Δm_{W} could indicate that FSI effects are biasing the value of m_{W} determined from $\mathrm{W^+W^-}\rightarrow\mathrm{q\overline{q}q\overline{q}}$ events. Since Δm_{W} is primarily of interest as a check of the possible effects of final state interactions, the errors from CR and BEC are set to zero in its determination, giving:

$$\Delta m_{\mathrm{W}}(\mathrm{q\overline{q}q\overline{q}} - \mathrm{q\overline{q}}\ell\overline{\nu}_\ell) = +5 \pm 51 \text{ MeV}.$$

This result is obtained from a fit to the results of the four experiments taking into account correlations between: the experiments, the two channels and different years. This result is almost unchanged if the systematic part of the error on m_{W} from fragmentation effects is considered as uncorrelated between experiments and channels, although the uncertainty increases by about 17%. The masses from the two channels obtained from this fit are

$$m_{\mathrm{W}}(\mathrm{W^+W^-}\rightarrow\mathrm{q\overline{q}}\ell\overline{\nu}_\ell) = 80.427 \pm 0.038(\text{stat.}) \pm 0.035(\text{syst.}) \text{ GeV},$$
$$m_{\mathrm{W}}(\mathrm{W^+W^-}\rightarrow\mathrm{q\overline{q}q\overline{q}}) = 80.432 \pm 0.034(\text{stat.}) \pm 0.064(\text{syst.}) \text{ GeV}.$$

These two results are correlated having a correlation coefficient of 0.29. The value of χ^2/d.o.f is 27.1/28, corresponding to a χ^2 probability of 52%. These results and the correlation between them can be used to combine the two measurements or to form the mass difference.

Experimentally, separate m_{W} measurements are obtained from the $\mathrm{W^+W^-}\rightarrow\mathrm{q\overline{q}}\ell\overline{\nu}_\ell$ and $\mathrm{W^+W^-}\rightarrow\mathrm{q\overline{q}q\overline{q}}$ channels. The combination using only the $\mathrm{q\overline{q}}\ell\overline{\nu}_\ell$ measurements yields

$$m_{\mathrm{W}}^{indep}(\mathrm{W^+W^-}\rightarrow\mathrm{q\overline{q}}\ell\overline{\nu}_\ell) = 80.429 \pm 0.038(\text{stat.}) \pm 0.035(\text{syst.}) \text{ GeV}.$$

This result is independent of the measurements in the $\mathrm{W^+W^-}\rightarrow\mathrm{q\overline{q}q\overline{q}}$ channel. The systematic error is dominated by fragmentation uncertainties ($\pm$26 MeV) and the uncertainty in the LEP centre-of-mass

energy (±17 MeV). The independent average over all $q\overline{q}q\overline{q}$ measurements only gives

$$m_{\mathrm{W}}^{indep}(\mathrm{W^+W^-}\rightarrow q\overline{q}q\overline{q}) = 80.424 \pm 0.034(\mathrm{stat.}) \pm 0.064(\mathrm{syst.})\ \mathrm{GeV}.$$

where the dominant contributions to the systematic error arise from BE/CR (±56 MeV), fragmentation (±23 MeV) and from the uncertainty in the LEP centre-of-mass energy (±17 MeV).

8.3.4 LEP Combined W Boson Width

The method of direct reconstruction is also used for the direct measurement of the width of the W boson. The results of the four LEP experiments are shown in Table 26.

Experiment	Γ_{W}/GeV
ALEPH	$2.17 \pm 0.16 \pm 0.12$
DELPHI	$2.09 \pm 0.12 \pm 0.09$
L3	$2.19 \pm 0.14 \pm 0.16$
OPAL	$2.04 \pm 0.16 \pm 0.09$
Combined	$2.12 \pm 0.08 \pm 0.07$

Table 26: Preliminary W width measurements ($\sqrt{s} = 172-202$ GeV) from the individual experiments. The first error is statistical and the second systematic. The ALEPH results at 192-202 GeV do not use the $\mathrm{W^+W^-}\rightarrow q\overline{q}q\overline{q}$ channel and the OPAL results do not include data recorded at centre-of-mass energies greater than 189 GeV. Only OPAL and L3 include data from 172 GeV.

A simultaneous fit to the results of the four LEP collaborations is performed in the same way as for the m_{W} measurement. Correlated systematic uncertainties are taken into account to give:

$$\Gamma_{\mathrm{W}} = 2.12 \pm 0.08(\mathrm{stat.}) \pm 0.07(\mathrm{syst.})\ \mathrm{GeV},$$

with a χ^2/d.o.f. of 13.7/17.

Currently no LEP combined value for Γ_{W} is obtained from the $\mathrm{W^+W^-}\rightarrow q\overline{q}\ell\overline{\nu}_\ell$ and $\mathrm{W^+W^-}\rightarrow q\overline{q}q\overline{q}$ channels separately.

8.3.5 Summary

The results of the four LEP experiments on the mass and width of the W boson are combined taking into account correlated systematic uncertainties, giving:

$$\begin{aligned} m_{\mathrm{W}} &= 80.427 \pm 0.046\ \mathrm{GeV}, \\ \Gamma_{\mathrm{W}} &= 2.12 \pm 0.11\ \mathrm{GeV}. \end{aligned}$$

9 Single–W Production Cross Section

Updates with respect to last summer:
This is a new section.

Preliminary single–W results for data collected at $\sqrt{s} = 183$–202 GeV are available. No preliminary analysis of the data collected in the year 2000 at $\sqrt{s} > 200$ GeV was prepared in time for the summer conferences.

A common definition of the single–W production cross section is adopted, to allow direct comparisons and the combination of the results obtained by the four experiments. Single–W production is defined by the complete t-channel subset of Feynman diagrams contributing to the $e\nu ff'$ final states, with additional cuts on kinematic variables to exclude the regions of the phase space dominated by multiperipheral diagrams, where the cross section calculation is affected by large uncertainties. The advantage of this definition is that a gauge invariant set of diagrams is taken, which has a small interference with the s-channel one. In addition, no angular cuts due to the specific detector acceptances are used.

The kinematic cuts used in the cross section definition are (charge conjugation is implied in the definition):

- $M_{\mathrm{qq}'} > 45$ GeV for the $e\nu\mathrm{qq}'$ final states,
- $E_{\ell^+} > 20$ GeV for the $e\nu\ell\nu$ final states (with $\ell = \mu, \tau$),
- $|cos(\theta_{\mathrm{e}^-})| > 0.95, |cos(\theta_{\mathrm{e}^+})| < 0.95, E_{\mathrm{e}^+} > 20$ GeV for the $e\nu e\nu$ final state.

The results of the single experiments and of the LEP average are summarised for the different centre-of-mass energies in Table 27. Given the statistical precision of the single–W measurements, results are combined assuming uncorrelated systematic errors between experiments and using expected statistical errors.

Since winter 2000 conferences [129], the only update concerns the addition of one theoretical prediction [130] to the single–W production cross section curve as a function of the centre-of-mass energy for the hadronic final state, based on the exact treatment of the evolution of the energy scale for α_{em} [131] in the 4f matrix element. This evolution is only approximated (at the level of 1–2%) by one of the codes previously used [132], and introduced by rescaling the cross section in one other code [133]. The data at $\sqrt{s} = 183$–202 GeV are compared with the theoretical predictions in Figure 11.

It should be remarked that all the theoretical predictions are scaled upward by 4% , since all codes implement QED radiative corrections (mainly due to initial state radiation) using the wrong energy scale s in the ISR structure functions which is not adequate for this process dominated by t-channel exchange diagrams. The correction factor of 4% is derived in [134] from a comparison of `grc4f` [135] and SWAP [136] for different scales in the structure functions. Since this is only an approximation of the complete $\mathcal{O}(\alpha)$ correction for the single W process, a 100% uncertainty is conservatively assigned to this 4% correction. This constitutes the major part of the theoretical uncertainty currently assigned to the predictions (5%, as discussed in [134]), which is becoming a limiting factor for the extraction of triple gauge couplings from the single W events [137].

$\sqrt{s}$	Cross section (pb)					χ^2/d.o.f.
(GeV)	ALEPH	DELPHI	L3	OPAL	LEP	
182.67	0.40 ± 0.24		$0.58^{+0.23}_{-0.20}$		0.50 ± 0.16	0.33/1
188.63	0.31 ± 0.14	$0.44^{+0.28}_{-0.25}$	$0.52^{+0.14}_{-0.13}$	$0.53^{+0.13}_{-0.13}$	0.46 ± 0.07	1.71/3
191.6	0.94 ± 0.44	$0.01^{+0.19}_{-0.07}$	$0.85^{+0.45}_{-0.37}$		0.73 ± 0.26	1.70/2
195.5	0.45 ± 0.23	$0.78^{+0.38}_{-0.34}$	$0.66^{+0.25}_{-0.23}$		0.60 ± 0.15	0.79/2
199.5	0.82 ± 0.26	$0.16^{+0.29}_{-0.17}$	$0.34^{+0.23}_{-0.20}$		0.45 ± 0.15	3.26/2
201.6	0.68 ± 0.35	$0.55^{+0.47}_{-0.40}$	$1.09^{+0.42}_{-0.37}$		0.80 ± 0.22	1.03/2

Table 27: Single–W cross section for the hadronic decay of the W, from the four experiments and LEP combined value for the five centre-of-mass energies. All numbers are preliminary.

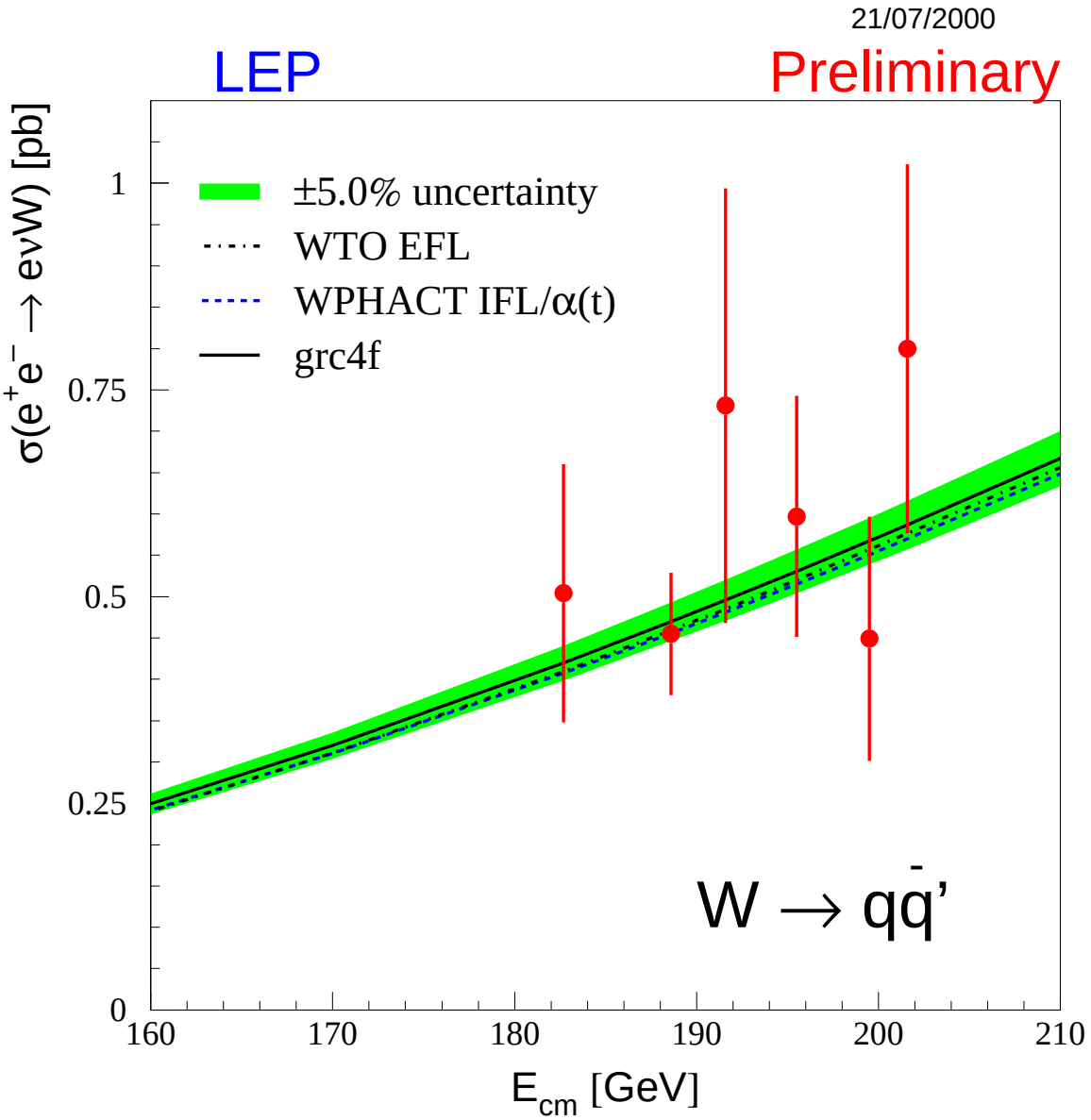

Figure 11: Measurements of the single–W production cross section in the hadronic decay channel of the W boson compared to the predictions of WTO, WPHACT and `grc4f`. The shaded area represents a ±5% uncertainty on the predictions.

10 Measurement of the ZZ Production Cross Section

Updates with respect to last summer:
All experiments have published results up to 189 GeV, new results at higher energies are available.

At centre-of-mass energies above twice the Z boson mass, the production of pairs of Z bosons is possible. All experiments have published final results [138–141] on the Z–pair (NC02) production cross section at $\sqrt{s} = 183$ and 189 GeV. L3 [142] has updated its preliminary results for $\sqrt{s} = 192$–202 GeV, whereas ALEPH [143], DELPHI [144] and OPAL [145] preliminary results are unchanged since the winter conferences. All experiments have provided preliminary results [94, 96–98] based on an integrated luminosity of approximately 90 pb^{-1} collected in the year 2000 at centre-of-mass energies between 200 and 208 GeV.

The combination of results is performed using the expected statistical error of each analysis, to avoid biases due to the limited number of events selected. The following components of the systematic errors are considered correlated between experiments:

- $\pm 5\%$ uncertainty on the 2–fermion background rate.
- $\pm 2\%$ uncertainty on the WW background rate.
- $\pm 10\%$ uncertainty on the $\mathrm{Z^0e^+e^-}$ background rate.
- the uncertainty on the b quark modelling.

The common error ranges from 0.01 to 0.03 pb.

The results of the single experiments and of the LEP average are summarised for the different centre-of-mass energies in Table 28. All results are preliminary, with the exception of those at $\sqrt{s} = 183$ and 189 GeV. The results are shown in Figure 12 as a function of the LEP centre-of-mass energy and compared to the YFSZZ [146] and ZZTO [147] predictions, which have an estimated uncertainty of $\pm 2\%$ [134]. These results supersede those presented in [148] for $\sqrt{s} = 183$–202 GeV. The data do not show any significant deviation from the theoretical expectations.

$\sqrt{s}$	Cross section (pb)					χ^2/d.o.f.
(GeV)	ALEPH	DELPHI	L3	OPAL	LEP	
182.67	$0.11^{+0.16*}_{-0.12}$	$0.38 \pm 0.18^*$	$0.31^{+0.17*}_{-0.15}$	$0.12^{+0.20*}_{-0.18}$	$0.23 \pm 0.08^*$	2.28/3
188.63	$0.67^{+0.14*}_{-0.13}$	$0.60 \pm 0.15^*$	$0.73^{+0.15*}_{-0.14}$	$0.80^{+0.15*}_{-0.14}$	$0.70 \pm 0.08^*$	0.92/3
191.6	$0.53^{+0.34}_{-0.27}$	0.55 ± 0.34	$0.27^{+0.20}_{-0.23}$	$1.13^{+0.47}_{-0.41}$	0.60 ± 0.18	2.99/3
195.5	$0.69^{+0.23}_{-0.20}$	1.17 ± 0.28	1.11 ± 0.23	$1.28^{+0.29}_{-0.27}$	1.04 ± 0.12	3.43/3
199.5	$0.70^{+0.22}_{-0.20}$	1.08 ± 0.26	1.19 ± 0.24	$1.01^{+0.26}_{-0.23}$	0.99 ± 0.13	2.31/3
201.6	$0.70^{+0.33}_{-0.28}$	0.87 ± 0.33	$0.89^{+0.36}_{-0.37}$	$1.09^{+0.40}_{-0.35}$	0.88 ± 0.18	0.57/3
204.9	$0.86^{+0.29}_{-0.26}$	1.28 ± 0.34	0.56 ± 0.28	$1.41^{+0.35}_{-0.32}$	1.00 ± 0.15	4.74/3
206.7	$0.51^{+0.35}_{-0.28}$	1.11 ± 0.42	0.84 ± 0.39	$0.30^{+0.37}_{-0.29}$	0.70 ± 0.21	2.13/3

Table 28: Z–pair production cross section from the four LEP experiments and combined values for the eight centre-of-mass energies. All results are preliminary with the exception of those indicated by *. A common systematic error of (0.01–0.03) pb is taken into account in the averaging procedure.

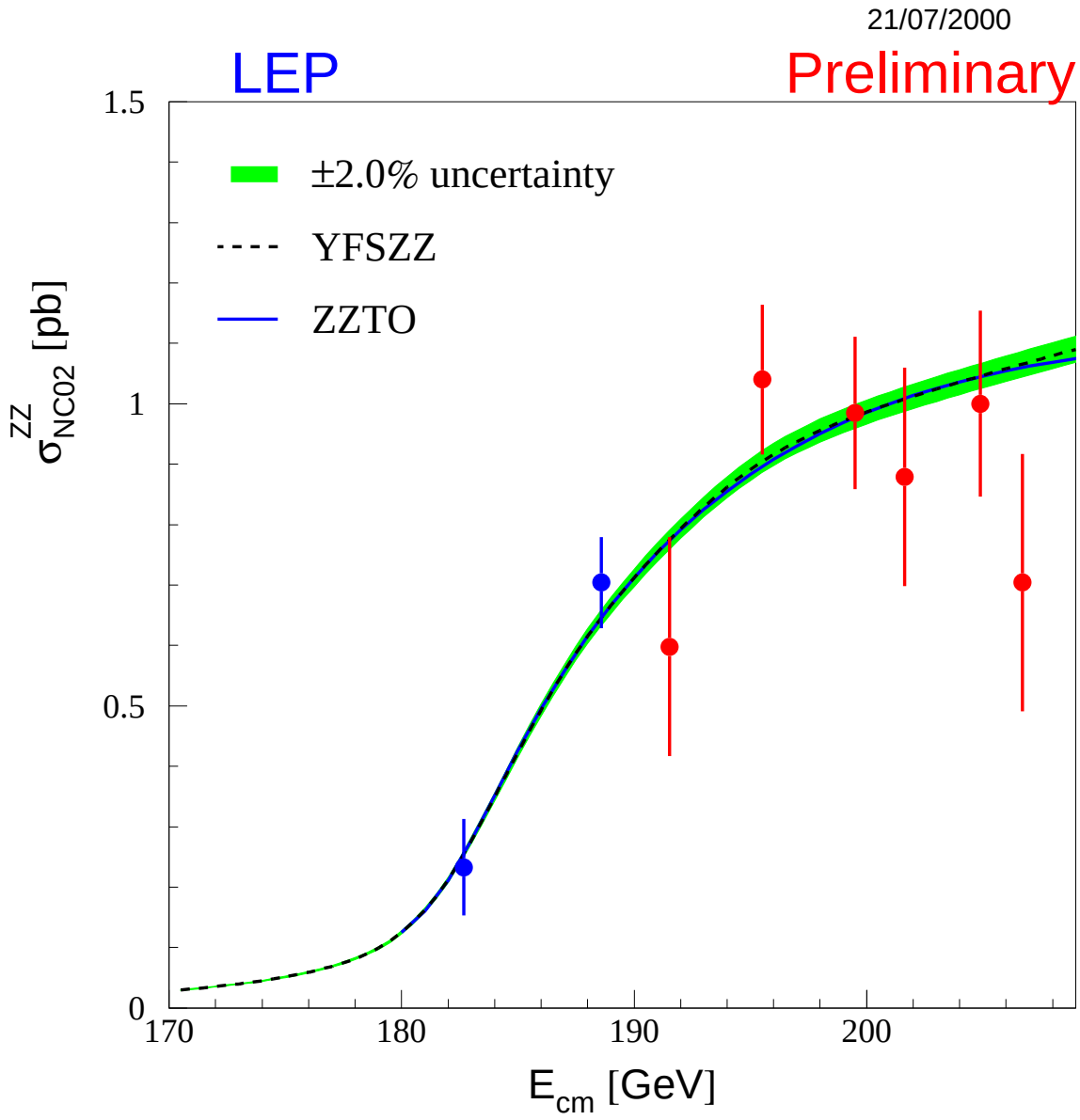

Figure 12: Measurements of the Z–pair production cross section compared to the predictions of YFSZZ and ZZTO. The shaded area represent a ±2% uncertainty on the predictions.

11 Electroweak Gauge Boson Couplings

Updates with respect to last summer:
This is a new section

The W-pair production process, $e^+e^- \to W^+W^-$, involves the triple gauge boson vertices between the W^+W^- and the Z or the photon. Up-to the end of 1999, more than 7000 W-pair events were collected by each experiment. Single W ($e\nu W$) and single photon ($\nu\bar{\nu}\gamma$) production at LEP are sensitive to the $WW\gamma$ vertex. The measurement of these charged triple gauge boson couplings and the search for possible anomalous contributions due to the effects of new physics beyond the Standard Model is one of the principal physics goals at LEP-II [149].

At centre-of-mass energies exceeding twice the Z boson mass, pair production of Z bosons is kinematically allowed. Here, one searches for the possible existence of triple vertices involving only neutral electroweak gauge bosons. Such vertices could also contribute to $Z\gamma$ production. In contrast to triple gauge boson vertices with two charged gauge bosons, purely neutral gauge boson vertices do not occur in the Standard Model of electroweak interactions.

Within the Standard Model, quartic electroweak gauge boson vertices with at least two charged gauge bosons exist. In e^+e^- collisions at LEP-II centre-of-mass energies, the $WWZ\gamma$ and $WW\gamma\gamma$ vertices contribute to $WW\gamma$ and $\nu\bar{\nu}\gamma\gamma$ production in s-channel and t-channel, respectively. The effect of the Standard Model quartic electroweak vertices is below the sensitivity of LEP-II. Thus, anomalous quartic vertices are searched for in the production of $WW\gamma$ and $\nu\bar{\nu}\gamma\gamma$ but also $Z\gamma\gamma$ final states.

In this note we present the combination of results on electroweak gauge boson couplings based on the data collected by the four LEP experiments at LEP-II. Charged TGCs [150–153], neutral TGCs [154–159] as well as QGCs [160–162] are combined.

11.1 Charged Triple Gauge Boson Couplings

The parametrisation of the charged triple gauge boson vertices is described in References [149,163–168]. The most general Lorentz invariant Lagrangian which describes the charged triple gauge boson interaction contains fourteen independent complex couplings, seven describing the $WW\gamma$ vertex and seven describing the WWZ vertex. Assuming electromagnetic gauge invariance as well as CP conservation, the number of independent TGCs reduces to six. One common set is $\{g_1^z,\ \kappa_\gamma,\ \kappa_z,\ \lambda_\gamma,\ \lambda_z,\ g_5^Z\}$ where $g_1^z = \kappa_\gamma = \kappa_z = 1$ and $\lambda_\gamma = \lambda_z = g_5^Z = 0$ in the Standard Model. Except g_5^Z, all these couplings also conserve C and P separately.

The parameters proposed in [149] and used here are:

$$\Delta g_1^z \equiv g_1^z - 1\,, \tag{23}$$
$$\Delta\kappa_\gamma \equiv \kappa_\gamma - 1\,, \tag{24}$$
$$\lambda_\gamma \quad and \quad g_5^Z \tag{25}$$

with the gauge constraints:

$$\Delta\kappa_z \equiv \kappa_z - 1 = \Delta g_1^z - \Delta\kappa_\gamma \tan^2\theta_W \tag{26}$$
$$\lambda_z = \lambda_\gamma\,, \tag{27}$$

where Δ indicates the deviation of the respective coupling from its Standard Model value of unity, and θ_W is the weak mixing angle. The couplings are considered as real, with the imaginary parts fixed to zero.

11.2 Neutral Triple Gauge Boson Couplings

There are two possible anomalous triple vertices in the neutral sector. Each is parametrised by the most general Lorentz and $U(1)_{\rm EM}$ invariant Lagrangian plus Bose symmetry, as described in References [164, 169].

The first vertex refers to anomalous Z$\gamma\gamma$ and ZZγ couplings which are accessible at LEP in the process $e^+e^- \to Z\gamma$. The parametrisation contains eight couplings: h_i^V with $i = 1, ..., 4$ and $V = \gamma$,Z. The superscript γ refers to Z$\gamma\gamma$ couplings and superscript Z refers to ZZγ couplings. The photon and the Z boson in the final state are considered as on-shell particles, while the third boson at the triple vertex is off shell. The couplings h_1^V and h_2^V are CP-odd while h_3^V and h_4^V are CP-even.

The second vertex refers to anomalous ZZγ and ZZZ couplings which are accessible at LEP in the process $e^+e^- \to ZZ$. This anomalous vertex is parametrised in terms of four couplings: f_i^V with $i = 4, 5$ and $V = \gamma$,Z. The superscript γ refers to ZZγ couplings and the superscript Z refers to ZZZ couplings. Both Z bosons in the final state are assumed to be on-shell, while the third boson at the triple vertex is off-shell. The couplings f_4^V are CP-odd whereas f_5^V are CP-even.

Note that the h_i^V and f_i^V couplings are independent of each other. They are considered as real, with the imaginary parts fixed to zero. They vanish in the Standard Model at tree level.

11.3 Quartic Gauge Boson Couplings

Anomalous contributions to electroweak quartic vertices are considered in the framework of References [170–172]. Three lowest-dimensional operators leading to quartic vertices not causing anomalous TGCs are considered. The corresponding couplings are a_0/Λ^2, a_c/Λ^2 and a_n/Λ^2, where Λ represents the energy scale of new physics. The couplings a_0/Λ^2 and a_c/Λ^2 parametrise variations in the WW$\gamma\gamma$ and ZZ$\gamma\gamma$ vertices, while a_n/Λ^2 affects purely the WWZγ vertex. The couplings a_0/Λ^2 and a_c/Λ^2 conserve C and P, while the coupling a_n/Λ^2 is CP violating. The production of WWγ depends on all three couplings. The production of $\nu\bar{\nu}\gamma\gamma$ and Z$\gamma\gamma$ depends only on a_0/Λ^2 and a_c/Λ^2, the former through the WW$\gamma\gamma$ vertex, the latter through the ZZ$\gamma\gamma$ vertex. The couplings are considered as real, with the imaginary parts fixed to zero. They vanish in the Standard Model at tree level.

A more detailed description of QGCs has recently appeared [173], in which it is suggested that the coupling a_0/Λ^2 and a_c/Λ^2 describing the anomalous WW$\gamma\gamma$ vertex should not be assumed to be the same couplings as those describing the anomalous ZZ$\gamma\gamma$ vertex. The experimental results on these vertices are therefore also given separately.

11.4 Measurements

The results presented comprise measurements of all electroweak gauge boson couplings discussed above. In most cases, the results are based on the data collected at LEP-II until the end of 1999 at centre-of-mass energies up to 202 GeV. The experiments already combine different processes and final

states for each coupling. In each case, the individual references should be consulted for the details on the data samples used.

For charged TGCs, the experimental analyses study different channels, typically the semileptonic, fully hadronic and fully leptonic W-pair decays [150–153]. Anomalous TGCs affect both the total production cross section and the shape of the differential cross section as a function of the polar W^- production angle. The relative contributions of each helicity state of the W bosons are also changed, which in turn affects the distributions of their decay products. The analyses presented by each experiment make use of different combinations of each of these quantities. In general, however, all analyses use at least the expected variations of the total production cross section and the W^- production angle. Results from $e\nu W$ and $\nu\bar{\nu}\gamma$ production are included by some experiments. Single W production is particularly sensitive to κ_γ, thus providing information complementary to that from W-pair production.

For neutral TGCs, the analyses mainly use measurements of the total cross sections of $Z\gamma$ and ZZ production, though the use of differential distributions increases the sensitivity. The individual references should be consulted concerning the details of the analyses for the h_i^V couplings [154–156] and the f_i^V couplings [157–159].[9]

For QGCs, the experiments investigate $WW\gamma$, $\nu\bar{\nu}\gamma\gamma$ and $Z\gamma\gamma$ production. Besides the total cross section, the sensitive variables analysed are photon energies ($WW\gamma$ and $Z\gamma\gamma$) and recoil masses ($\nu\bar{\nu}\gamma\gamma$). Again, the individual references should be consulted for the details in the determination of the QGCs a_0/Λ^2, a_c/Λ^2 and a_n/Λ^2 [160–162].

11.5 Combination Procedure

The combination procedure is modified compared to previous LEP combinations of electroweak gauge boson couplings [1,174] in order to treat systematic uncertainties correlated between the experiments.

Each experiment provides the negative log likelihood, $-\Delta \log \mathcal{L}$, as a function of the coupling parameters (one, two, or three) to be combined. The single parameter analyses are performed fixing the values of all other parameters to their Standard Model value. The two- and three-parameter analyses are performed setting the remaining parameters to their Standard Model value. For the charged TGCs, the gauge constraints listed in Section 11.1 are always enforced.

The $-\Delta \log \mathcal{L}$ functions from each experiment include statistical as well as all systematic uncertainties considered as uncorrelated between experiments. For both single- and multi-parameter combinations, the individual $-\Delta \log \mathcal{L}$ functions are added. It is necessary to use the $-\Delta \log \mathcal{L}$ functions directly for the combination as in some cases they are not parabolic, so that it is not possible to combine the results correctly by simply taking weighted averages of the measurements.

The main contributions to the systematic uncertainties uncorrelated between experiments arise from detector effects, backgrounds in the selected samples, limited Monte Carlo statistics and the fitting methods. Their importance varies for each experiment and the individual references should be consulted for details.

The systematic uncertainties arising from the following sources are treated as correlated between

[9] For quoting results on the f_i^V couplings, DELPHI [157] uses a convention for the sign of f_i^V opposite to that used by L3 [158] and OPAL [159]. For DELPHI and combined LEP results presented in this note, the DELPHI f_i^V measurements are modified to conform to the same sign convention as used by L3 and OPAL.

the experiments: the uncertainty on the theoretical cross section prediction (W^+W^-, $e\nu W$ and $Z\gamma$ production), fragmentation effects (W^+W^- production), and Bose-Einstein correlations and colour-reconnection effects (fully hadronic W-pair decays). While the correlated systematic uncertainties are small in $Z\gamma$ production, they are sizeable for charged TGCs. In particular, the uncertainty on the theoretical cross section prediction for the $e\nu W$ process causes a large reduction in the sensitivity of this process to charged TGCs. For ZZ production, the uncertainty on the theoretical cross section prediction is small compared to the statistical accuracy and is neglected. For other sources of correlated systematic uncertainties, such as those arising from the LEP beam energy or the W mass, the effect of their correlation on the combination result is negligible.

The correlated systematic uncertainties are applied by scaling the likelihood functions by the squared ratio of the statistical and uncorrelated systematic uncertainty over the total uncertainty including all correlated uncertainties. This procedure to treat correlations is an approximation in the case where the log-likelihood function is not parabolic.

The one standard deviation uncertainties (68% confidence level) are obtained by taking the coupling values where $-\Delta \log \mathcal{L} = +0.5$ above the minimum. The 95% confidence level (C.L.) limits are given by the coupling values where $-\Delta \log \mathcal{L} = +1.92$ above the minimum. These cut-off values are used for obtaining the results of both single- and multi-parameter analyses reported here. Note that in the case of the neutral TGCs and the QGCs, double minima structures appear in the negative log-likelihood curves. For multi-parameter analyses, the 68% C.L. contour curves for any pair of couplings are obtained by requiring $-\Delta \log \mathcal{L} = +1.15$, while for the 95% C.L. contour curves $-\Delta \log \mathcal{L} = +3.0$ is required.

11.6 Results

We present below results on combination of the four LEP experiments on the various electroweak gauge boson couplings. The results quoted individually for each experiment, summarised in Appendix B are calculated using the method described in Section 11.5. Thus, they sometimes differ slightly from those reported in the individual references.

11.6.1 Charged Triple Gauge Boson Couplings

Results of the combination of charged triple gauge boson couplings are given in Tables 29, 30 and 31 for the single, two and three-parameter analyses respectively. Individual $-\Delta \log \mathcal{L}$ curves and their sum are shown in Figure 13 for the single-parameter analysis. The 68% C.L. and 95% C.L. contours curves resulting from the combinations of the two-dimensional likelihood curves are shown in Figure 14.

Parameter	68% C.L.	95% C.L.
g_5^Z	$+0.05^{+0.16}_{-0.17}$	$[-0.28, \quad +0.36]$
Δg_1^z	$-0.025^{+0.026}_{-0.026}$	$[-0.074, \quad +0.028]$
$\Delta\kappa_\gamma$	$-0.002^{+0.067}_{-0.065}$	$[-0.13, \quad +0.13]$
λ_γ	$-0.036^{+0.028}_{-0.027}$	$[-0.089, \quad +0.020]$

Table 29: Single-parameter analyses : the central values, 68% C.L. uncertainties and 95% C.L. intervals ($-\Delta \log \mathcal{L} = 0.5,\ 1.92$) obtained combining the results from the four LEP experiments. In each case the parameter listed is varied while the remaining ones are fixed to their Standard Model value. Both statistical and systematic uncertainties are included.

Parameter	68% C.L.	95% C.L.	Correlations	
Δg_1^z	$-0.038^{+0.041}_{-0.034}$	$[-0.10, \quad +0.03]$	1.00	-0.43
$\Delta\kappa_\gamma$	$+0.053^{+0.074}_{-0.089}$	$[-0.10, \quad +0.21]$	-0.43	1.00
Δg_1^z	$+0.006^{+0.035}_{-0.039}$	$[-0.072, \quad +0.076]$	1.00	-0.70
λ_γ	$-0.048^{+0.043}_{-0.036}$	$[-0.12, \quad +0.03]$	-0.70	1.00
λ_γ	$-0.046^{+0.041}_{-0.031}$	$[-0.11, \quad +0.02]$	1.00	-0.19
$\Delta\kappa_\gamma$	$+0.037^{+0.060}_{-0.069}$	$[-0.09, \quad +0.16]$	-0.19	1.00

Table 30: Two-parameter analyses : the central values, 68% C.L. uncertainties and 95% C.L. intervals ($-\Delta \log \mathcal{L} = 0.5,\ 1.92$) obtained combining the results from the four LEP experiments. In each case the two parameters listed are varied while the remaining one is fixed to its Standard Model value. Both statistical and systematic uncertainties are included. Since the shape of the log-likelihood is not parabolic, there is some ambiguity in the definition of the correlation coefficients and the values quoted here are approximate.

Parameter	68% C.L.	95% C.L.	Correlations		
Δg_1^z	$+0.023^{+0.039}_{-0.041}$	$[-0.06, \quad +0.10]$	1.00	-0.20	-0.66
$\Delta\kappa_\gamma$	$+0.027^{+0.073}_{-0.072}$	$[-0.11, \quad +0.18]$	-0.20	1.00	-0.15
λ_γ	$-0.067^{+0.044}_{-0.037}$	$[-0.14, \quad +0.02]$	-0.66	-0.15	1.00

Table 31: Three-parameter analyses : the central values, 68% C.L. uncertainties and 95% C.L. intervals ($-\Delta \log \mathcal{L} = 0.5,\ 1.92$) obtained combining the results from ALEPH, L3 and OPAL. All three parameters listed are varied. Both statistical and systematic uncertainties are included. Since the shape of the log-likelihood is not parabolic, there is some ambiguity in the definition of the correlation coefficients and the values quoted here are approximate.

11.6.2 Neutral Triple Gauge Boson Couplings in Zγ Production

Results of the combination of neutral triple gauge boson couplings in Zγ production are given in Tables 32 and 33 for the single, two-parameter analyses respectively. The 68% C.L. and 95% C.L. contours curves resulting from the combinations of the two-dimensional likelihood curves are shown in Figure 15.

Parameter	95% C.L.
h_1^γ	$[-0.10, \quad +0.03]$
h_2^γ	$[-0.036, \quad +0.061]$
h_3^γ	$[-0.075, \quad -0.004]$
h_4^γ	$[+0.005, \quad +0.056]$
h_1^Z	$[-0.13, \quad +0.04]$
h_2^Z	$[-0.041, \quad +0.080]$
h_3^Z	$[-0.16, \quad +0.07]$
h_4^Z	$[-0.04, \quad +0.10]$

Table 32: Single-parameter analyses : The 95% C.L. intervals ($-\Delta \log \mathcal{L} = 1.92$) obtained combining the results from DELPHI, L3 and OPAL. In each case the parameter listed is varied while the remaining ones are fixed to their Standard Model value. Both statistical and systematic uncertainties are included.

Parameter	95% C.L.	Correlations	
h_1^γ	$[-0.21, \quad +0.10]$	1.00	+0.88
h_2^γ	$[-0.11, \quad +0.10]$	+0.88	1.00
h_3^γ	$[-0.20, \quad +0.13]$	1.00	+0.98
h_4^γ	$[-0.11, \quad +0.12]$	+0.98	1.00
h_1^Z	$[-0.44, \quad +0.20]$	1.00	+0.96
h_2^Z	$[-0.28, \quad +0.16]$	+0.96	1.00
h_3^Z	$[-0.38, \quad +0.35]$	1.00	+0.95
h_4^Z	$[-0.21, \quad +0.26]$	+0.95	1.00

Table 33: Two-parameter analyses : The 95% C.L. intervals ($-\Delta \log \mathcal{L} = 1.92$) obtained combining the results from DELPHI and L3. In each case the two parameters listed are varied while the remaining ones are fixed to their Standard Model value. Both statistical and systematic uncertainties are included. Since the shape of the log-likelihood is not parabolic, there is some ambiguity in the definition of the correlation coefficients and the values quoted here are approximate.

11.6.3 Neutral Triple Gauge Boson Couplings in ZZ Production

Results of the combination of neutral triple gauge boson couplings in ZZ production are given in Tables 34 and 35 for the single, two-parameter analyses respectively. The 68% C.L. and 95% C.L. contours curves resulting from the combinations of the two-dimensional likelihood curves are shown in Figure 16.

Parameter	95% C.L.
f_4^γ	$[-0.41, \ +0.39]$
f_4^Z	$[-0.66, \ +0.68]$
f_5^γ	$[-0.89, \ +0.84]$
f_5^Z	$[-1.1, \ +0.5]$

Table 34: Single-parameter analyses : The 95% C.L. intervals ($-\Delta \log \mathcal{L} = 1.92$) obtained combining the results from DELPHI, L3 and OPAL. In each case the parameter listed is varied while the remaining ones are fixed to their Standard Model value. Both statistical and systematic uncertainties are included.

Parameter	95% C.L.	Correlations	
f_4^γ	$[-0.40, \ +0.38]$	1.00	+0.88
f_4^Z	$[-0.66, \ +0.68]$	+0.88	1.00
f_5^γ	$[-0.88, \ +0.86]$	1.00	−0.52
f_5^Z	$[-1.1, \ +0.7]$	−0.52	1.00

Table 35: Two-parameter analyses : The 95% C.L. intervals ($-\Delta \log \mathcal{L} = 1.92$) obtained combining the results from DELPHI, L3 and OPAL. In each case the two parameters listed are varied while the remaining ones are fixed to their Standard Model value. Both statistical and systematic uncertainties are included. Since the shape of the log-likelihood is not parabolic, there is some ambiguity in the definition of the correlation coefficients and the values quoted here are approximate.

11.6.4 Quartic Gauge Boson Couplings

The individual $-\Delta \log \mathcal{L}$ curves and their sum are shown in Figure 17 for the WWγ and $\nu\bar{\nu}\gamma\gamma$ channels. The results of the combination are given in Table 36.

Parameter [GeV^{-2}]	95% C.L.
a_0/Λ^2	$[-0.037, \quad +0.036]$
a_c/Λ^2	$[-0.077, \quad +0.095]$
a_n/Λ^2	$[-0.45, \quad +0.41]$
a_0/Λ^2	$[-0.0048, \quad +0.0056]$
a_c/Λ^2	$[-0.0052, \quad +0.0099]$

Table 36: The 95% C.L. intervals ($-\Delta \log \mathcal{L} = 1.92$) obtained combining the results from ALEPH, L3 and OPAL. In each case the parameter listed is varied while the remaining ones are fixed to their Standard Model value. Both statistical and systematic uncertainties are included. Top: WWγ and $\nu\bar{\nu}\gamma\gamma$. Bottom: Z$\gamma\gamma$.

11.7 Conclusions

The existence of triple gauge boson couplings among the electroweak gauge bosons is experimentally verified. No significant deviation from the Standard Model predictions is seen for any of the electroweak gauge boson couplings investigated. As an example, these data allow the Kaluza-Klein theory [175], in which $\kappa_\gamma = -2$, to be excluded [176].

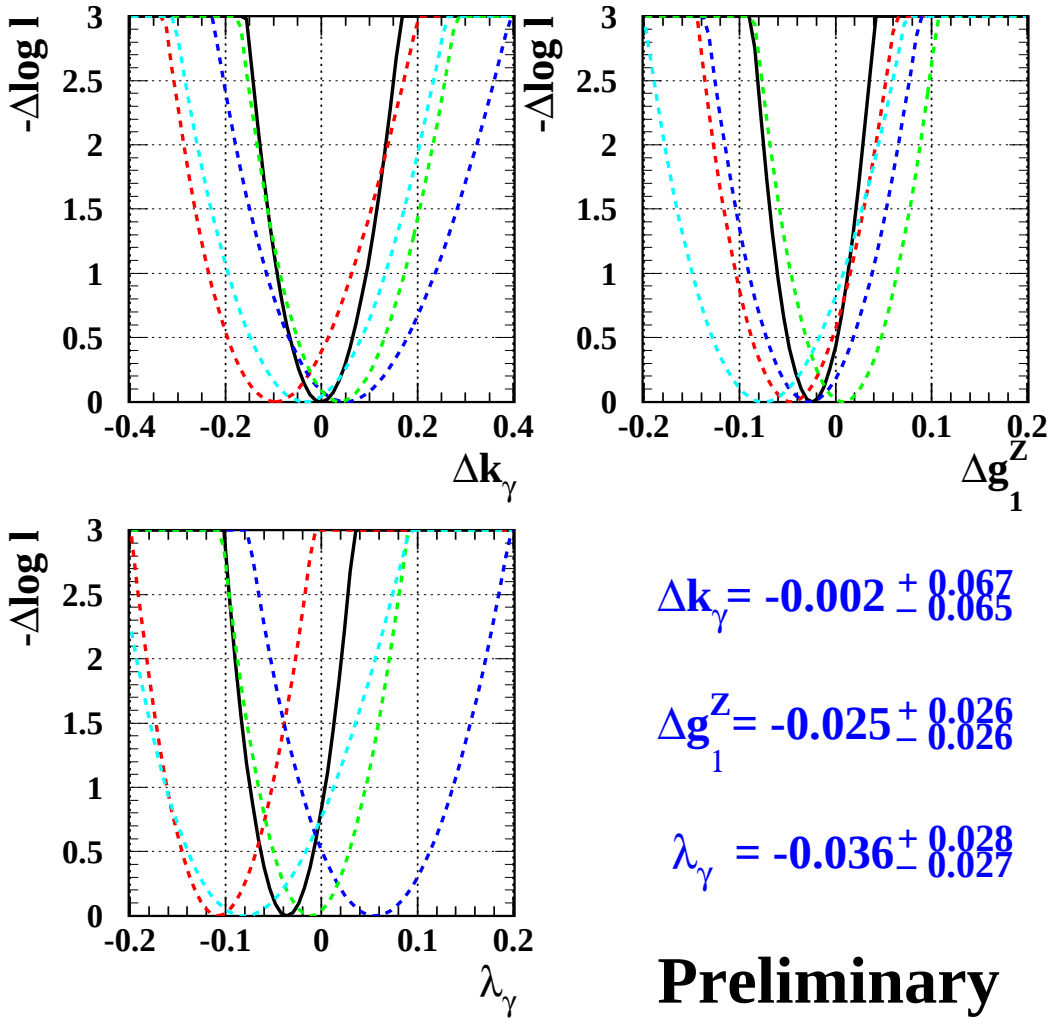

Figure 13: The $-\Delta \log \mathcal{L}$ curves of the four experiments (dashed lines) and the LEP combined curve (solid line) for the three charged TGCs Δg_1^z, $\Delta\kappa_\gamma$ and λ_γ. In each case, the minimal value is subtracted.

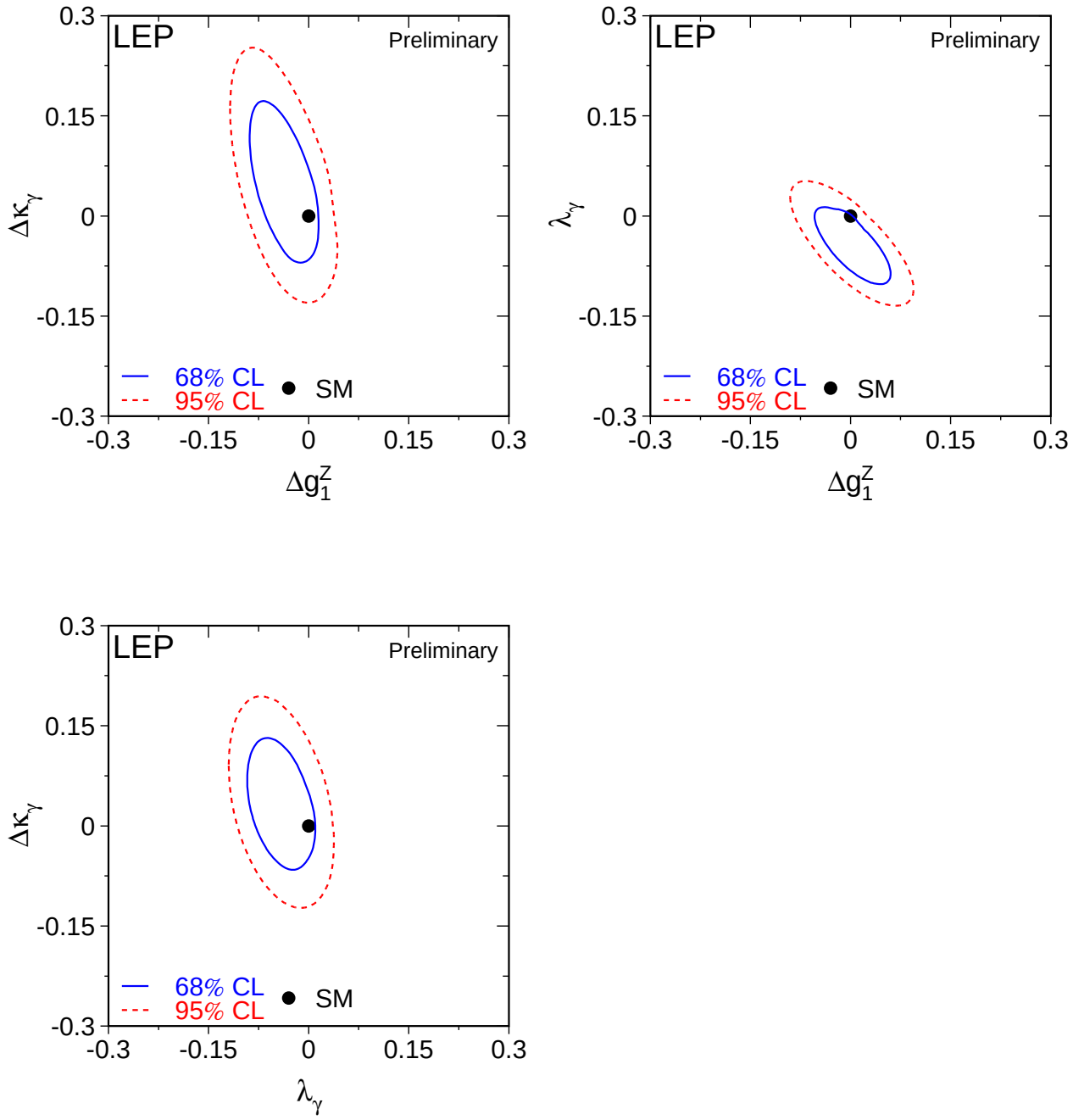

Figure 14: Contour curves of 68% C.L. and 95% C.L. in the planes $(\Delta g_1^z, \Delta\kappa_\gamma)$, $(\Delta g_1^z, \lambda_\gamma)$, $(\lambda_\gamma, \Delta\kappa_\gamma)$ showing the LEP combined results.

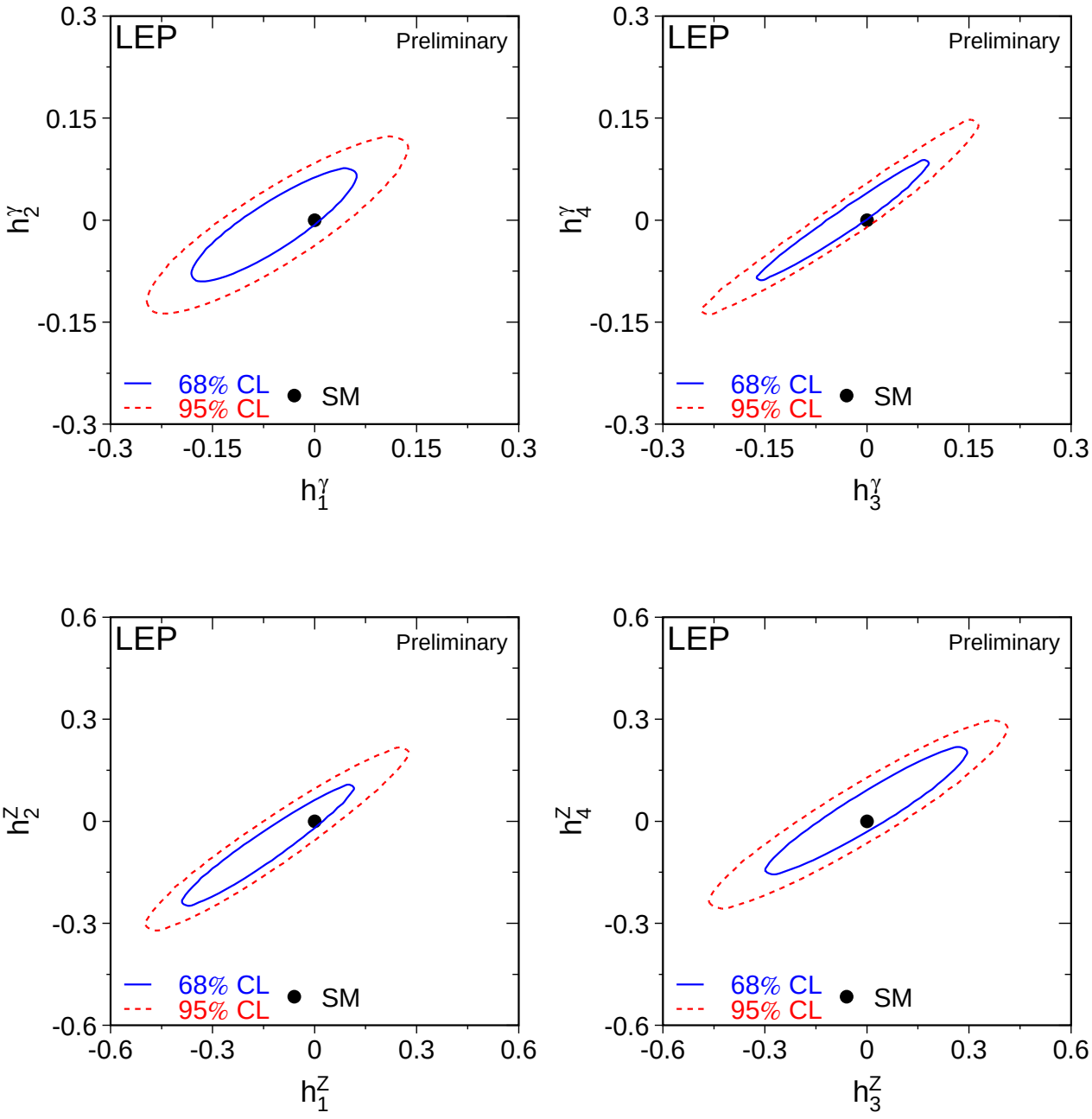

Figure 15: Contour curves of 68% C.L. and 95% C.L. in the planes (h_1^γ, h_2^γ), (h_3^γ, h_4^γ), (h_1^Z, h_2^Z) and (h_3^Z, h_4^Z) showing the LEP combined results.

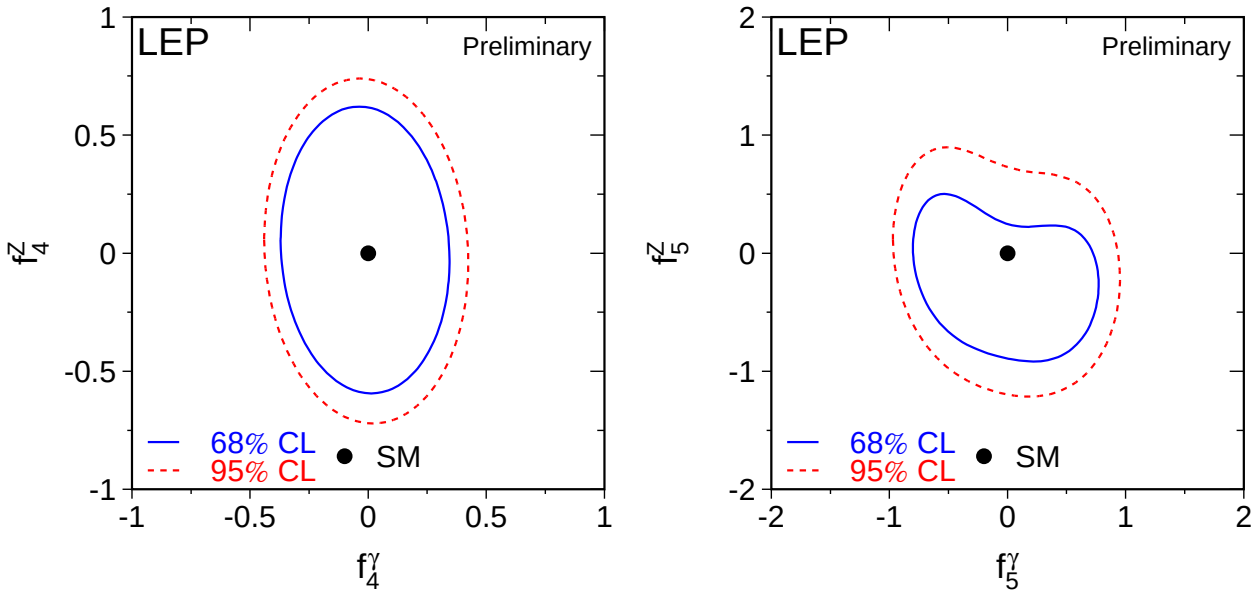

Figure 16: Contour curves of 68% C.L. and 95% C.L. in the planes (f_4^γ, f_4^Z) and (f_5^γ, f_5^Z) showing the LEP combined results.

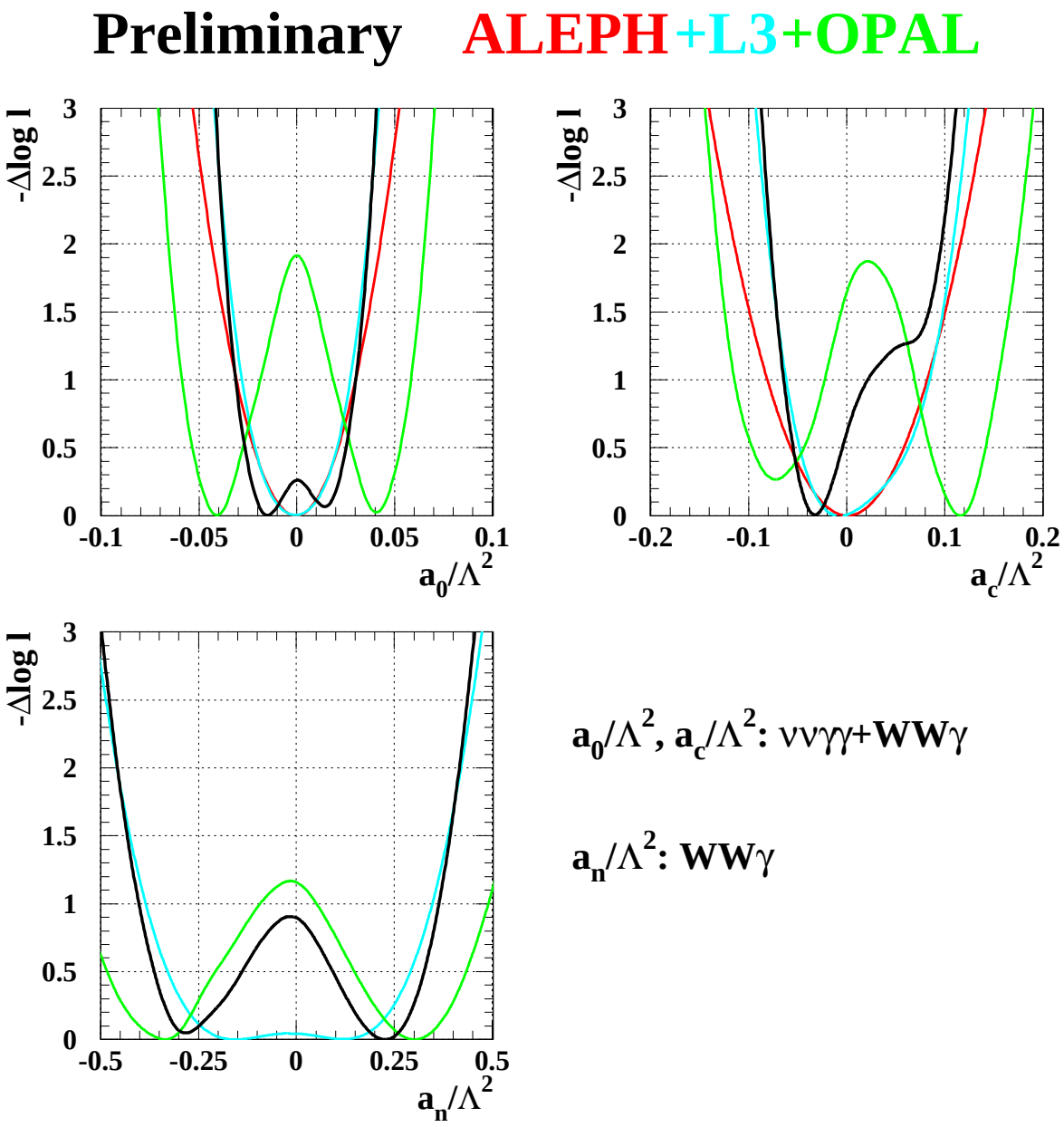

Figure 17: The $-\Delta \log \mathcal{L}$ curves of ALEPH, L3 and OPAL, and the LEP combined curve for the QGCs derived from WWγ and $\nu\bar{\nu}\gamma\gamma$ production. In each case, the minimal value is subtracted.

12 Interpretation of Results

Updates with respect to last summer:
Results on $\sin^2\theta^{\rm lept}_{\rm eff}$ from asymmetries are averaged for leptonic and hadronic channels separately. A new fit for the top mass is performed where all data except the direct measurement of $m_{\rm t}$ is included.

12.1 Number of Neutrino Species

An important aspect of our measurement concerns the information related to Z decays into invisible channels. Using the results of Table 3, the ratio of the Z decay width into invisible particles and the leptonic decay width is determined:

$$\Gamma_{\rm inv}/\Gamma_{\ell\ell} \quad = \quad 5.942 \pm 0.016\,. \tag{28}$$

The Standard Model value for the ratio of the partial widths to neutrinos and charged leptons is:

$$(\Gamma_{\nu\nu}/\Gamma_{\ell\ell})_{\rm SM} \quad = \quad 1.9912 \pm 0.0012\,. \tag{29}$$

The central value is evaluated for $m_{\rm Z} = 91.1875$ GeV and the error quoted accounts for a variation of $m_{\rm t}$ in the range $m_{\rm t} = 174.3 \pm 5.1$ GeV and a variation of $m_{\rm H}$ in the range 100 GeV $\leq m_{\rm H} \leq$ 1000 GeV. The number of light neutrino species is given by the ratio of the two expressions listed above:

$$N_\nu \quad = \quad 2.9841 \pm 0.0083, \tag{30}$$

which is 2 standard deviations below the expected value of 3.

Alternatively, one can assume 3 neutrino species and determine the width from additional invisible decays of the Z. This yields

$$\Delta\Gamma_{\rm inv} \quad = \quad -2.7 \pm 1.6 \text{ MeV}. \tag{31}$$

The measured total width is below the Standard Model expectation. If a conservative approach is taken to limit the result to only positive values of $\Delta\Gamma_{\rm inv}$, then the 95% CL upper limit on additional invisible decays of the Z is

$$\Delta\Gamma_{\rm inv} \quad < \quad 2.0 \text{ MeV}. \tag{32}$$

The uncertainties on N_ν and $\Delta\Gamma_{\rm inv}$ are dominated by the theoretical error on the luminosity. These results have therefore improved due to the improved theoretical calculations on Bhabha scattering [14].

12.2 The Coupling Parameters $\mathcal{A}_{\rm f}$

The coupling parameters $\mathcal{A}_{\rm f}$ are defined in terms of the effective vector and axial-vector neutral current couplings of fermions (Equation (4)). The LEP measurements of the forward-backward asymmetries of charged leptons (Section 2) and b and c quarks (Section 5) determine the products $A_{\rm FB}^{0,\,\rm f} = \frac{3}{4}\mathcal{A}_{\rm e}\mathcal{A}_{\rm f}$ (Equation (3)). The LEP measurements of the τ polarisation (Section 3), $\mathcal{P}_\tau(\cos\theta)$, determine $\mathcal{A}_\tau$ and $\mathcal{A}_{\rm e}$ separately (Equation (6)).

	$\mathcal{A}_\ell$	Cumulative Average	χ^2/d.o.f.
$A_{\rm FB}^{0,\ell}$	0.1512 ± 0.0042		
$\mathcal{P}_\tau(\cos\theta)$	0.1464 ± 0.0032	0.1482 ± 0.0025	0.8/1
$\mathcal{A}_\ell$ (SLD)	0.1513 ± 0.0021	0.1500 ± 0.0016	1.7/2

Table 37: Determination of the leptonic coupling parameter $\mathcal{A}_\ell$ assuming lepton universality. The second column lists the $\mathcal{A}_\ell$ values derived from the quantities listed in the first column. The third column contains the cumulative averages of these $\mathcal{A}_\ell$ results. The averages are derived assuming no correlations between the measurements. The χ^2 per degree of freedom for the cumulative averages is given in the last column.

	LEP ($\mathcal{A}_\ell = 0.1482 \pm 0.0025$)	SLD	LEP+SLD ($\mathcal{A}_\ell = 0.1500 \pm 0.0016$)	Standard Model fit
$\mathcal{A}_{\rm b}$	0.890 ± 0.024	0.922 ± 0.023	0.898 ± 0.015	0.935
$\mathcal{A}_{\rm c}$	0.619 ± 0.035	0.631 ± 0.026	0.623 ± 0.020	0.668

Table 38: Determination of the quark coupling parameters $\mathcal{A}_{\rm b}$ and $\mathcal{A}_{\rm c}$ from LEP data alone (using the LEP average for $\mathcal{A}_\ell$), from SLD data alone, and from LEP+SLD data (using the LEP+SLD average for $\mathcal{A}_\ell$) assuming lepton universality.

Table 37 shows the results for the leptonic coupling parameter $\mathcal{A}_\ell$ from the LEP and SLD measurements, assuming lepton universality.

Using the measurements of $\mathcal{A}_\ell$ one can extract $\mathcal{A}_{\rm b}$ and $\mathcal{A}_{\rm c}$ from the LEP measurements of the b and c quark asymmetries. The SLD measurements of the left-right forward-backward asymmetries for b and c quarks are direct determinations of $\mathcal{A}_{\rm b}$ and $\mathcal{A}_{\rm c}$. Table 38 shows the results on the quark coupling parameters $\mathcal{A}_{\rm b}$ and $\mathcal{A}_{\rm c}$ derived from LEP or SLD measurements separately (Equations 17 and 18) and from the combination of LEP+SLD measurements (Equation 18). The LEP extracted values of $\mathcal{A}_{\rm b}$ and $\mathcal{A}_{\rm c}$ in excellent agreement with the SLD measurements, and in reasonable agreement with the Standard Model predictions (0.935 and 0.668, respectively, essentially independent of $m_{\rm t}$ and $m_{\rm H}$). The combination of LEP and SLD of $\mathcal{A}_{\rm b}$ and $\mathcal{A}_{\rm c}$ are 2.5 and 2.3 sigma below the Standard Model respectively. This is mainly because the $\mathcal{A}_{\rm b}$ value deduced from the measured $A_{\rm FB}^{0,\rm b}$ and the combined $\mathcal{A}_\ell$ is low compared to both the Standard Model and the direct measurement of $\mathcal{A}_{\rm b}$, this can also be seen in Figure 18.

12.3 The Effective Vector and Axial-Vector Coupling Constants

The partial widths of the Z into leptons and the lepton forward-backward asymmetries (Section 2), the τ polarisation and the τ polarisation asymmetry (Section 3) are combined to determine the effective vector and axial-vector couplings for e, μ and τ. The asymmetries (Equations (3) and (6)) determine the ratio $g_{V\ell}/g_{A\ell}$ (Equation (4)), while the leptonic partial widths determine the sum of the squares of the couplings:

$$\Gamma_{\ell\ell} \;=\; \frac{G_{\rm F} m_{\rm Z}^3}{6\pi\sqrt{2}}(g_{V\ell}^2 + g_{A\ell}^2)(1+\delta_\ell^{QED})\,, \tag{33}$$

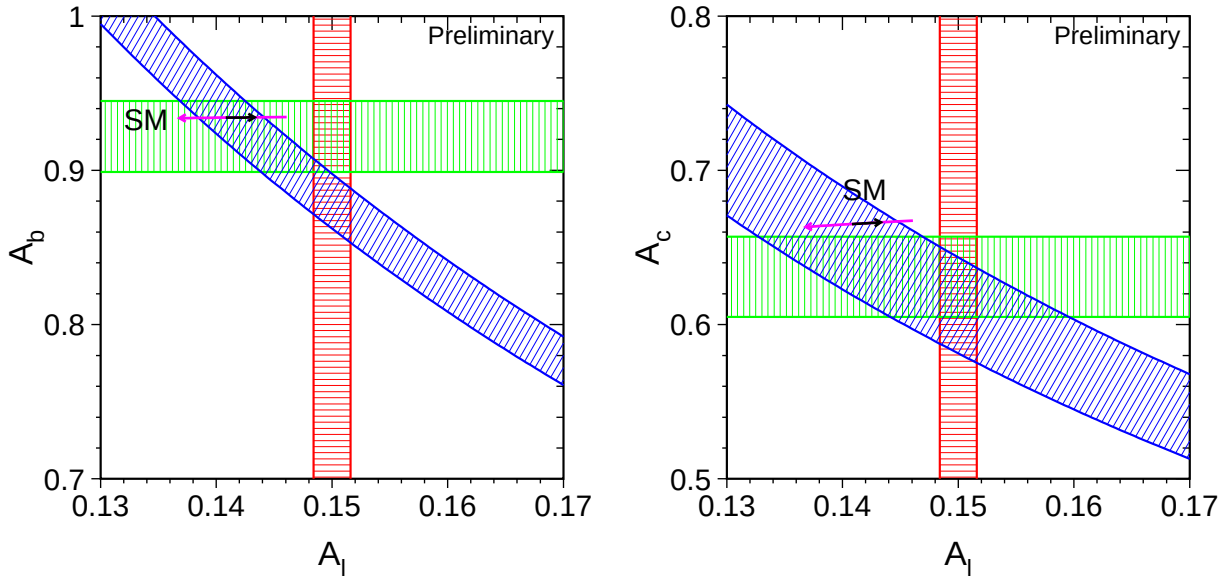

Figure 18: The measurements of the combined LEP+SLD $\mathcal{A}_\ell$ (vertical band), SLD $\mathcal{A}_\mathrm{b}$,$\mathcal{A}_\mathrm{c}$ (horizontal bands) and LEP $A_\mathrm{FB}^{0,\mathrm{b}}$,$A_\mathrm{FB}^{0,\mathrm{c}}$ (diagonal bands), compared to the Standard Model expectations (arrows). The arrow pointing to the left shows the variation in the SM prediction for m_H in the range 300^{+700}_{-187} GeV, and the arrow pointing to the right for m_t in the range 174.3 ± 5.1 GeV. Although the $A_\mathrm{FB}^{0,\mathrm{b}}$ measurements prefer a high Higgs mass, the Standard Model fit to the full set of measurements prefers a low Higgs mass, for example because of the influence of $\mathcal{A}_\ell$.

where $\delta_\ell^{QED} = 3q_\ell^2\alpha(m_\mathrm{Z}^2)/(4\pi)$ accounts for final state photonic corrections. Corrections due to lepton masses, neglected in Equation 33, are taken into account for the results presented below.

The averaged results for the effective lepton couplings are given in Table 39 for both the LEP data alone as well as for the LEP and SLD measurements. Figure 19 shows the 68% probability contours in the $g_{A\ell}$-$g_{V\ell}$ plane for the individual lepton species from the LEP data. The signs of $g_{A\ell}$ and $g_{V\ell}$ are based on the convention $g_{A\mathrm{e}} < 0$. With this convention the signs of the couplings of all charged leptons follow from LEP data alone. For comparison, the $g_{V\ell}$-$g_{A\ell}$ relation following from the measurement of $\mathcal{A}_\ell$ from SLD [177] is indicated as a band in the $g_{A\ell}$-$g_{V\ell}$-plane of Figure 19. The measured ratios of the e, μ and τ couplings provide a test of lepton universality and are shown in Table 39. All values are consistent with lepton universality. The combined results assuming universality are also given in the table and are shown as a solid contour in Figure 19.

The neutrino couplings to the Z can be derived from the measured value of the invisible width of the Z, Γ_inv (see Table 4), attributing it exclusively to the decay into three identical neutrino generations ($\Gamma_\mathrm{inv} = 3\Gamma_{\nu\nu}$) and assuming $g_{A\nu} \equiv g_{V\nu} \equiv g_\nu$. The relative sign of g_ν is chosen to be in agreement with neutrino scattering data [178], resulting in $g_\nu = +0.50068 \pm 0.00075$.

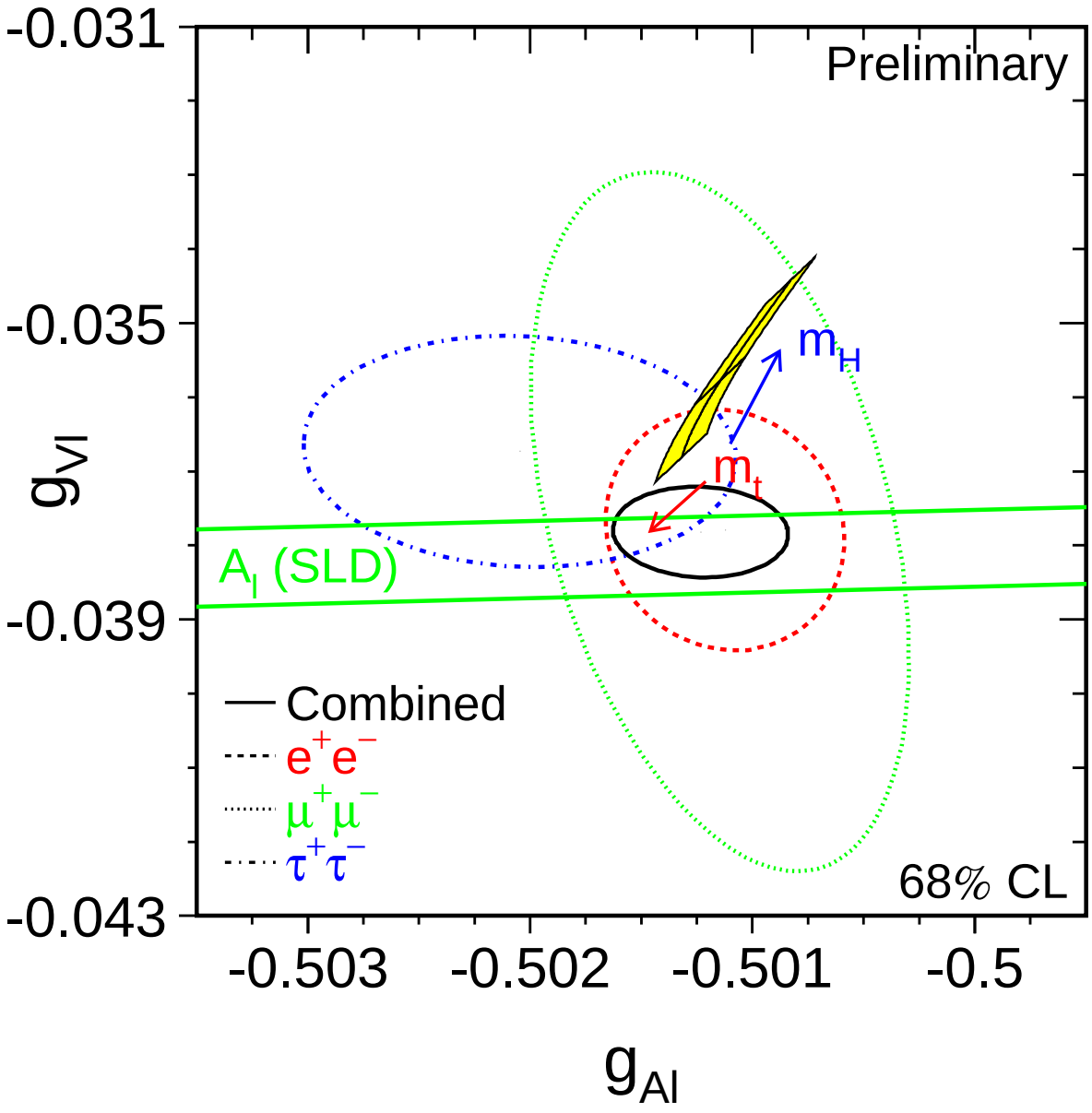

Figure 19: Contours of 68% probability in the $g_{V\ell}$-$g_{A\ell}$ plane from LEP measurements. Also shown is the one standard deviation band resulting from the $\mathcal{A}_\ell$ measurement of SLD. The solid contour results from a fit to the LEP and SLD results assuming lepton universality. The shaded region corresponds to the Standard Model prediction for $m_{\rm t} = 174.3 \pm 5.1$ GeV and $m_{\rm H} = 300^{+700}_{-187}$ GeV. The arrows point in the direction of increasing values of $m_{\rm t}$ and $m_{\rm H}$.

	Without Lepton Universality:	
	LEP	LEP+SLD
$g_{V\mathrm{e}}$	-0.0378 ± 0.0011	-0.03809 ± 0.00047
$g_{V\mu}$	-0.0376 ± 0.0031	-0.0360 ± 0.0024
$g_{V\tau}$	-0.0367 ± 0.0010	-0.0364 ± 0.0010
$g_{A\mathrm{e}}$	-0.50112 ± 0.00035	-0.50111 ± 0.00035
$g_{A\mu}$	-0.50115 ± 0.00056	-0.50120 ± 0.00054
$g_{A\tau}$	-0.50205 ± 0.00064	-0.50204 ± 0.00064
	Ratios of couplings:	
	LEP	LEP+SLD
$g_{V\mu}/g_{V\mathrm{e}}$	0.995 ± 0.093	0.962 ± 0.062
$g_{V\tau}/g_{V\mathrm{e}}$	0.972 ± 0.039	0.958 ± 0.029
$g_{A\mu}/g_{A\mathrm{e}}$	1.0001 ± 0.0014	1.0002 ± 0.0014
$g_{A\tau}/g_{A\mathrm{e}}$	1.0018 ± 0.0015	1.0019 ± 0.0015
	With Lepton Universality:	
	LEP	LEP+SLD
$g_{V\ell}$	-0.03734 ± 0.00065	-0.03782 ± 0.00040
$g_{A\ell}$	-0.50126 ± 0.00026	-0.50123 ± 0.00026
g_{ν}	$+0.50068 \pm 0.00075$	$+0.50068 \pm 0.00075$

Table 39: Results for the effective vector and axial-vector couplings derived from the combined LEP data without and with the assumption of lepton universality. For the right column the SLD measurements of A^0_{LR}, $\mathcal{A}_{\mathrm{e}}$, $\mathcal{A}_\mu$ and $\mathcal{A}_\tau$ are also included.

12.4 The Effective Electroweak Mixing Angle $\sin^2\theta^{\mathrm{lept}}_{\mathrm{eff}}$

The asymmetry measurements from LEP and SLD can be combined into a single observable, the effective electroweak mixing angle, $\sin^2\theta^{\mathrm{lept}}_{\mathrm{eff}}$, defined as:

$$\sin^2\theta^{\mathrm{lept}}_{\mathrm{eff}} \equiv \frac{1}{4}\left(1 - \frac{g_{V\ell}}{g_{A\ell}}\right), \tag{34}$$

without making strong model-specific assumptions.

For a combined average of $\sin^2\theta^{\mathrm{lept}}_{\mathrm{eff}}$ from $A^{0,\ell}_{\mathrm{FB}}$, $\mathcal{A}_\tau$ and $\mathcal{A}_{\mathrm{e}}$ only the assumption of lepton universality, already inherent in the definition of $\sin^2\theta^{\mathrm{lept}}_{\mathrm{eff}}$, is needed. Also the value derived from the measurements of $\mathcal{A}_\ell$ from SLD is given. We can also include the hadronic forward-backward asymmetries if we assume the quark couplings to be given by the Standard Model. This is justified within the Standard Model as the hadronic asymmetries $A^{0,\mathrm{b}}_{\mathrm{FB}}$ and $A^{0,\mathrm{c}}_{\mathrm{FB}}$ have a reduced sensitivity to corrections particular to the quark vertex. The results of these determinations of $\sin^2\theta^{\mathrm{lept}}_{\mathrm{eff}}$ and their combination are shown in Table 40 and in Figure 20. The combinations based on leptonic and hadronic results show a difference of 3.0 sigma, mainly caused by the two most precise measurements of $\sin^2\theta^{\mathrm{lept}}_{\mathrm{eff}}$, A^0_{LR} (SLD) and $A^{0,\mathrm{b}}_{\mathrm{FB}}$ (LEP). This is the same effect as discussed in section 12.2 and shown in Figure 18.

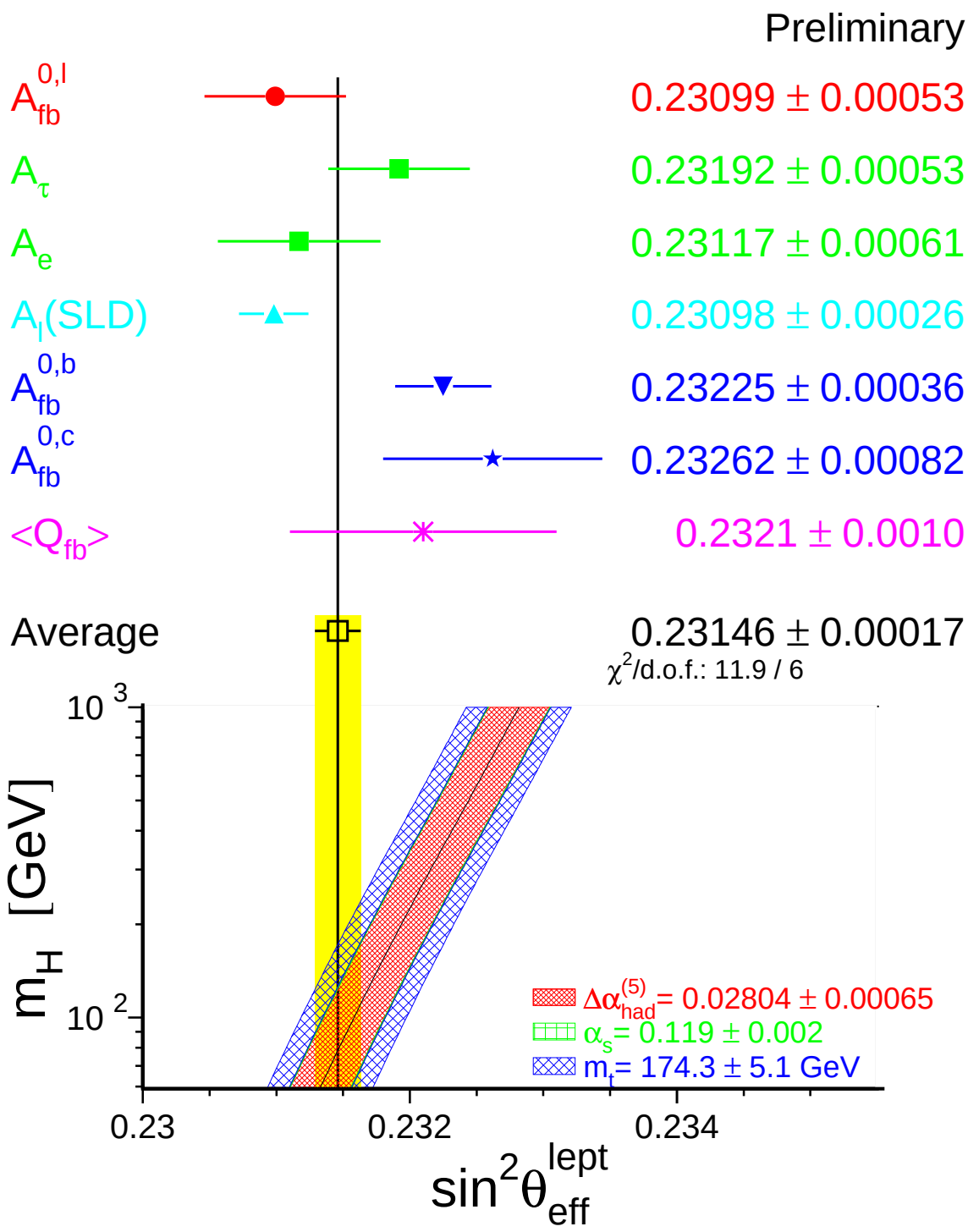

Figure 20: Comparison of several determinations of $\sin^2\theta_{\rm eff}^{\rm lept}$ from asymmetries. In the average, the small correlation between $A_{\rm FB}^{0,\,\rm b}$ and $A_{\rm FB}^{0,\,\rm c}$ is included. Also shown is the prediction of the Standard Model as a function of $m_{\rm H}$. The width of the Standard Model band is due to the uncertainties in $\Delta\alpha_{\rm had}^{(5)}(m_{\rm Z}^2)$ (see Section 12.5), $\alpha_{\rm s}(m_{\rm Z}^2)$ and $m_{\rm t}$. The total width of the band is the linear sum of these effects.

	$\sin^2\theta^{\rm lept}_{\rm eff}$	Average by Group of Observations	Cumulative Average	χ^2/d.o.f.
$A^{0,\ell}_{\rm FB}$	0.23099 ± 0.00053			
$\mathcal{A}_\tau$	0.23192 ± 0.00053			
$\mathcal{A}_{\rm e}$	0.23117 ± 0.00061	0.23138 ± 0.00032	0.23138 ± 0.00032	1.7/2
$\mathcal{A}_\ell$ (SLD)	0.23098 ± 0.00026	0.23098 ± 0.00026	0.23114 ± 0.00020	2.6/3
$A^{0,\rm b}_{\rm FB}$	0.23225 ± 0.00036			
$A^{0,\rm c}_{\rm FB}$	0.23262 ± 0.00082			
$\langle Q_{\rm FB}\rangle$	0.2321 ± 0.0010	0.23228 ± 0.00032	0.23146 ± 0.00017	11.9/6

Table 40: Determinations of $\sin^2\theta^{\rm lept}_{\rm eff}$ from asymmetries. The second column lists the $\sin^2\theta^{\rm lept}_{\rm eff}$ values derived from the quantities listed in the first column. The third column contains the averages of these numbers by groups of observations, where the groups are separated by the horizontal lines. The fourth column shows the cumulative averages. The χ^2 per degree of freedom for the cumulative averages is also given. The averages have been performed including the small correlation between $A^{0,\rm b}_{\rm FB}$ and $A^{0,\rm c}_{\rm FB}$.

12.5 Constraints on the Standard Model

The precise electroweak measurements performed at LEP and SLC and elsewhere can be used to check the validity of the Standard Model and, within its framework, to infer valuable information about its fundamental parameters. The accuracy of the measurements makes them sensitive to the mass of the top quark $m_{\rm t}$, and to the mass of the Higgs boson $m_{\rm H}$ through loop corrections. While the leading $m_{\rm t}$ dependence is quadratic, the leading $m_{\rm H}$ dependence is logarithmic. Therefore, the inferred constraints on $m_{\rm H}$ are not very strong.

The LEP and SLD [177] measurements used are summarised in Table 41 together with the results of the Standard Model fit. Also shown are the results of measurements of $m_{\rm W}$ from UA2 [179], CDF [180, 181], and DØ [182][10], measurements of the top quark mass by CDF [184] and DØ [185][11], and measurements of the neutrino-nucleon neutral to charged current ratios from CCFR [187] and NuTeV [188]. Although these latter results are quoted in terms of $\sin^2\theta_W = 1 - m_{\rm W}^2/m_{\rm Z}^2$, radiative corrections result in small $m_{\rm t}$ and $m_{\rm H}$ dependences[12] that are included in the fit. In addition, the value of the electromagnetic coupling constant $\alpha(m_{\rm Z}^2)$, which is used in the fits, is shown. An additional input parameter, not shown in the table, is the Fermi constant G_F, determined from the μ lifetime, $G_F = (1.16637 \pm 0.00001) \times 10^{-5}{\rm GeV}^{-2}$ [189]. The relative error of G_F is comparable to that of $m_{\rm Z}$; both errors have negligible effects in the fit results.

Detailed studies of the theoretical uncertainties in the Standard Model predictions due to missing higher-order electroweak corrections and their interplay with QCD corrections have been carried out in the working group on 'Precision calculations for the Z resonance' [192]. Theoretical uncertainties are evaluated by comparing different but, within our present knowledge, equivalent treatments of aspects such as resummation techniques, momentum transfer scales for vertex corrections and factorisation schemes. The effects of these theoretical uncertainties have been reduced by the inclusion of higher-order corrections [193, 194] in the electroweak libraries [195]. The use of the new QCD corrections [194] increases the value of $\alpha_{\rm s}(m_{\rm Z}^2)$ by 0.001, as expected. The effects of missing higher-order QCD corrections on $\alpha_{\rm s}(m_{\rm Z}^2)$ covers missing higher-order electroweak corrections and uncertainties in the interplay of electroweak and QCD corrections and is estimated to be about 0.002 [196]. A discussion of theoretical uncertainties in the determination of $\alpha_{\rm s}$ can be found in References 192 and 196. For the moment, the determination of the size of remaining theoretical uncertainties is still under study. All theoretical errors discussed in this paragraph are neglected for the results presented in Table 42.

At present the impact of theoretical uncertainties on the determination of SM parameters from the precise electroweak measurements is small compared with the error due to the uncertainty in the value of $\alpha(m_{\rm Z}^2)$. The uncertainty in $\alpha(m_{\rm Z}^2)$ arises from the contribution of light quarks to the photon vacuum polarisation ($\Delta\alpha^{(5)}_{\rm had}(m_{\rm Z}^2)$):

$$\alpha(m_{\rm Z}^2) = \frac{\alpha(0)}{1 - \Delta\alpha_\ell(m_{\rm Z}^2) - \Delta\alpha^{(5)}_{\rm had}(m_{\rm Z}^2) - \Delta\alpha_{\rm top}(m_{\rm Z}^2)}. \tag{35}$$

The top contribution depends on the mass of the top quark, and is therefore determined inside the electroweak libraries [195]. The leptonic contribution is calculated to third order [191] to be 0.031498. For the hadronic contribution, we use the value 0.02804 ± 0.00065 [190], which results in $1/\alpha^{(5)}(m_{\rm Z}^2) = 128.878 \pm 0.090$. This uncertainty causes an error of 0.00023 on the Standard Model

[10] See Reference 183 for a combination of these $m_{\rm W}$ measurements.

[11] See Reference 186 for a combination of these $m_{\rm t}$ measurements.

[12] The formula used is $\delta\sin^2\theta_W = -0.00142\frac{m_{\rm t}^2-(175{\rm GeV})^2}{(100{\rm GeV})^2} + 0.00048\ln(\frac{m_{\rm H}}{150{\rm GeV}})$. See Reference 188 for details.

	Measurement with Total Error	Systematic Error	Standard Model fit	Pull
$\Delta\alpha^{(5)}_{\rm had}(m^2_{\rm Z})$ [190, 191]	0.02804 ± 0.00065	0.00064	0.02804	0.0
a) LEP				
line-shape and				
lepton asymmetries:				
$m_{\rm Z}$ [GeV]	91.1875 ± 0.0021	[a] 0.0017	91.1874	0.0
$\Gamma_{\rm Z}$ [GeV]	2.4952 ± 0.0023	[a] 0.0012	2.4962	−0.4
$\sigma^0_{\rm h}$ [nb]	41.540 ± 0.037	[b] 0.028	41.480	1.6
R_ℓ	20.767 ± 0.025	[b] 0.007	20.740	1.1
$A^{0,\ell}_{\rm FB}$	0.0171 ± 0.0010	[b] 0.0003	0.0164	0.8
+ correlation matrix Table 3				
τ polarisation:				
$\mathcal{A}_\tau$	0.1439 ± 0.0042	0.0026	0.1480	−1.0
$\mathcal{A}_{\rm e}$	0.1498 ± 0.0048	0.0009	0.1480	0.4
$q\overline{q}$ charge asymmetry:				
$\sin^2\theta^{\rm lept}_{\rm eff}$ ($\langle Q_{\rm FB}\rangle$)	0.2321 ± 0.0010	0.0008	0.23140	0.7
$m_{\rm W}$ [GeV]	80.427 ± 0.046	0.035	80.402	0.5
b) SLD [177]				
$\sin^2\theta^{\rm lept}_{\rm eff}$ ($\mathcal{A}_\ell$)	0.23098 ± 0.00026	0.00018	0.23140	−1.6
c) LEP and SLD Heavy Flavour				
$R^0_{\rm b}$	0.21653 ± 0.00069	0.00053	0.21578	1.1
$R^0_{\rm c}$	0.1709 ± 0.0034	0.0022	0.1723	−0.4
$A^{0,{\rm b}}_{\rm FB}$	0.0990 ± 0.0020	0.0009	0.1038	−2.4
$A^{0,{\rm c}}_{\rm FB}$	0.0689 ± 0.0035	0.0017	0.0742	−1.5
$\mathcal{A}_{\rm b}$	0.922 ± 0.023	0.016	0.935	−0.6
$\mathcal{A}_{\rm c}$	0.631 ± 0.026	0.016	0.668	−1.4
+ correlation matrix Table 10				
d) $p\overline{p}$ and νN				
$m_{\rm W}$ [GeV] ($p\overline{p}$ [183])	80.452 ± 0.062	0.050	80.402	0.8
$1 - m^2_{\rm W}/m^2_{\rm Z}$ (νN [187, 188])	0.2255 ± 0.0021	0.0010	0.2226	1.2
$m_{\rm t}$ [GeV] ($p\overline{p}$ [186])	174.3 ± 5.1	4.0	174.3	0.0

Table 41: Summary of measurements included in the combined analysis of Standard Model parameters. Section a) summarises LEP averages, Section b) SLD results ($\sin^2\theta^{\rm lept}_{\rm eff}$ includes $A_{\rm LR}$ and the polarised lepton asymmetries), Section c) the LEP and SLD heavy flavour results and Section d) electroweak measurements from $p\overline{p}$ colliders and νN scattering. The total errors in column 2 include the systematic errors listed in column 3. Although the systematic errors include both correlated and uncorrelated sources, the determination of the systematic part of each error is approximate. The Standard Model results in column 4 and the pulls (difference between measurement and fit in units of the total measurement error) in column 5 are derived from the Standard Model fit including all data (Table 42, column 5) with the Higgs mass treated as a free parameter.

[a] The systematic errors on $m_{\rm Z}$ and $\Gamma_{\rm Z}$ contain the errors arising from the uncertainties in the LEP energy only.

[b] Only common systematic errors are indicated.

prediction of $\sin^2\theta^{\rm lept}_{\rm eff}$, an error of 1 GeV on $m_{\rm t}$, and 0.2 on $\log(m_{\rm H})$, which are included in the results. The effect on the Standard Model prediction for $\Gamma_{\ell\ell}$ is negligible. The $\alpha_{\rm s}(m^2_{\rm Z})$ values for the Standard Model fits presented in this Section are stable against a variation of $\alpha(m^2_{\rm Z})$ in the interval quoted.

At the ICHEP 2000 conference in Osaka, the BES collaboration reported on new preliminary measurements of the hadronic cross section in electron-positron collisions at 2 to 5 GeV centre-of-mass energy [197]. With these data, the hadronic vacuum polarisation is determined with improved precision: $\Delta\alpha^{(5)}_{\rm had}(m^2_{\rm Z}) = 0.02755 \pm 0.00046$ [198]. To show the effects of the uncertainty of $\alpha(m^2_{\rm Z})$, we also use this evaluation of the hadronic vacuum polarisation. There are also several evaluations of $\Delta\alpha^{(5)}_{\rm had}(m^2_{\rm Z})$ [190, 199–207] which are more theory driven. The most recent of these (Reference 206) also includes the new preliminary results from BES. All these evaluations obtain values for $\Delta\alpha^{(5)}_{\rm had}(m^2_{\rm Z})$ consistently lower than the old value of 0.02804 ± 0.00065.

Figure 21 shows a comparison of the leptonic partial width from LEP (Table 4) and the effective electroweak mixing angle from asymmetries measured at LEP and SLD (Table 40), with the Standard Model. Good agreement with the Standard Model prediction is observed. The point with the arrow shows the prediction if among the electroweak radiative corrections only the photon vacuum polarisation is included, which shows an example of evidence that LEP+SLD data are sensitive to electroweak corrections. Note that the error due to the uncertainty on $\alpha(m^2_{\rm Z})$ (shown as the length of the arrow) is larger than the experimental error on $\sin^2\theta^{\rm lept}_{\rm eff}$ from LEP and SLD. This underlines the growing importance of a precise measurement of $\sigma(\mathrm{e^+e^-} \to \text{hadrons})$ at low centre-of-mass energies.

Of the measurements given in Table 41, R_ℓ is one of the most sensitive to QCD corrections. For $m_{\rm Z} = 91.1875$ GeV, and imposing $m_{\rm t} = 174.3 \pm 5.1$ GeV as a constraint, $\alpha_{\rm s} = 0.123 \pm 0.004$ is obtained. Alternatively, σ^0_ℓ (see Table 4) which has higher sensitivity to QCD corrections and less dependence on $m_{\rm H}$ yields : $\alpha_{\rm s} = 0.118 \pm 0.003$. Typical errors arising from variation $m_{\rm H}$ are of the order of 0.001, somewhat smaller for σ^0_ℓ. These results are in very good agreement with the world average ($\alpha_{\rm s}(m^2_{\rm Z}) = 0.119 \pm 0.002$ [107]).

To test the agreement between the LEP data and the Standard Model, a fit to the data (including the LEP-II $m_{\rm W}$ determination) leaving the top quark mass and the Higgs mass as free parameters is performed. The result is shown in Table 42, column 1. This fit shows that the LEP data prefer a light top quark and a light Higgs boson, albeit with very large errors. The strongly asymmetric errors on $m_{\rm H}$ are due to the fact that to first order, the radiative corrections in the Standard Model are proportional to $\log(m_{\rm H})$. The correlation between the top quark mass and the Higgs mass is 0.63 (see Figure 22).

The data can also be used within the Standard Model to determine the top quark and W masses indirectly, which can be compared to the direct measurements performed at the $\mathrm{p\overline{p}}$ colliders and LEP. In the second fit, all the results in Table 41, except the LEP-II and $\mathrm{p\overline{p}}$ colliders $m_{\rm W}$ and $m_{\rm t}$ results are used. The results are shown in column 2 of Table 42. The indirect measurements of $m_{\rm W}$ and $m_{\rm t}$ from this data sample are shown in Figure 23, compared with the direct measurements. Also shown is the Standard Model predictions for Higgs masses between 113 and 1000 GeV. As can be seen in the figure, the indirect and direct measurements of $m_{\rm W}$ and $m_{\rm t}$ are in good agreement, and both sets prefer a low Higgs mass.

For the third fit, the direct $m_{\rm t}$ measurements is used to obtain the best indirect determination of $m_{\rm W}$. The result is shown in column 3 of Table 42. Also here, the indirect determination of W boson mass 80.386 ± 0.025 GeV is in excellent agreement with the combination of direct measurements from LEP and $\mathrm{p\overline{p}}$ colliders [183] of $m_{\rm W} = 80.436 \pm 0.037$ GeV.

For the next fit, (column 4 of Table 42), the direct $m_{\rm W}$ measurements from LEP and $\rm p\overline{p}$ colliders are included to obtain $m_{\rm t} = 174.4^{+9.3}_{-6.7}$ GeV, in good agreement with the direct measurement of $m_{\rm t} = 174.3 \pm 5.1$ GeV.

Finally, the best constraints on $m_{\rm H}$ are obtained when all data are used in the fit. The results of this fit are shown in column 5 of Table 42 and in Figure 22. In Figures 24 and 25 the sensitivity of the LEP and SLD measurements to the Higgs mass is shown. As can be seen, the most sensitive measurements are the asymmetries. A reduced uncertainty for the value of $\alpha(m_{\rm Z}^2)$ would therefore result in an improved constraint on $m_{\rm H}$, as shown in Figures 21 and 26.

In Figure 26 the observed value of $\Delta\chi^2 \equiv \chi^2 - \chi^2_{\rm min}$ as a function of $m_{\rm H}$ is plotted for the fit including all data. The solid curve is the result using ZFITTER, and corresponds to the last column of Table 42. The shaded band represents the uncertainty due to uncalculated higher-order corrections, as estimated by ZFITTER and TOPAZ0. The 95% confidence level upper limit on $m_{\rm H}$ (taking the band into account) is 165 GeV. The lower limit on $m_{\rm H}$ of approximately 113 GeV obtained from direct searches [208] has not been used in this limit determination. Also shown is the result (dashed curve) obtained when using $\alpha^{(5)}(m_{\rm Z}^2)$ of Reference 198. The fit results in $\log(m_{\rm H}/{\rm GeV}) = 1.94^{+0.22}_{-0.24}$ corresponding to $m_{\rm H} = 88^{+60}_{-37}$ GeV and an upper limit on $m_{\rm H}$ of approximately 206 GeV.

	- 1 - LEP including LEP-II $m_{\rm W}$	- 2 - all data except $m_{\rm W}$ and $m_{\rm t}$	- 3 - all data except $m_{\rm W}$	- 4 - all data except $m_{\rm t}$	- 5 - all data
$m_{\rm t}$ [GeV]	179^{+13}_{-10}	169^{+10}_{-8}	$173.0^{+4.7}_{-4.5}$	$174.4^{+9.3}_{-6.7}$	$174.3^{+4.4}_{-4.1}$
$m_{\rm H}$ [GeV]	135^{+262}_{-83}	56^{+75}_{-27}	74^{+68}_{-37}	61^{+94}_{-32}	60^{+52}_{-29}
$\log(m_{\rm H}/{\rm GeV})$	$2.13^{+0.47}_{-0.41}$	$1.75^{+0.37}_{-0.29}$	$1.87^{+0.28}_{-0.30}$	$1.78^{+0.41}_{-0.32}$	$1.78^{+0.27}_{-0.28}$
$\alpha_{\rm s}(m_{\rm Z}^2)$	0.120 ± 0.003	0.119 ± 0.003	0.119 ± 0.003	0.118 ± 0.003	0.118 ± 0.003
χ^2/d.o.f.	13/9	19/12	20/13	21/14	21/15
$\sin^2\theta^{\rm lept}_{\rm eff}$	0.23167	0.23147	0.23147	0.23140	0.23140
	± 0.00020	± 0.00017	± 0.00017	± 0.00016	± 0.00016
$1 - m_{\rm W}^2/m_{\rm Z}^2$	0.2229	0.2231	0.2229	0.2226	0.2226
	± 0.0006	± 0.0007	± 0.0005	± 0.0005	± 0.0004
$m_{\rm W}$ [GeV]	80.383 ± 0.029	80.374 ± 0.034	80.386 ± 0.025	80.402 ± 0.025	80.402 ± 0.020

Table 42: Results of the fits to LEP data alone, to all data except the direct determinations of $m_{\rm t}$ and $m_{\rm W}$ ($\rm p\overline{p}$ collider and LEP-II), to all data except direct $m_{\rm W}$ determinations, and to all data. As the sensitivity to $m_{\rm H}$ is logarithmic, both $m_{\rm H}$ as well as $\log(m_{\rm H}/{\rm GeV})$ are quoted. The bottom part of the table lists derived results for $\sin^2\theta^{\rm lept}_{\rm eff}$, $1 - m_{\rm W}^2/m_{\rm Z}^2$ and $m_{\rm W}$. See text for a discussion of theoretical errors not included in the errors above.

13 Prospects for the Future

Most of the measurements from data taken at or near the Z resonance, both at LEP as well as at SLC, that are presented in this report are either final or are being finalised. The major improvements will therefore take place in the high energy data. With more than 600 pb^{-1} per experiment, LEP-II will lead to substantially improved measurements of certain electroweak parameters. As a result, the measurements of m_{W} are likely to match the error obtained via the radiative corrections of the Z data, providing a further important test of the Standard Model. In the measurement of the $\mathrm{WW}\gamma$ and WWZ triple-gauge-boson couplings the increase in LEP-II statistics, together with the increased sensitivity at higher beam energies, will lead to an improvement in the current precision.

14 Conclusions

The combination of the many precise electroweak results yields stringent constraints on the Standard Model. All measurements agree with the predictions. In addition, the results are sensitive to the Higgs mass.

The experiments wish to stress that this report reflects a preliminary status at the time of the 2000 summer conferences. A definitive statement on these results must wait for publication by each collaboration.

Acknowledgements

We would like to thank the CERN accelerator divisions for the efficient operation of the LEP accelerator, the precise information on the absolute energy scale and their close cooperation with the four experiments. The SLD collaboration would like to thank the SLAC accelerator department for the efficient operation of the SLC accelerator. We would also like to thank members of the CDF, DØ and NuTeV Collaborations for making results available to us in advance of the conferences and for useful discussions concerning their combination. Finally, the results of the section on Standard Model constraints would not have been possible without the close collaboration of many theorists.

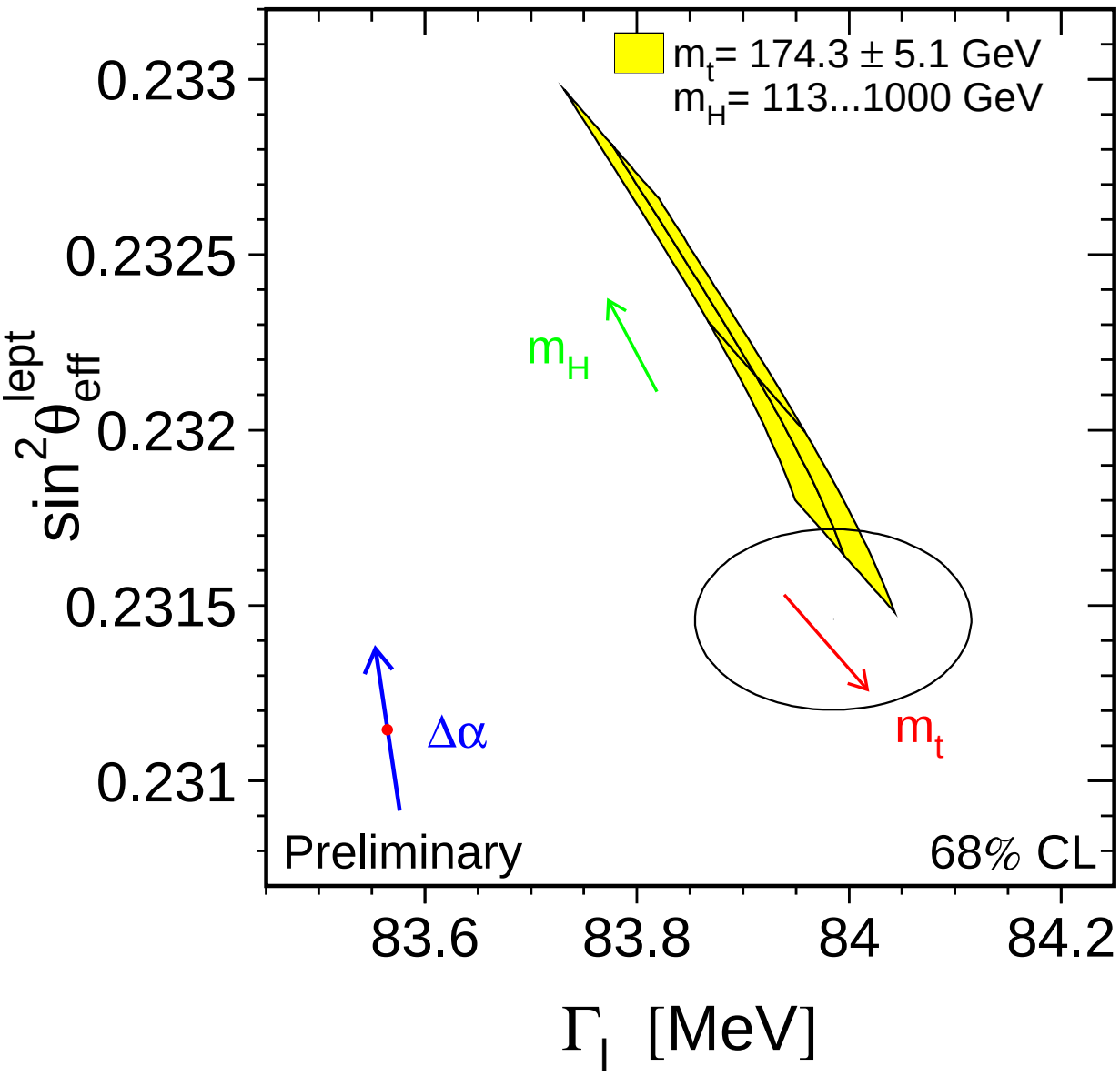

Figure 21: LEP-I+SLD measurements of $\sin^2\theta^{\rm lept}_{\rm eff}$ (Table 40) and $\Gamma_{\ell\ell}$ (Table 4) and the Standard Model prediction. The point shows the predictions if among the electroweak radiative corrections only the photon vacuum polarisation is included. The corresponding arrow shows variation of this prediction if $\alpha(m_{\rm Z}^2)$ is changed by one standard deviation. This variation gives an additional uncertainty to the Standard Model prediction shown in the figure.

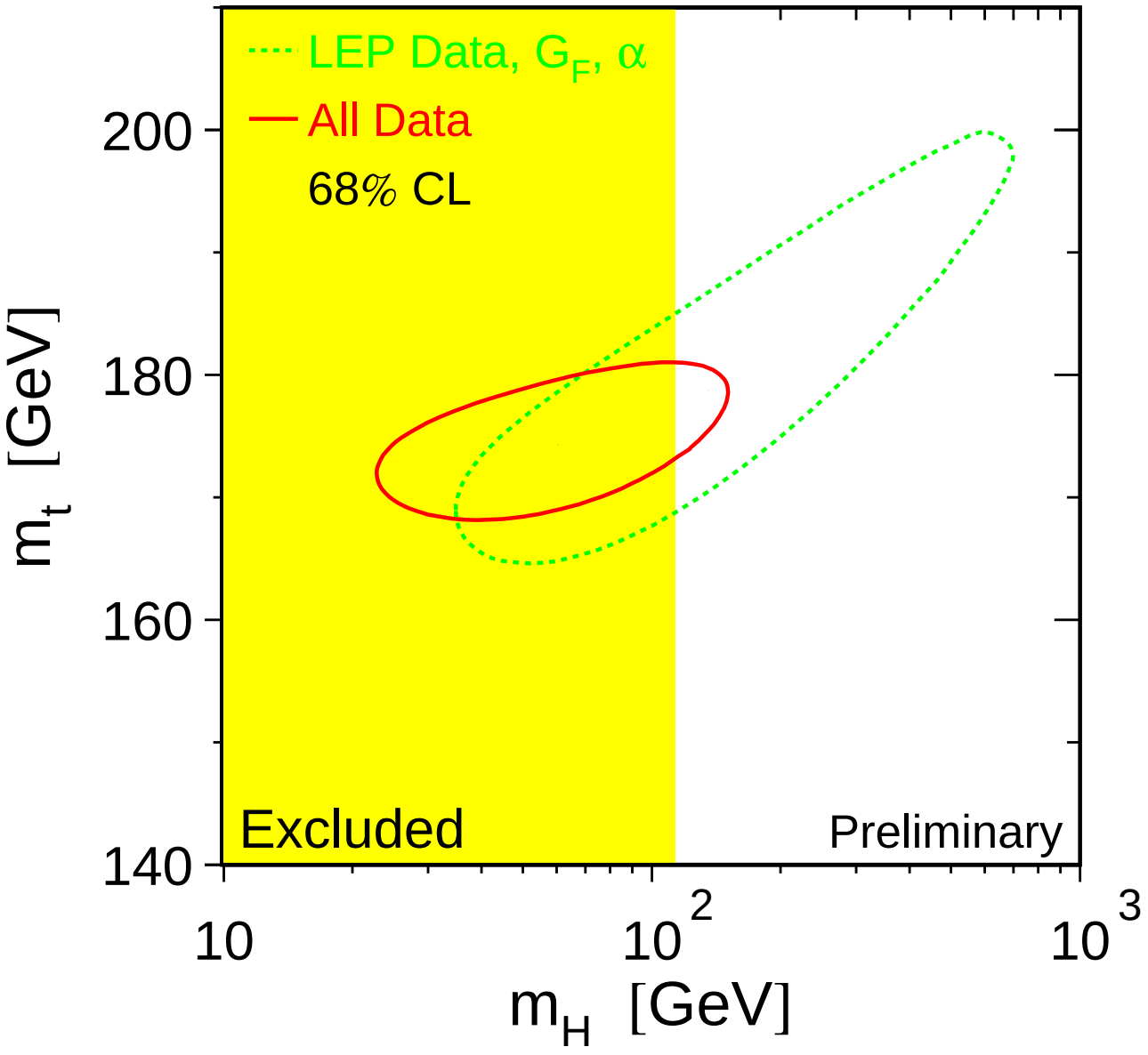

Figure 22: The 68% confidence level contours in m_t and m_H for the fits to LEP data only (dashed curve) and to all data including the CDF/DØ m_t measurement (solid curve). The vertical band shows the 95% CL exclusion limit on m_H from the direct search.

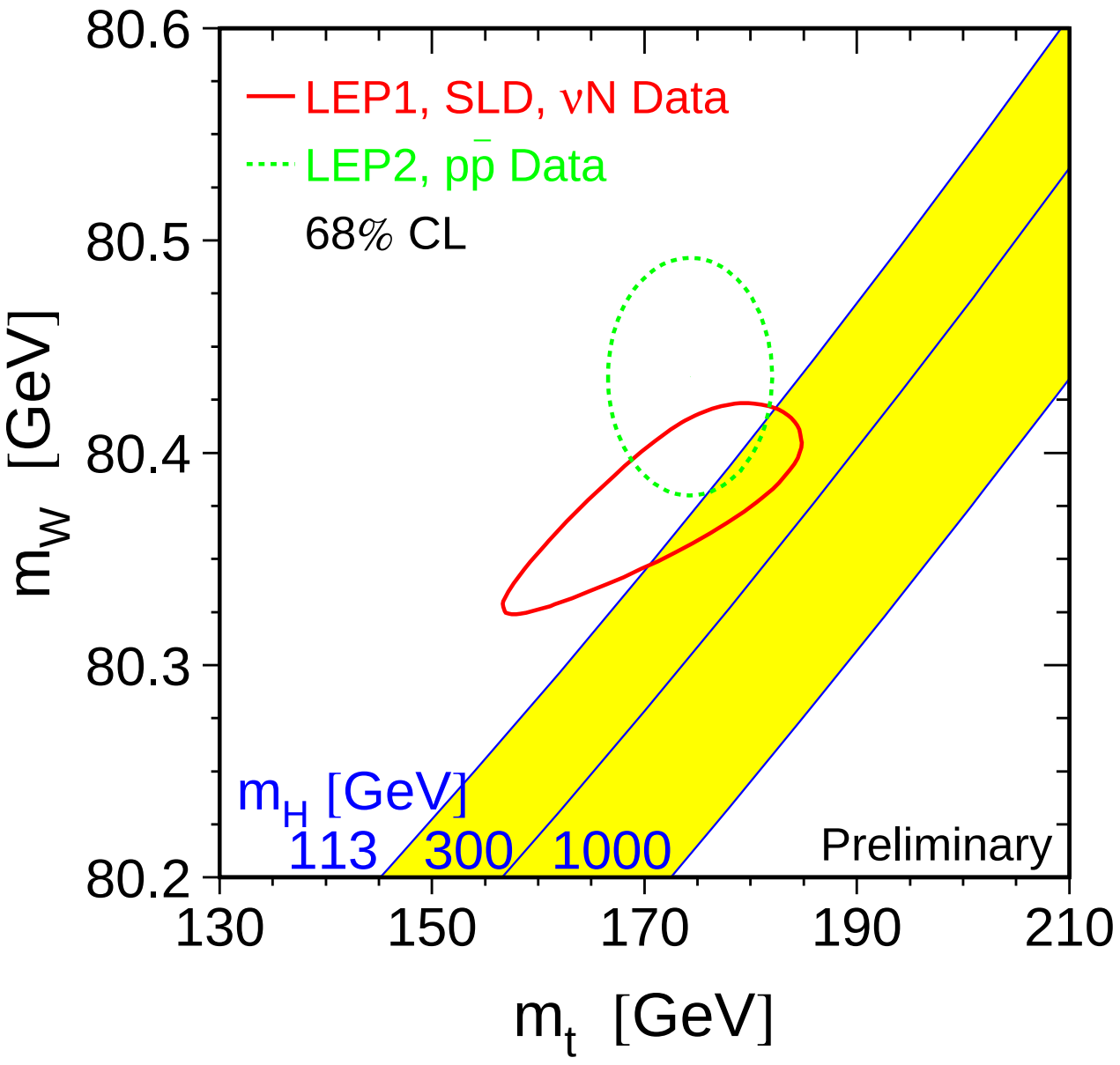

Figure 23: The comparison of the indirect measurements of m_{W} and m_{t} (LEP-I+SLD+νN data) (solid contour) and the direct measurements ($\mathrm{p\overline{p}}$ colliders and LEP-II data) (dashed contour). In both cases the 68% CL contours are plotted. Also shown is the Standard Model relationship for the masses as a function of the Higgs mass.

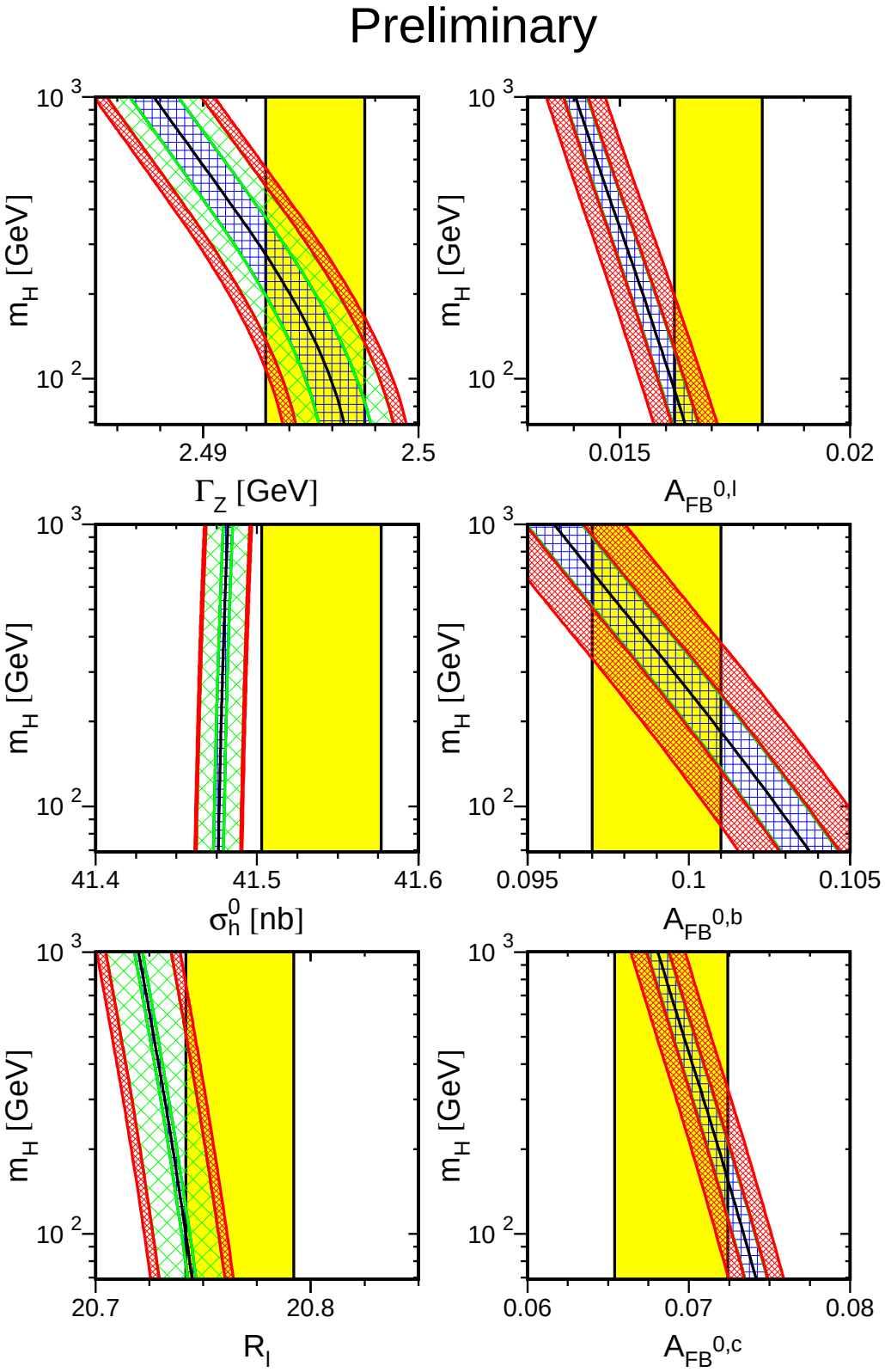

Figure 24: Comparison of LEP-I measurements with the Standard Model prediction as a function of m_{H}. The measurement with its error is shown as the vertical band. The width of the Standard Model band is due to the uncertainties in $\Delta\alpha^{(5)}_{\mathrm{had}}(m^2_{\mathrm{Z}})$, $\alpha_{\mathrm{s}}(m^2_{\mathrm{Z}})$ and m_{t}. The total width of the band is the linear sum of these effects. See Figure 25 for the definition of these uncertainties.

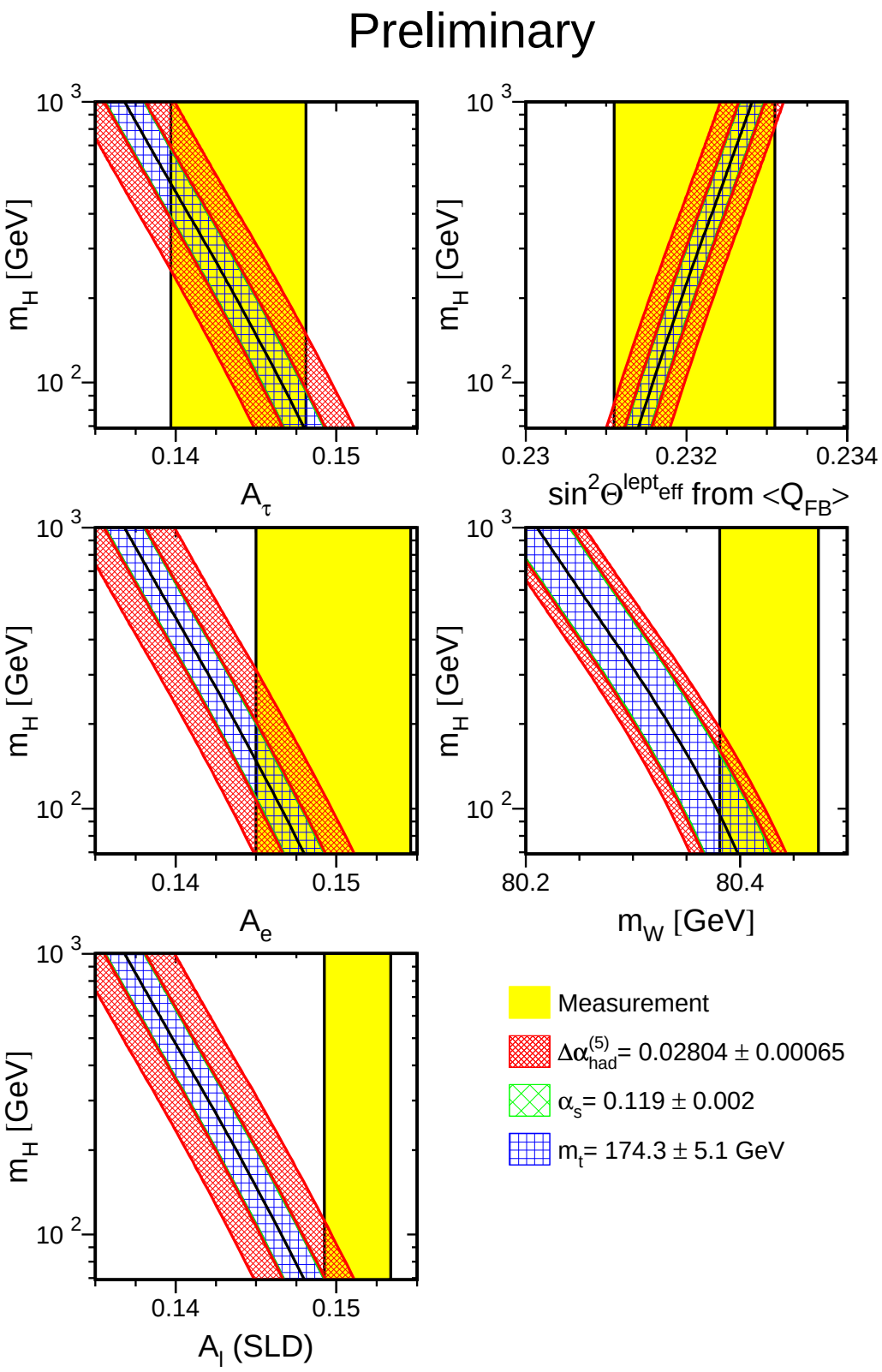

Figure 25: Comparison of LEP-I measurements with the Standard Model prediction as a function of $m_{\rm H}$ (*c.f.* Figure 24). Also shown is the comparison of the SLD measurement of $A^0_{\rm LR}$ with the Standard Model.

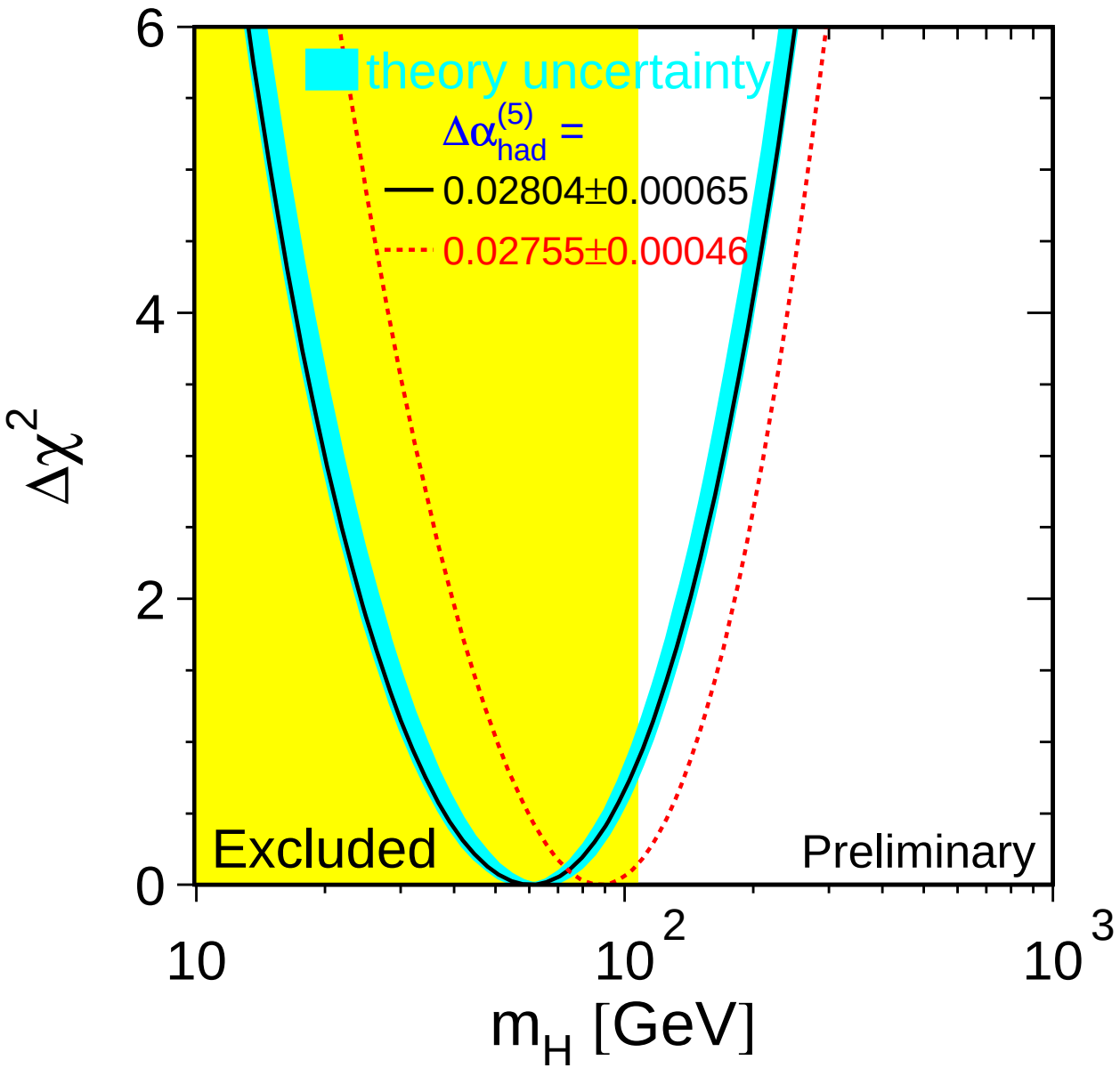

Figure 26: $\Delta\chi^2 = \chi^2 - \chi^2_{min}$ *vs.* $m_{\rm H}$ curve. The line is the result of the fit using all data (last column of Table 42); the band represents an estimate of the theoretical error due to missing higher order corrections. The vertical band shows the 95% CL exclusion limit on $m_{\rm H}$ from the direct search. The dashed curve is the result obtained using the evaluation of $\Delta\alpha^{(5)}_{\rm had}(m^2_{\rm Z})$ from Reference 198.

Appendix

A Heavy-Flavour Fit including Off-Peak Asymmetries

The full 18 parameter fit to the LEP and SLD data gave the following results:

$$
\begin{aligned}
R_{\mathrm{b}}^{0} &= 0.21652 \pm 0.00069 \\
R_{\mathrm{c}}^{0} &= 0.1702 \pm 0.0034 \\
A_{\mathrm{FB}}^{\mathrm{b\bar{b}}}(-2) &= 0.0572 \pm 0.0075 \\
A_{\mathrm{FB}}^{\mathrm{c\bar{c}}}(-2) &= -0.027 \pm 0.016 \\
A_{\mathrm{FB}}^{\mathrm{b\bar{b}}}(\mathrm{pk}) &= 0.0973 \pm 0.0021 \\
A_{\mathrm{FB}}^{\mathrm{c\bar{c}}}(\mathrm{pk}) &= 0.0621 \pm 0.0036 \\
A_{\mathrm{FB}}^{\mathrm{b\bar{b}}}(+2) &= 0.1106 \pm 0.0065 \\
A_{\mathrm{FB}}^{\mathrm{c\bar{c}}}(+2) &= 0.131 \pm 0.013 \\
\mathcal{A}_{\mathrm{b}} &= 0.922 \pm 0.022 \\
\mathcal{A}_{\mathrm{c}} &= 0.631 \pm 0.026 \\
\mathrm{BR}(\mathrm{b} \to \ell) &= 0.1056 \pm 0.0019 \\
\mathrm{BR}(\mathrm{b} \to \mathrm{c} \to \bar{\ell}) &= 0.0801 \pm 0.0026 \\
\mathrm{BR}(\mathrm{c} \to \ell) &= 0.0984 \pm 0.0032 \\
\overline{\chi} &= 0.1194 \pm 0.0043 \\
f(\mathrm{D}^{+}) &= 0.237 \pm 0.016 \\
f(\mathrm{D_s}) &= 0.121 \pm 0.025 \\
f(\mathrm{c_{baryon}}) &= 0.090 \pm 0.022 \\
\mathrm{P}(\mathrm{c} \to \mathrm{D}^{*+}) \times \mathrm{BR}(\mathrm{D}^{*+} \to \pi^{+}\mathrm{D}^{0}) &= 0.1631 \pm 0.0050
\end{aligned}
$$

with a χ^2/d.o.f. of $52/(98-18)$. The corresponding correlation matrix is given in Table 43. The energy for the peak-2, peak and peak$+2$ results are respectively 89.55 GeV, 91.26 GeV and 92.94 GeV. Note that the asymmetry results shown here are not the pole asymmetries shown in Section 5.2.2. The non-electroweak parameters do not depend on the treatment of the asymmetries.

	1) R_b	2) R_c	3) $A_{FB}^{b\bar{b}}$ (−2)	4) $A_{FB}^{c\bar{c}}$ (−2)	5) $A_{FB}^{b\bar{b}}$ (pk)	6) $A_{FB}^{c\bar{c}}$ (pk)	7) $A_{FB}^{b\bar{b}}$ (+2)	8) $A_{FB}^{c\bar{c}}$ (+2)	9) $\mathcal{A}_b$	10) $\mathcal{A}_c$	11) BR (1)	12) BR (2)	13) BR (3)	14) $\overline{\chi}$	15) $f(D^+)$	16) $f(D_s)$	17) $f(c_{bar.})$	18) PcDst
1)	1.00	−0.13	0.00	−0.01	−0.02	0.01	−0.01	0.00	−0.04	0.02	−0.09	−0.02	−0.02	−0.02	−0.16	−0.04	0.12	0.11
2)	−0.13	1.00	0.01	0.01	0.05	−0.01	0.02	−0.01	0.02	−0.02	0.05	−0.01	−0.32	0.04	−0.13	0.19	0.18	−0.49
3)	0.00	0.01	1.00	0.14	0.04	0.01	0.02	0.00	0.01	0.00	0.02	−0.03	0.01	0.06	0.00	0.00	0.00	−0.01
4)	−0.01	0.01	0.14	1.00	0.01	0.02	0.00	0.00	0.00	0.00	0.01	−0.01	0.02	0.01	0.00	0.00	0.00	0.01
5)	−0.02	0.05	0.04	0.01	1.00	0.10	0.10	0.00	0.02	0.00	0.01	−0.09	0.02	0.16	0.01	0.03	0.00	−0.03
6)	0.01	−0.01	0.01	0.02	0.10	1.00	0.00	0.09	0.00	0.01	0.14	−0.17	−0.05	0.16	0.00	0.00	−0.01	0.00
7)	−0.01	0.02	0.02	0.00	0.10	0.00	1.00	0.13	0.01	0.00	−0.01	−0.03	0.01	0.07	0.01	0.01	0.00	−0.01
8)	0.00	−0.01	0.00	0.00	0.00	0.09	0.13	1.00	0.00	0.00	0.02	−0.04	−0.03	0.02	−0.01	−0.01	0.00	0.00
9)	−0.04	0.02	0.01	0.00	0.02	0.00	0.01	0.00	1.00	0.14	−0.02	0.00	0.05	0.09	−0.01	0.00	0.00	−0.01
10)	0.02	−0.02	0.00	0.00	0.00	0.01	0.00	0.00	0.14	1.00	0.02	−0.03	−0.03	0.01	−0.01	0.00	0.01	0.01
11)	−0.09	0.05	0.02	0.01	0.01	0.14	−0.01	0.02	−0.02	0.02	1.00	−0.33	0.14	0.43	0.04	0.01	−0.02	−0.02
12)	−0.02	−0.01	−0.03	−0.01	−0.09	−0.17	−0.03	−0.04	0.00	−0.03	−0.33	1.00	−0.03	−0.40	0.01	−0.01	0.00	0.01
13)	−0.02	−0.32	0.01	0.02	0.02	−0.05	0.01	−0.03	0.05	−0.03	0.14	−0.03	1.00	0.20	0.02	−0.04	−0.04	0.16
14)	−0.02	0.04	0.06	0.01	0.16	0.16	0.07	0.02	0.09	0.01	0.43	−0.40	0.20	1.00	0.01	0.01	−0.01	−0.03
15)	−0.16	−0.13	0.00	0.00	0.01	0.00	0.01	−0.01	−0.01	−0.01	0.04	0.01	0.02	0.01	1.00	−0.38	−0.27	0.11
16)	−0.04	0.19	0.00	0.00	0.03	0.00	0.01	−0.01	0.00	0.00	0.01	−0.01	−0.04	0.01	−0.38	1.00	−0.46	−0.11
17)	0.12	0.18	0.00	0.00	0.00	−0.01	0.00	0.00	0.00	0.01	−0.02	0.00	−0.04	−0.01	−0.27	−0.46	1.00	−0.17
18)	0.11	−0.49	−0.01	0.01	−0.03	0.00	−0.01	0.00	−0.01	0.01	−0.02	0.01	0.16	−0.03	0.11	−0.11	−0.17	1.00

Table 43: The correlation matrix for the set of the 18 heavy flavour parameters. BR(1), BR(2) and BR(3) denote BR($b \to \ell$), BR($b \to c \to \bar{\ell}$) and BR($c \to \ell$) respectively, PcDst denotes P($c \to D^{*+}$) × BR($D^{*+} \to \pi^+ D^0$).

The Measurements used in the Heavy Flavour Averages

In the following 20 tables the results used in the combination are listed. In each case an indication of the dataset used and the type of analysis is given. Preliminary results are indicated by the symbol "†". The values of centre-of-mass energy are given where relevant. In each table, the result used as input to the average procedure is given followed by the statistical error, the correlated and uncorrelated systematic errors, the total systematic error, and any dependence on other electroweak parameters. In the case of the asymmetries, the measurement moved to a common energy (89.55 GeV, 91.26 GeV and 92.94 GeV, respectively, for peak−2, peak and peak+2 results) is quoted as *corrected* asymmetry.

Contributions to the correlated systematic error quoted here are from any sources of error shared with one or more other results from different experiments in the same table, and the uncorrelated errors from the remaining sources. In the case of $\mathcal{A}_c$ and $\mathcal{A}_b$ from SLD the quoted correlated systematic error has contributions from any source shared with one or more other measurements from LEP experiments. Constants such as $a(x)$ denote the dependence on the assumed value of $x^{\rm used}$, which is also given.

	ALEPH	DELPHI	L3	OPAL	SLD
	92-95 [24]	92-95 [25]	94-95 [26]	92-95 [27]	93-98† [28]
R_b	0.2157	0.2163	0.2174	0.2174	0.2167
Statistical	0.0009	0.0007	0.0015	0.0011	0.0009
Uncorrelated	0.0007	0.0004	0.0015	0.0009	0.0008
Correlated	0.0007	0.0004	0.0018	0.0008	0.0005
Total Systematic	0.0009	0.0006	0.0023	0.0012	0.0010
$a(R_c)$	-0.0033	-0.0041	-0.0376	-0.0122	-0.0057
$R_c^{\rm used}$	0.1720	0.1720	0.1734	0.1720	0.1710
$a({\rm BR}(c\to\ell))$			-0.0133	-0.0067	
${\rm BR}(c\to\ell)^{\rm used}$			9.80	9.80	
$a(f(D^+))$	-0.0010	-0.0010	-0.0086	-0.0029	-0.0008
$f(D^+)^{\rm used}$	0.2330	0.2330	0.2330	0.2380	0.2370
$a(f(D_s))$	-0.0001	0.0001	-0.0005	-0.0001	-0.0003
$f(D_s)^{\rm used}$	0.1020	0.1030	0.1030	0.1020	0.1140
$a(f(\Lambda_c))$	0.0002	0.0003	0.0008	0.0003	-0.0003
$f(\Lambda_c)^{\rm used}$	0.0650	0.0630	0.0630	0.0650	0.0730

Table 44: The measurements of R_b. All measurements use a lifetime tag enhanced by other features like invariant mass cuts or high p_T leptons.

	ALEPH			DELPHI		OPAL		SLD
	91-95 c-count [33]	91-95 D meson [29]	92-95 lepton [29]	92-95 c-count [31]	92-95 D meson [31]	91-94 c-count [34]	90-95 D meson [32]	93-97† vtx-mass [28]
R_c	0.1734	0.1679	0.1668	0.1692	0.1610	0.164	0.1760	0.1732
Statistical	0.0049	0.0082	0.0062	0.0047	0.0104	0.011	0.0095	0.0041
Uncorrelated	0.0057	0.0078	0.0059	0.0050	0.0064	0.012	0.0102	0.0025
Correlated	0.0101	0.0026	0.0010	0.0083	0.0060	0.010	0.0062	0.0004
Total Systematic	0.0116	0.0082	0.0059	0.0097	0.0088	0.016	0.0120	0.0025
$a(R_b)$		-0.0050						-0.0239
R_b^{used}		0.2159						0.2175
$a(BR(c \to \ell))$			-0.1646					
$BR(c \to \ell)^{used}$			9.80					

Table 45: The measurements of R_c^0. "c-count" denotes the determination of R_c^0 from the sum of production rates of weakly decaying charmed hadrons. "D meson" denotes any single/double tag analysis using exclusive and/or inclusive D meson reconstruction.

	ALEPH				DELPHI			L3	OPAL		
	90-95 lepton [37]	90-95 lepton [37]	90-95 lepton [37]	91-95 jet charge [41]	93-95† lepton [38]	92-95 D-meson [46]	92-95 jet charge [42]	90-95 lepton [39]	91-95 jet charge [44]	90-95† lepton [40]	90-95 D-meson [47]
$\sqrt{s}$ (GeV)	88.380	89.380	90.210	89.430	89.433	89.434	89.550	89.500	89.440	89.490	89.490
$A_{\rm FB}^{\rm bb}(-2)$	-3.53	5.47	9.11	7.46	5.90	5.65	6.80	6.14	4.10	3.56	-9.30
$A_{\rm FB}^{\rm bb}(-2)$Corrected	5.87			7.75	6.18	5.93	6.80	6.26	4.36	3.70	-9.16
Statistical	1.90			1.78	2.20	7.59	1.80	2.93	2.10	1.73	10.80
Uncorrelated	0.39			0.19	0.08	0.91	0.12	0.37	0.25	0.16	2.51
Correlated	0.70			0.15	0.08	0.08	0.01	0.19	0.02	0.04	1.41
Total Systematic	0.80			0.24	0.12	0.91	0.13	0.41	0.25	0.16	2.88
$a(R_{\rm b})$	-0.3069			-0.2430	-1.1543		-0.1962	-1.4467	-0.7300	-0.1000	
$R_{\rm b}^{\rm used}$	0.2192			0.2155	0.2164		0.2158	0.2170	0.2150	0.2155	
$a(R_{\rm c})$	0.0362			1.4800	1.0444		0.3200	0.3612	0.0700	0.1000	
$R_{\rm c}^{\rm used}$	0.1710			0.1726	0.1671		0.1720	0.1734	0.1730	0.1720	
$a(A_{\rm FB}^{\rm c\bar{c}}(-2))$	-0.2244			-0.2501				-0.1000	-0.3156		
$A_{\rm FB}^{\rm c\bar{c}}(-2)^{\rm used}$	-2.34			-2.70				-2.50	-2.81		
$a({\rm BR}({\rm b}\to\ell))$	-0.2486				-1.0154			-1.0290		0.3406	
${\rm BR}({\rm b}\to\ell)^{\rm used}$	11.34				10.56			10.50		10.90	
$a({\rm BR}({\rm b}\to{\rm c}\to\bar{\ell}))$	-0.1074				-0.1424			-0.1440		-0.5298	
${\rm BR}({\rm b}\to{\rm c}\to\bar{\ell})^{\rm used}$	7.86				8.07			8.00		8.30	
$a({\rm BR}({\rm c}\to\ell))$	-0.0474				0.7224			0.5096		0.1960	
${\rm BR}({\rm c}\to\ell)^{\rm used}$	9.80				9.90			9.80		9.80	
$a(\overline{\chi})$	5.259				1.3054						
$\overline{\chi}^{\rm used}$	0.12460				0.11770						
$a(f({\rm D}^+))$						0.5083	0.0949				
$f({\rm D}^+)^{\rm used}$						0.2210	0.2330				
$a(f({\rm D_s}))$						0.1742	0.0035				
$f({\rm D_s})^{\rm used}$						0.1120	0.1020				
$a(f(\Lambda_{\rm c}))$						-0.0191	-0.0225				
$f(\Lambda_{\rm c})^{\rm used}$						0.0840	0.0630				

Table 46: The measurements of $A_{\rm FB}^{\rm b\bar{b}}(-2)$. All numbers are given in %.

	ALEPH	DELPHI		OPAL	
	91-95 D-meson [45]	93-95† lepton [38]	92-95 D-meson [46]	90-95† lepton [40]	90-95 D-meson [47]
$\sqrt{s}$ (GeV)	89.370	89.433	89.434	89.490	89.490
$A_{\rm FB}^{\rm c\bar{c}}(-2)$	-1.10	1.11	-5.04	-6.92	3.90
$A_{\rm FB}^{\rm c\bar{c}}(-2)$Corrected	-0.02	1.81	-4.35	-6.56	4.26
Statistical	4.30	3.60	3.69	2.44	5.10
Uncorrelated	1.00	0.53	0.40	0.38	0.80
Correlated	0.09	0.16	0.09	0.23	0.30
Total Systematic	1.00	0.55	0.41	0.44	0.86
$a(R_{\rm b})$		-0.2886		-3.4000	
$R_{\rm b}^{\rm used}$		0.2164		0.2155	
$a(R_{\rm c})$		1.0096		3.2000	
$R_{\rm c}^{\rm used}$		0.1671		0.1720	
$a(A_{\rm FB}^{\rm b\bar{b}}(-2))$	-1.3365				
$A_{\rm FB}^{\rm b\bar{b}}(-2)^{\rm used}$	6.13				
$a({\rm BR}({\rm b}\to\ell))$		-1.0966		-1.7031	
${\rm BR}({\rm b}\to\ell)^{\rm used}$		10.56		10.90	
$a({\rm BR}({\rm b}\to{\rm c}\to\bar{\ell}))$		1.1156		-1.4128	
${\rm BR}({\rm b}\to{\rm c}\to\bar{\ell})^{\rm used}$		8.07		8.30	
$a({\rm BR}({\rm c}\to\ell))$		1.0703		3.3320	
${\rm BR}({\rm c}\to\ell)^{\rm used}$		9.90		9.80	
$a(\overline{\chi})$		-0.0856			
$\overline{\chi}^{\rm used}$		0.11770			
$a(f({\rm D}^+))$			-0.3868		
$f({\rm D}^+)^{\rm used}$			0.2210		
$a(f({\rm D_s}))$			-0.1742		
$f({\rm D_s})^{\rm used}$			0.1120		
$a(f(\Lambda_{\rm c}))$			-0.0878		
$f(\Lambda_{\rm c})^{\rm used}$			0.0840		

Table 47: The measurements of $A_{\rm FB}^{\rm c\bar{c}}(-2)$. All numbers are given in %.

	ALEPH		DELPHI				L3		OPAL		
	91-95† lepton [37]	91-95 jet charge [41]	91-92 lepton [38]	93-95† lepton [38]	92-95 D-meson [46]	92-95 jet charge [42]	91-95 jet charge [43]	90-95 lepton [39]	91-95 jet charge [44]	90-95† lepton [40]	90-95 D-meson [47]
$\sqrt{s}$ (GeV)	91.210	91.250	91.270	91.223	91.235	91.260	91.240	91.260	91.210	91.240	91.240
$A_{\rm FB}^{\rm bb}$(pk)	9.71	10.40	10.89	9.86	7.59	9.83	9.31	9.85	10.06	9.14	8.90
$A_{\rm FB}^{\rm bb}$(pk)Corrected	9.81	10.42	10.87	9.93	7.63	9.83	9.35	9.85	10.15	9.18	8.94
Statistical	0.40	0.40	1.30	0.64	1.97	0.47	1.01	0.67	0.52	0.44	2.70
Uncorrelated	0.16	0.23	0.33	0.15	0.77	0.14	0.51	0.27	0.41	0.14	2.15
Correlated	0.12	0.22	0.27	0.14	0.07	0.04	0.21	0.14	0.20	0.15	0.45
Total Systematic	0.20	0.32	0.43	0.20	0.77	0.14	0.55	0.31	0.46	0.20	2.20
$a(R_{\rm b})$	-0.9545	-0.2430	-2.8933	-2.0201		-0.1962	-9.1622	-2.1700	-7.6300	-0.7000	
$R_{\rm b}^{\rm used}$	0.2172	0.2155	0.2170	0.2164		0.2158	0.2170	0.2170	0.2150	0.2155	
$a(R_{\rm c})$	0.6450	1.4900	1.0993	1.1488		0.8400	1.0831	1.3005	0.4600	0.6000	
$R_{\rm c}^{\rm used}$	0.1720	0.1726	0.1710	0.1671		0.1720	0.1733	0.1734	0.1730	0.1720	
$a(A_{\rm FB}^{\rm c\bar{c}}$(pk))		0.6345					1.1603	0.9262	0.6870		
$A_{\rm FB}^{\rm c\bar{c}}(pk)^{\rm used}$		6.85					6.91	7.41	6.19		
$a({\rm BR}({\rm b}\to\ell))$	-1.8480		-3.8824	-2.0308				-2.0160		-0.3406	
${\rm BR}({\rm b}\to\ell)^{\rm used}$	10.78		11.00	10.56				10.50		10.90	
$a({\rm BR}({\rm b}\to{\rm c}\to\bar{\ell}))$	0.4233		0.4740	-0.3798				-0.1280		-0.3532	
${\rm BR}({\rm b}\to{\rm c}\to\bar{\ell})^{\rm used}$	8.14		7.90	8.07				8.00		8.30	
$a({\rm BR}({\rm c}\to\ell))$	0.5096		0.7840	1.0703				1.5288		0.5880	
${\rm BR}({\rm c}\to\ell)^{\rm used}$	9.80		9.80	9.90				9.80		9.80	
$a(\overline{\chi})$	2.9904		3.4467	1.6692							
$\overline{\chi}^{\rm used}$	0.12460		0.12100	0.11770							
$a(f({\rm D}^+))$					0.0442	0.2761					
$f({\rm D}^+)^{\rm used}$					0.2210	0.2330					
$a(f({\rm D_s}))$					-0.0788	0.0106					
$f({\rm D_s})^{\rm used}$					0.1120	0.1020					
$a(f(\Lambda_{\rm c}))$					-0.0115	-0.0495					
$f(\Lambda_{\rm c})^{\rm used}$					0.0840	0.0630					

Table 48: The measurements of $A_{\rm FB}^{\rm b\bar{b}}$(pk). All numbers are given in %.

	ALEPH		DELPHI			L3	OPAL	
	91-95† lepton [37]	91-95 D-meson [45]	91-92 lepton [38]	93-95† lepton [38]	92-95 D-meson [46]	90-95 lepton [39]	90-95† lepton [40]	90-95 D-meson [47]
$\sqrt{s}$ (GeV)	91.210	91.220	91.270	91.223	91.235	91.240	91.240	91.240
$A_{\rm FB}^{\rm c\bar{c}}$(pk)	5.69	6.20	8.05	6.28	6.58	7.94	5.97	6.60
$A_{\rm FB}^{\rm c\bar{c}}$(pk)Corrected	5.94	6.39	8.00	6.46	6.70	8.04	6.07	6.70
Statistical	0.53	0.90	2.26	1.00	0.97	3.70	0.59	1.20
Uncorrelated	0.24	0.23	1.25	0.53	0.25	2.40	0.37	0.49
Correlated	0.36	0.17	0.49	0.27	0.04	0.49	0.32	0.24
Total Systematic	0.44	0.28	1.35	0.60	0.25	2.45	0.49	0.54
$a(R_{\rm b})$	1.4318		2.8933	-2.3087		4.3200	4.1000	
$R_{\rm b}^{\rm used}$	0.2172		0.2170	0.2164		0.2160	0.2155	
$a(R_{\rm c})$	-2.9383		-6.4736	5.4307		-6.7600	-3.8000	
$R_{\rm c}^{\rm used}$	0.1720		0.1710	0.1671		0.1690	0.1720	
$a(A_{\rm FB}^{\rm b\bar{b}}({\rm pk}))$		-2.1333				6.4274		
$A_{\rm FB}^{\rm b\bar{b}}({\rm pk})^{\rm used}$		9.79				8.84		
$a({\rm BR}({\rm b}\to\ell))$	1.8993		4.8529	-2.7618		3.5007	5.1094	
${\rm BR}({\rm b}\to\ell)^{\rm used}$	10.78		11.00	10.56		10.50	10.90	
$a({\rm BR}({\rm b}\to{\rm c}\to\bar{\ell}))$	-1.0745		-3.9500	2.2786		-3.2917	-1.7660	
${\rm BR}({\rm b}\to{\rm c}\to\bar{\ell})^{\rm used}$	8.14		7.90	8.07		7.90	8.30	
$a({\rm BR}({\rm c}\to\ell))$	-3.2732		-7.2520	4.8965		-6.5327	-3.9200	
${\rm BR}({\rm c}\to\ell)^{\rm used}$	9.80		9.80	9.90		9.80	9.80	
$a(\overline{\chi})$	0.0453			0.3852				
$\overline{\chi}^{\rm used}$	0.12460			0.11770				
$a(f({\rm D}^+))$					-0.0221			
$f({\rm D}^+)^{\rm used}$					0.2210			
$a(f({\rm D_s}))$					0.0788			
$f({\rm D_s})^{\rm used}$					0.1120			
$a(f(\Lambda_{\rm c}))$					0.0115			
$f(\Lambda_{\rm c})^{\rm used}$					0.0840			

Table 49: The measurements of $A_{\rm FB}^{\rm c\bar{c}}$(pk). All numbers are given in %.

	ALEPH				DELPHI			L3	OPAL		
	90-95 lepton [37]	90-95 lepton [37]	90-95 lepton [37]	91-95 jet charge [41]	93-95† lepton [38]	92-95 D-meson [46]	92-95 jet charge [42]	90-95 lepton [39]	91-95 jet charge [44]	90-95† lepton [40]	90-95 D-meson [47]
$\sqrt{s}$ (GeV)	92.050	92.940	93.900	92.970	92.990	92.990	92.940	93.100	92.910	92.950	92.950
$A_{\mathrm{FB}}^{\mathrm{bb}}(+2)$	3.93	10.60	9.03	9.24	10.10	8.78	12.30	13.78	14.60	10.75	-3.40
$A_{\mathrm{FB}}^{\mathrm{bb}}(+2)$Corrected	10.03			9.21	10.05	8.73	12.30	13.62	14.63	10.74	-3.41
Statistical	1.51			1.79	1.80	6.37	1.60	2.40	1.70	1.43	9.00
Uncorrelated	0.14			0.45	0.14	0.97	0.25	0.34	0.64	0.25	2.03
Correlated	0.24			0.26	0.16	0.13	0.05	0.20	0.34	0.28	1.74
Total Systematic	0.28			0.52	0.21	0.98	0.26	0.40	0.73	0.37	2.68
$a(R_{\mathrm{b}})$	-1.964			-0.2430	-2.8859		-0.1962	-3.3756	-12.9000	-0.8000	
$R_{\mathrm{b}}^{\mathrm{used}}$	0.2192			0.2155	0.2164		0.2158	0.2170	0.2150	0.2155	
$a(R_{\mathrm{c}})$	1.575			1.4900	1.3577		1.2000	1.9869	0.6900	0.8000	
$R_{\mathrm{c}}^{\mathrm{used}}$	0.1710			0.1726	0.1671		0.1720	0.1734	0.1730	0.1720	
$a(A_{\mathrm{FB}}^{\mathrm{c\bar{c}}}(+2))$	1.081			1.2018				0.5206	1.3287		
$A_{\mathrm{FB}}^{\mathrm{c\bar{c}}}(+2)^{\mathrm{used}}$	12.51			12.96				12.39	12.08		
$a(\mathrm{BR}(\mathrm{b}\to\ell))$	-1.762				-2.3557			-2.0790		-1.3625	
$\mathrm{BR}(\mathrm{b}\to\ell)^{\mathrm{used}}$	11.34				10.56			10.50		10.90	
$a(\mathrm{BR}(\mathrm{b}\to\mathrm{c}\to\bar{\ell}))$	-0.2478				-0.7595			-1.1200		0.7064	
$\mathrm{BR}(\mathrm{b}\to\mathrm{c}\to\bar{\ell})^{\mathrm{used}}$	7.86				8.07			8.00		8.30	
$a(\mathrm{BR}(\mathrm{c}\to\ell))$	1.524				1.0703			1.9796		0.7840	
$\mathrm{BR}(\mathrm{c}\to\ell)^{\mathrm{used}}$	9.80				9.90			9.80		9.80	
$a(\overline{\chi})$	6.584				1.6050						
$\overline{\chi}^{\mathrm{used}}$	0.12460				0.11770						
$a(f(\mathrm{D}^+))$						0.3978	0.4229				
$f(\mathrm{D}^+)^{\mathrm{used}}$						0.2210	0.2330				
$a(f(\mathrm{D_s}))$						-0.0788	0.0211				
$f(\mathrm{D_s})^{\mathrm{used}}$						0.1120	0.1020				
$a(f(\Lambda_{\mathrm{c}}))$						0.0573	-0.0855				
$f(\Lambda_{\mathrm{c}})^{\mathrm{used}}$						0.0840	0.0630				

Table 50: The measurements of $A_{\mathrm{FB}}^{\mathrm{b\bar{b}}}(+2)$. All numbers are given in %.

	ALEPH	DELPHI		OPAL	
	91-95 D-meson [45]	93-95† lepton [38]	92-95 D-meson [46]	90-95† lepton [40]	90-95 D-meson [47]
$\sqrt{s}$ (GeV)	92.960	92.990	92.990	92.950	92.950
$A_{\rm FB}^{\rm c\bar{c}}(+2)$	10.94	10.50	11.78	15.65	16.70
$A_{\rm FB}^{\rm c\bar{c}}(+2)$Corrected	10.89	10.37	11.65	15.62	16.67
Statistical	3.30	2.90	3.20	2.02	4.10
Uncorrelated	0.79	0.41	0.52	0.57	0.92
Correlated	0.18	0.29	0.07	0.62	0.51
Total Systematic	0.81	0.50	0.52	0.84	1.05
$a(R_{\rm b})$		-4.0402		9.6000	
$R_{\rm b}^{\rm used}$		0.2164		0.2155	
$a(R_{\rm c})$		7.5891		-8.9000	
$R_{\rm c}^{\rm used}$		0.1671		0.1720	
$a(A_{\rm FB}^{\rm b\bar{b}}(+2))$	-2.6333				
$A_{\rm FB}^{\rm b\bar{b}}(+2)^{\rm used}$	12.08				
$a({\rm BR}({\rm b}\to\ell))$		-3.2492		9.5375	
${\rm BR}({\rm b}\to\ell)^{\rm used}$		10.56		10.90	
$a({\rm BR}({\rm b}\to{\rm c}\to\bar{\ell}))$		1.5191		-1.5894	
${\rm BR}({\rm b}\to{\rm c}\to\bar{\ell})^{\rm used}$		8.07		8.30	
$a({\rm BR}({\rm c}\to\ell))$		8.1341		-9.2120	
${\rm BR}({\rm c}\to\ell)^{\rm used}$		9.90		9.80	
$a(\overline{\chi})$		-0.2140			
$\overline{\chi}^{\rm used}$		0.11770			
$a(f({\rm D}^+))$			-0.2984		
$f({\rm D}^+)^{\rm used}$			0.2210		
$a(f({\rm D_s}))$			0.0539		
$f({\rm D_s})^{\rm used}$			0.1120		
$a(f(\Lambda_{\rm c}))$			0.0764		
$f(\Lambda_{\rm c})^{\rm used}$			0.0840		

Table 51: The measurements of $A_{\rm FB}^{\rm c\bar{c}}(+2)$. All numbers are given in %.

	SLD			
	93-98† lepton [48]	93-98† jet charge [51]	94-98† $K^{\pm}$ [52]	97-98† multi [53]
$\sqrt{s}$ (GeV)	91.280	91.280	91.280	91.280
$\mathcal{A}_{\rm b}$	0.922	0.882	0.960	0.926
Statistical	0.029	0.020	0.040	0.019
Uncorrelated	0.019	0.029	0.056	0.027
Correlated	0.008	0.001	0.002	0.001
Total Systematic	0.021	0.029	0.056	0.027
$a(R_{\rm b})$	-0.0542			
$R_{\rm b}^{\rm used}$	0.2168			
$a(R_{\rm c})$	0.0424			
$R_{\rm c}^{\rm used}$	0.1697			
$a(\mathcal{A}_{\rm c})$	0.0449	0.0134	-0.0112	0.0133
$\mathcal{A}_{\rm c}{}^{\rm used}$	0.667	0.670	0.666	0.667
$a({\rm BR}({\rm b}\to\ell))$	-0.2160			
${\rm BR}({\rm b}\to\ell)^{\rm used}$	10.80			
$a({\rm BR}({\rm b}\to{\rm c}\to\bar{\ell}))$	0.0888			
${\rm BR}({\rm b}\to{\rm c}\to\bar{\ell})^{\rm used}$	8.05			
$a({\rm BR}({\rm c}\to\ell))$	0.0479			
${\rm BR}({\rm c}\to\ell)^{\rm used}$	9.83			
$a(\overline{\chi})$	0.3052			
$\overline{\chi}^{\rm used}$	0.11990			

Table 52: The measurements of $\mathcal{A}_{\rm b}$.

	SLD		
	93-98† lepton [49]	93-97† D-meson [50]	93-97† K+vertex [54]
$\sqrt{s}$ (GeV)	91.280	91.280	91.280
$\mathcal{A}_{\rm c}$	0.567	0.688	0.603
Statistical	0.051	0.035	0.028
Uncorrelated	0.056	0.020	0.023
Correlated	0.018	0.003	0.001
Total Systematic	0.059	0.021	0.023
$a(R_{\rm b})$	0.2173		
$R_{\rm b}^{\rm used}$	0.2173		
$a(R_{\rm c})$	-0.4089		
$R_{\rm c}^{\rm used}$	0.1730		
$a(\mathcal{A}_{\rm b})$	0.2151	-0.0673	-0.0306
$\mathcal{A}_{\rm b}{}^{\rm used}$	0.935	0.935	0.900
$a({\rm BR}({\rm b}\to\ell))$	0.2328		
${\rm BR}({\rm b}\to\ell)^{\rm used}$	11.06		
$a({\rm BR}({\rm b}\to{\rm c}\to\bar{\ell}))$	-0.1178		
${\rm BR}({\rm b}\to{\rm c}\to\bar{\ell})^{\rm used}$	8.02		
$a({\rm BR}({\rm c}\to\ell))$	-0.4077		
${\rm BR}({\rm c}\to\ell)^{\rm used}$	9.80		
$a(\overline{\chi})$	0.1138		
$\overline{\chi}^{\rm used}$	0.12170		
$a(f({\rm D}^+))$			-0.0140
$f({\rm D}^+)^{\rm used}$			0.2300
$a(f({\rm D_s}))$			-0.0028
$f({\rm D_s})^{\rm used}$			0.1150
$a(f(\Lambda_{\rm c}))$			0.0005
$f(\Lambda_{\rm c})^{\rm used}$			0.0740

Table 53: The measurements of $\mathcal{A}_{\rm c}$.

	ALEPH	DELPHI	L3		OPAL
	91-95† multi [55]	94-95† multi [56]	92 lepton [57]	94-95† multi [26]	92-95 multi [58]
$BR(b \to \ell)$	11.55	10.65	10.68	10.21	10.83
Statistical	0.09	0.07	0.11	0.13	0.10
Uncorrelated	0.17	0.23	0.36	0.20	0.20
Correlated	0.22	0.42	0.22	0.31	0.21
Total Systematic	0.27	0.48	0.42	0.36	0.29
$a(R_b)$			-9.2571		-0.1808
R_b^{used}			0.2160		0.2169
$a(R_c)$				1.4450	0.4867
R_c^{used}				0.1734	0.1770
$a(BR(b \to c \to \bar{\ell}))$			-1.1700	0.1618	
$BR(b \to c \to \bar{\ell})^{used}$			9.00	8.09	
$a(BR(c \to \ell))$	-0.3078	-0.1960	-2.5480	0.9212	
$BR(c \to \ell)^{used}$	9.85	9.80	9.80	9.80	
$a(\overline{\chi})$	0.7683				
$\overline{\chi}^{used}$	0.1178				
$a(f(D^+))$				0.5523	0.1445
$f(D^+)^{used}$				0.2330	0.2380
$a(f(D_s))$				0.0213	0.0055
$f(D_s)^{used}$				0.1030	0.1020
$a(f(\Lambda_c))$				-0.0427	-0.0157
$f(\Lambda_c)^{used}$				0.0630	0.0650

Table 54: The measurements of $BR(b \to \ell)$. All numbers are given in %.

	ALEPH	DELPHI	OPAL
	91-95† multi [55]	94-95† multi [56]	92-95 multi [58]
$\mathrm{BR}(\mathrm{b} \to \mathrm{c} \to \bar{\ell})$	8.04	7.88	8.40
Statistical	0.14	0.13	0.16
Uncorrelated	0.20	0.26	0.19
Correlated	0.14	0.36	0.34
Total Systematic	0.25	0.45	0.39
$a(R_\mathrm{b})$			-0.1808
$R_\mathrm{b}^\mathrm{used}$			0.2169
$a(R_\mathrm{c})$	0.8916		0.3761
$R_\mathrm{c}^\mathrm{used}$	0.1694		0.1770
$a(\mathrm{BR}(\mathrm{c} \to \ell))$	0.3078	-0.1960	
$\mathrm{BR}(\mathrm{c} \to \ell)^\mathrm{used}$	9.85	9.80	
$a(\overline{\chi})$	-1.2804		
$\overline{\chi}^\mathrm{used}$	0.11780		
$a(f(\mathrm{D}^+))$			0.1190
$f(\mathrm{D}^+)^\mathrm{used}$			0.2380
$a(f(\mathrm{D_s}))$			0.0028
$f(\mathrm{D_s})^\mathrm{used}$			0.1020
$a(f(\Lambda_\mathrm{c}))$			-0.0110
$f(\Lambda_\mathrm{c})^\mathrm{used}$			0.0660

Table 55: The measurements of $\mathrm{BR}(\mathrm{b} \to \mathrm{c} \to \bar{\ell})$. All numbers are given in %.

	DELPHI	OPAL
	92-95 D+lepton [30]	90-95 D+lepton [59]
$\mathrm{BR}(\mathrm{c} \to \ell)$	9.59	9.60
Statistical	0.42	0.60
Uncorrelated	0.24	0.49
Correlated	0.14	0.43
Total Systematic	0.27	0.65
$a(\mathrm{BR}(\mathrm{b} \to \ell))$	-0.5600	-1.4335
$\mathrm{BR}(\mathrm{b} \to \ell)^\mathrm{used}$	11.20	10.99
$a(\mathrm{BR}(\mathrm{b} \to \mathrm{c} \to \bar{\ell}))$	-0.4100	-0.7800
$\mathrm{BR}(\mathrm{b} \to \mathrm{c} \to \bar{\ell})^\mathrm{used}$	8.20	7.80

Table 56: The measurements of $\mathrm{BR}(\mathrm{c} \to \ell)$. All numbers are given in %.

	ALEPH	DELPHI	L3	OPAL
	90-95 multi [37]	94-95† multi [56]	90-95 lepton [39]	90-95† lepton [40]
$\overline{\chi}$	0.12461	0.12700	0.11920	0.11390
Statistical	0.00515	0.01300	0.00680	0.00540
Uncorrelated	0.00252	0.00566	0.00214	0.00306
Correlated	0.00397	0.00554	0.00252	0.00324
Total Systematic	0.00470	0.00792	0.00330	0.00446
$a(R_{\mathrm{b}})$	0.0341		0.0000	
$R_{\mathrm{b}}^{\mathrm{used}}$	0.2192		0.2170	
$a(R_{\mathrm{c}})$	0.0009		0.0004	
$R_{\mathrm{c}}^{\mathrm{used}}$	0.1710		0.1734	
$a(\mathrm{BR}(\mathrm{b} \to \ell))$	0.0524		0.0550	0.0170
$\mathrm{BR}(\mathrm{b} \to \ell)^{\mathrm{used}}$	11.34		10.50	10.90
$a(\mathrm{BR}(\mathrm{b} \to \mathrm{c} \to \bar{\ell}))$	-0.0440		-0.0466	-0.0318
$\mathrm{BR}(\mathrm{b} \to \mathrm{c} \to \bar{\ell})^{\mathrm{used}}$	7.86		8.00	8.30
$a(\mathrm{BR}(\mathrm{c} \to \ell))$	0.0035	-0.0020	0.0006	0.0039
$\mathrm{BR}(\mathrm{c} \to \ell)^{\mathrm{used}}$	9.80	9.80	9.80	9.80

Table 57: The measurements of $\overline{\chi}$.

	DELPHI	OPAL
	92-95 D-meson [30]	90-95 D-meson [32]
$\mathrm{P}(\mathrm{c} \to \mathrm{D}^{*+}) \times \mathrm{BR}(\mathrm{D}^{*+} \to \pi^+\mathrm{D}^0)$	0.1740	0.1513
Statistical	0.0100	0.0096
Uncorrelated	0.0040	0.0088
Correlated	0.0007	0.0011
Total Systematic	0.0041	0.0089
$a(R_{\mathrm{b}})$	0.0293	
$R_{\mathrm{b}}^{\mathrm{used}}$	0.2166	
$a(R_{\mathrm{c}})$	-0.0158	
$R_{\mathrm{c}}^{\mathrm{used}}$	0.1735	

Table 58: The measurements of $\mathrm{P}(\mathrm{c} \to \mathrm{D}^{*+}) \times \mathrm{BR}(\mathrm{D}^{*+} \to \pi^+\mathrm{D}^0)$.

	ALEPH	DELPHI	OPAL
	91-95 D meson [33]	92-95 D meson [31]	91-94 D meson [34]
$R_c f_{D^+}$	0.0406	0.0384	0.0390
Statistical	0.0013	0.0013	0.0050
Uncorrelated	0.0014	0.0015	0.0042
Correlated	0.0032	0.0025	0.0031
Total Systematic	0.0035	0.0030	0.0052
$a(f(D^+))$		0.0008	
$f(D^+)^{\text{used}}$		0.2210	
$a(f(D_s))$		-0.0002	
$f(D_s)^{\text{used}}$		0.1120	
$a(f(\Lambda_c))$		0.0000	
$f(\Lambda_c)^{\text{used}}$		0.0840	

Table 59: The measurements of $R_c f_{D^+}$.

	ALEPH	DELPHI	OPAL
	91-95 D meson [33]	92-95 D meson [31]	91-94 D meson [34]
$R_c f_{D_s}$	0.0207	0.0213	0.0160
Statistical	0.0033	0.0017	0.0042
Uncorrelated	0.0011	0.0010	0.0016
Correlated	0.0053	0.0054	0.0043
Total Systematic	0.0054	0.0055	0.0046
$a(f(D^+))$		0.0007	
$f(D^+)^{\text{used}}$		0.2210	
$a(f(D_s))$		-0.0009	
$f(D_s)^{\text{used}}$		0.1120	
$a(f(\Lambda_c))$		-0.0001	
$f(\Lambda_c)^{\text{used}}$		0.0840	

Table 60: The measurements of $R_c f_{D_s}$.

	ALEPH	DELPHI	OPAL
	91-95 D meson [33]	92-95 D meson [31]	91-94 D meson [34]
$R_c f_{\Lambda_c}$	0.0157	0.0169	0.0091
Statistical	0.0016	0.0035	0.0050
Uncorrelated	0.0005	0.0016	0.0015
Correlated	0.0044	0.0045	0.0035
Total Systematic	0.0045	0.0048	0.0038
$a(f(D^+))$		0.0002	
$f(D^+)^{\text{used}}$		0.2210	
$a(f(D_s))$		-0.0001	
$f(D_s)^{\text{used}}$		0.1120	
$a(f(\Lambda_c))$		-0.0002	
$f(\Lambda_c)^{\text{used}}$		0.0840	

Table 61: The measurements of $R_c f_{\Lambda_c}$.

	ALEPH	DELPHI	OPAL
	91-95 D meson [33]	92-95 D meson [31]	91-94 D meson [34]
$R_c f_{D^0}$	0.0964	0.0926	0.0997
Statistical	0.0029	0.0026	0.0070
Uncorrelated	0.0040	0.0038	0.0057
Correlated	0.0045	0.0023	0.0041
Total Systematic	0.0060	0.0044	0.0070
$a(f(D^+))$		0.0020	
$f(D^+)^{\text{used}}$		0.2210	
$a(f(D_s))$		-0.0004	
$f(D_s)^{\text{used}}$		0.1120	
$a(f(\Lambda_c))$		-0.0004	
$f(\Lambda_c)^{\text{used}}$		0.0840	

Table 62: The measurements of $R_c f_{D^0}$.

	DELPHI	OPAL
	92-95 D meson [31]	90-95 D-meson [32]
$R_c P(c \to D^{*+}) \times BR(D^{*+} \to \pi^+ D^0)$	0.0282	0.0266
Statistical	0.0007	0.0005
Uncorrelated	0.0010	0.0010
Correlated	0.0007	0.0009
Total Systematic	0.0012	0.0014
$a(f(D^+))$	0.0006	
$f(D^+)^{\text{used}}$	0.2210	
$a(f(D_s))$	-0.0001	
$f(D_s)^{\text{used}}$	0.1120	
$a(f(\Lambda_c))$	-0.0004	
$f(\Lambda_c)^{\text{used}}$	0.0840	

Table 63: The measurements of $R_c P(c \to D^{*+}) \times BR(D^{*+} \to \pi^+ D^0)$.

B The Measurements used in the Electroweak Gauge Boson Couplings

In the following, results from individual experiments used in the electroweak gauge boson couplings averages are summarised.

Charged Triple Gauge Boson Couplings

Results from each experiment are shown in Tables 64, 65 and 66 for the single, two and three-parameter analyses respectively. Uncertainties include both statistical and systematic effects.

Parameter	ALEPH [150]	DELPHI [151]	L3 [152]	OPAL [153]
g_5^Z	$+0.13^{+0.21}_{-0.21}$	—	$-0.04^{+0.24}_{-0.25}$	—
Δg_1^z	$+0.008^{+0.040}_{-0.039}$	$-0.028^{+0.046}_{-0.045}$	$-0.075^{+0.058}_{-0.054}$	$-0.046^{+0.043}_{-0.041}$
$\Delta\kappa_\gamma$	$+0.04^{+0.09}_{-0.09}$	$+0.05^{+0.13}_{-0.12}$	$-0.03^{+0.12}_{-0.11}$	$-0.10^{+0.11}_{-0.10}$
λ_γ	$-0.012^{+0.041}_{-0.039}$	$+0.056^{+0.057}_{-0.056}$	$-0.081^{+0.065}_{-0.058}$	$-0.108^{+0.040}_{-0.038}$

Table 64: The measured central values and one standard deviation uncertainties ($\Delta - \Delta \log \mathcal{L} = 0.5$) obtained by the four LEP experiments. In each case the parameter listed is varied while the remaining ones are fixed to their Standard Model value. Both statistical and systematic uncertainties are included.

Parameter	ALEPH [150]	DELPHI [151]	L3 [152]	OPAL [153]
Δg_1^z	$-0.001^{+0.043}_{-0.045}$	$-0.048^{+0.049}_{-0.046}$	$-0.088^{+0.095}_{-0.064}$	$-0.017^{+0.049}_{-0.061}$
$\Delta\kappa_\gamma$	$+0.02^{+0.09}_{-0.09}$	$+0.14^{+0.11}_{-0.11}$	$+0.04^{+0.13}_{-0.17}$	$-0.11^{+0.17}_{-0.10}$
Δg_1^z	$+0.019^{+0.052}_{-0.051}$	$-0.103^{+0.063}_{-0.058}$	$-0.02^{+0.10}_{-0.16}$	$+0.075^{+0.059}_{-0.059}$
λ_γ	$-0.026^{+0.053}_{-0.055}$	$+0.111^{+0.069}_{-0.072}$	$-0.06^{+0.19}_{-0.10}$	$-0.158^{+0.054}_{-0.051}$
λ_γ	$-0.019^{+0.044}_{-0.044}$	$+0.032^{+0.060}_{-0.058}$	$-0.088^{+0.093}_{-0.067}$	$-0.103^{+0.044}_{-0.044}$
$\Delta\kappa_\gamma$	$+0.03^{+0.09}_{-0.09}$	$+0.07^{+0.11}_{-0.10}$	$+0.03^{+0.12}_{-0.14}$	$-0.03^{+0.14}_{-0.11}$

Table 65: The measured central values and one standard deviation uncertainties ($\Delta - \Delta \log \mathcal{L} = 0.5$) obtained by the four LEP experiments. In each case the two parameters listed are varied while the remaining one is fixed to its Standard Model value. Both statistical and systematic uncertainties are included.

Parameter	ALEPH [150]	L3 [152]	OPAL [153]
Δg_1^z	$+0.018^{+0.043}_{-0.043}$	$-0.02^{+0.11}_{-0.18}$	$+0.081^{+0.054}_{-0.058}$
$\Delta\kappa_\gamma$	$+0.013^{+0.071}_{-0.071}$	$-0.02^{+0.14}_{-0.15}$	$-0.07^{+0.11}_{-0.09}$
λ_γ	$-0.028^{+0.044}_{-0.047}$	$-0.07^{+0.21}_{-0.11}$	$-0.149^{+0.055}_{-0.053}$

Table 66: The measured central values and one standard deviation uncertainties ($\Delta - \Delta \log \mathcal{L} = 0.5$) obtained by ALEPH, L3 and OPAL. All three parameters listed are varied. Both statistical and systematic uncertainties are included.

Neutral Triple Gauge Boson Couplings in Zγ Production

Results from each experiment are shown in Tables 67 and 68 for the single and two-parameter analyses respectively. Uncertainties include both statistical and systematic effects.

Parameter	DELPHI [154]	L3 [155]	OPAL [156]
h_1^γ	$[-0.17, +0.17]$	$[-0.14, +0.03]$	$[-0.11, +0.11]$
h_2^γ	$[-0.11, +0.11]$	$[-0.039, +0.079]$	$[-0.077, +0.077]$
h_3^γ	$[-0.058, +0.051]$	$[-0.095, -0.001]$	$[-0.17, -0.01]$
h_4^γ	$[-0.036, +0.041]$	$[+0.005, +0.072]$	$[+0.01, +0.14]$
h_1^Z	$[-0.28, +0.29]$	$[-0.16, +0.04]$	$[-0.19, +0.19]$
h_2^Z	$[-0.18, +0.18]$	$[-0.042, +0.093]$	$[-0.13, +0.13]$
h_3^Z	$[-0.37, +0.21]$	$[-0.16, +0.11]$	$[-0.27, +0.12]$
h_4^Z	$[-0.14, +0.22]$	$[-0.05, +0.11]$	$[-0.08, +0.18]$

Table 67: The 95% C.L. intervals ($\Delta - \Delta \log \mathcal{L} = 1.92$) measured by DELPHI, L3 and OPAL. In each case the parameter listed is varied while the remaining ones are fixed to their Standard Model value. Both statistical and systematic uncertainties are included.

Parameter	DELPHI [154]	L3 [155]
h_1^γ	$[-0.35, +0.35]$	$[-0.23, +0.10]$
h_2^γ	$[-0.23, +0.23]$	$[-0.12, +0.10]$
h_3^γ	$[-0.26, +0.38]$	$[-0.20, +0.12]$
h_4^γ	$[-0.32, +0.43]$	$[-0.10, +0.12]$
h_1^Z	$[-0.58, +0.58]$	$[-0.49, +0.19]$
h_2^Z	$[-0.38, +0.38]$	$[-0.31, +0.16]$
h_3^Z	$[-0.70, +0.50]$	$[-0.37, +0.40]$
h_4^Z	$[-0.41, +0.37]$	$[-0.20, +0.28]$

Table 68: The 95% C.L. intervals ($\Delta - \Delta \log \mathcal{L} = 1.92$) measured by DELPHI and L3. In each case the two parameters listed are varied while the remaining ones are fixed to their Standard Model value. Both statistical and systematic uncertainties are included.

Neutral Triple Gauge Boson Couplings in ZZ Production

Results from each experiment are shown in Tables 69 and 70 for the single and two-parameter analyses respectively. Uncertainties include both statistical and systematic effects.

Parameter	DELPHI [157]	L3 [158]	OPAL [159]
f_4^γ	$[-0.49, \ +0.49]$	$[-0.59, \ +0.58]$	$[-0.45, \ +0.43]$
f_4^Z	$[-0.82, \ +0.83]$	$[-0.97, \ +0.99]$	$[-0.74, \ +0.75]$
f_5^γ	$[-1.2, \ +1.2]$	$[-1.4, \ +1.4]$	$[-0.9, \ +0.8]$
f_5^Z	$[-1.9, \ +2.1]$	$[-2.2, \ +2.5]$	$[-1.0, \ +0.5]$

Table 69: The 95% C.L. intervals ($\Delta - \Delta \log \mathcal{L} = 1.92$) measured by DELPHI, L3 and OPAL. In each case the parameter listed is varied while the remaining ones are fixed to their Standard Model value. Both statistical and systematic uncertainties are included.

Parameter	DELPHI [157]	L3 [158]	OPAL [159]
f_4^γ	$[-0.49, \ +0.49]$	$[-0.58, \ +0.58]$	$[-0.45, \ +0.43]$
f_4^Z	$[-0.82, \ +0.83]$	$[-0.97, \ +0.99]$	$[-0.73, \ +0.75]$
f_5^γ	$[-1.2, \ +1.2]$	$[-1.4, \ +1.4]$	$[-0.9, \ +0.9]$
f_5^Z	$[-1.9, \ +2.1]$	$[-2.2, \ +2.5]$	$[-1.0, \ +0.7]$

Table 70: The 95% C.L. intervals ($\Delta - \Delta \log \mathcal{L} = 1.92$) measured by DELPHI, L3 and OPAL. In each case the two parameters listed are varied while the remaining ones are fixed to their Standard Model value. Both statistical and systematic uncertainties are included.

Quartic Gauge Boson Couplings

Results from each experiment are shown in Table 71, where the uncertainties include both statistical and systematic effects.

Parameter [GeV^{-2}]	ALEPH [160]	L3 [161]	OPAL [162]
a_0/Λ^2	$[-0.043, \quad +0.042]$	$[-0.036, \quad +0.035]$	$[-0.065, \quad +0.065]$
a_c/Λ^2	$[-0.11, \quad +0.11]$	$[-0.08, \quad +0.11]$	$[-0.13, \quad +0.17]$
a_n/Λ^2	—	$[-0.45, \quad +0.42]$	$[-0.61, \quad +0.57]$
a_0/Λ^2	—	$[-0.006, \quad +0.006]$	$[-0.006, \quad +0.008]$
a_c/Λ^2	—	$[-0.006, \quad +0.010]$	$[-0.008, \quad +0.012]$

Table 71: The 95% C.L. intervals ($\Delta - \Delta \log \mathcal{L} = 1.92$) measured by ALEPH, L3 and OPAL. In each case the parameter listed is varied while the remaining ones are fixed to their Standard Model value. Both statistical and systematic uncertainties are included. Top: WWγ and $\nu\bar{\nu}\gamma\gamma$. Bottom: Z$\gamma\gamma$.

References

[1] The LEP Collaborations ALEPH, DELPHI, L3, OPAL and the LEP Electroweak Working Group, and the SLD Heavy Flavour and Electroweak Groups, *A Combination of Preliminary Electroweak Measurements and Constraints on the Standard Model*, CERN–EP/2000-16.

[2] The LEP Collaborations ALEPH, DELPHI, L3 and OPAL and the LEP Electroweak working group, *Combination procedure for the precise determination of Z boson parameters from results of the LEP experiments*, CERN–EP/2000-153, hep-ex/0101027.

[3] The LEP Experiments: ALEPH, DELPHI, L3 and OPAL, Nucl. Inst. Meth. **A378** (1996) 101.

[4] ALEPH Collaboration, D. Decamp *et al.*, Z. Phys. **C48** (1990) 365;
ALEPH Collaboration, D. Decamp *et al.*, Z. Phys. **C53** (1992) 1;
ALEPH Collaboration, D. Buskulic *et al.*, Z. Phys. **C60** (1993) 71;
ALEPH Collaboration, D. Buskulic *et al.*, Z. Phys. **C62** (1994) 539;
ALEPH Collaboration, R. Barate *et al.*, Europ. Phys. J. **C 14** (2000) 1.

[5] DELPHI Collaboration, P. Aarnio *et al.*, Nucl. Phys. **B367** (1991) 511;
DELPHI Collaboration, P. Abreu *et al.*, Nucl. Phys. **B417** (1994) 3;
DELPHI Collaboration, P. Abreu *et al.*, Nucl. Phys. **B418** (1994) 403;
DELPHI Collaboration, P. Abreu *et al.*, Europ. Phys. J. **C 16** (2000) 371.

[6] L3 Collaboration, B. Adeva *et al.*, Z. Phys. **C51** (1991) 179;
L3 Collaboration, O. Adriani *et al.*, Phys. Rep. **236** (1993) 1;
L3 Collaboration, M. Acciarri *et al.*, Z. Phys. **C62** (1994) 551;
L3 Collaboration, M. Acciarri *et al.*, Europ. Phys. J. **C16** (2000) 1-40.

[7] OPAL Collaboration, G. Alexander *et al.*, Z. Phys. **C52** (1991) 175;
OPAL Collaboration, P.D. Acton *et al.*, Z. Phys. **C58** (1993) 219;
OPAL Collaboration, R. Akers *et al.*, Z. Phys. **C61** (1994) 19;
OPAL Collaboration, G. Abbiendi *et al.*, *Precision Luminosity for Z0 Lineshape Measurements with a Silicon-Tungsten Calorimeter*, Eur. Phys. J. **C14** (2000) 373;
OPAL Collaboration, *Precise Determination of the Z Resonance Parameters at LEP : Zedometry*, CERN–EP/2000-148, Submitted to Eur. Phys. J. **C**.

[8] F.A. Berends et al., in *Z Physics at LEP 1, Vol. 1*, ed. G. Altarelli, R. Kleiss and C. Verzegnassi, (CERN Report: CERN 89-08, 1989), p. 89.
M. Böhm et al., in *Z Physics at LEP 1, Vol. 1*, ed. G. Altarelli, R. Kleiss and C. Verzegnassi, (CERN Report: CERN 89-08, 1989), p. 203.

[9] See, for example, M. Consoli *et al.*, in "Z Physics at LEP 1", CERN Report CERN 89-08 (1989), eds G. Altarelli, R. Kleiss and C. Verzegnassi, Vol. 1, p. 7.

[10] S. Jadach, *et al.*, Phys. Lett. **B257** (1991) 173.

[11] M. Skrzypek, Acta Phys. Pol. **B23** (1992) 135.

[12] G. Montagna, *et al.*, Phys. Lett. **B406** (1997) 243.

[13] G. Montagna *et al.*, Nucl. Phys. **B547** (1999) 39;
G. Montagna *et al.*, Phys. Rev. Lett. **459** (1999) 649.

[14] B.F.L Ward *et al.*, Phys. Lett. **B450** (1999) 262.

[15] D. Bardin, M. Grünewald and G. Passarino, *Precision Calculation Project Report*, hep-ph/9902452.

[16] ALEPH Collaboration, D. Buskulic *et al.*, Zeit. Phys. **C69** (1996) 183;
ALEPH Collaboration, *Measurement of the tau polarisation by ALEPH with the full LEP I data sample*, ALEPH 96-067 CONF 98-037, contributed paper to ICHEP 98 Vancouver **ICHEP'98 #939**.

[17] DELPHI Collaboration, *A Precise Measurement of τ Polarisation at LEP-I*, DELPHI 99-130 CONF 317, contributed paper to EPS-HEP 99, Tampere, 15-21 July 1999.

[18] L3 Collaboration, M. Acciarri *et al.*, Phys. Lett. **B429** (1998) 387.

[19] OPAL Collaboration, *Precision Tau and Electron Neutral Current Asymmetry Meausurements from the Tau Polarization at OPAL*, OPAL Physics Note PN438.

[20] The LEP Collaborations ALEPH, DELPHI, L3, OPAL and the LEP Electroweak Working Group, *Combined Preliminary Data on* Z *Parameters from the LEP Experiments and Constraints on the Standard Model*, CERN–PPE/94-187.

[21] SLD Collaboration, K. Abe *et al.*, Phys. Rev. Lett. **84** (2000) 5945.

[22] SLD Collaboration, K. Abe *et al.*, SLAC-PUB-8618, (2000). Submitted to Phys.Rev.Lett.

[23] The LEP Heavy Flavour Group, *Input Parameters for the LEP/SLD Electroweak Heavy Flavour Results for Summer 1998 Conferences* , LEPHF/98-01,
http://www.cern.ch/LEPEWWG/heavy/lephf9801.ps.gz.

[24] ALEPH Collaboration, R. Barate *et al.*, Physics Letters **B 401** (1997) 150;
ALEPH Collaboration, R. Barate *et al.*, Physics Letters **B 401** (1997) 163.

[25] DELPHI Collaboration, P.Abreu *et al.*, E. Phys. J. **C10** (1999) 415.

[26] L3 Collaboration, M. Acciarri *et al.*, Eur. Phys. J. **C13** (2000) 47.

[27] OPAL Collaboration, G. Abbiendi *et al.*, Eur. Phys. J. **C8** (1999) 217.

[28] SLD Collaboration, *Improved measurement of R_b, R_c at SLD*, SLAC-PUB-8667, Contributed Paper to ICHEP2000 , **#739**.

[29] ALEPH Collaboration, R. Barate *et al.*, Eur. Phys. J. **C4** (1998) 557.

[30] DELPHI Collaboration, P.Abreu *et al.*, E. Phys. J. **C12** (2000) 209.

[31] DELPHI Collaboration, P.Abreu *et al.*, E. Phys. J. **C12** (2000) 225.

[32] OPAL Collaboration, K. Ackerstaff *et al.*, Eur. Phys. J. **C1** (1998) 439.

[33] ALEPH Collaboration, R. Barate *et al.*, Eur. Phys. J. **C16** (2000) 597.

[34] OPAL Collaboration, G. Alexander *et al.*, Z. Phys. **C72** (1996) 1.

[35] D. Abbaneo *et al.*, Eur. Phys. J. **C4** (1998) 2, 185.

[36] D. Bardin *et al.*, Z. Phys. **C44** (1989) 493; Comp. Phys. Comm. **59** (1990) 303; Nucl. Phys. **B351**(1991) 1; Phys. Lett. **B255** (1991) 290 and CERN-TH 6443/92 (May 1992); the most recent version of ZFITTER (6.21) is described in hep-ph/9908433 and DESY 99-070 (Aug 1999).

[37] ALEPH Collaboration, D. Buskulic *et al.*, Phys. Lett. **B384** (1996)414;
ALEPH Collaboration, *Measurement of the b and c forward-backward asymmetries using leptons* ALEPH 99-076 CONF 99-048, contributed paper to EPS 99 Tampere **HEP'99 #6-65**.

[38] DELPHI Collaboration, P.Abreu *et al.*, Z. Phys **C65** (1995) 569;
DELPHI Collaboration, *Measurement of the Forward-Backward Asymmetries of* $e^+e^- \to Z \to b\bar{b}$ *and* $e^+e^- \to Z \to c\bar{c}$ *using prompt leptons* DELPHI 2000-101 CONF 400, contributed paper to ICHEP 2000 Osaka **ICHEP'00 #377** .
Delphi notes are available at http://wwwcn.cern.ch/~pubxx/www/delsec/delnote/.

[39] L3 Collaboration, O. Adriani *et al.*, Phys. Lett. **B292** (1992) 454;
L3 Collaboration, *L3 Results on* $A_{\rm FB}^{\rm b\bar{b}}$, $A_{\rm FB}^{\rm c\bar{c}}$ *and* χ *for the Glasgow Conference,* L3 Note 1624;
L3 Collaboration, M. Acciarri *et al.*, Phys. Lett. **B448** (1999) 152.

[40] OPAL Collaboration, G. Alexander *et al.*, Z. Phys. **C70** (1996) 357;
OPAL Collaboration, R. Akers *et al.*, *Updated Measurement of the Heavy Quark Forward-Backward Asymmetries and Average B Mixing Using Leptons in Multihadronic Events*, OPAL Physics Note PN226 contributed paper to ICHEP96, Warsaw, 25-31 July 1996 **PA05-007**
OPAL Collaboration, R. Akers *et al.*, *QCD corrections to the bottom and charm forward-backward asymmetries* OPAL Physics Note PN284.

[41] ALEPH Collaboration, R. Barate *et al.*, Phys. Lett. **B426**, (1998) 217.

[42] DELPHI Collaboration, P.Abreu *et al.*, E. Phys. J. **C9** (1999) 367.

[43] L3 Collaboration, M. Acciarri *et al.*, Phys. Lett. **B439** (1998) 225.

[44] OPAL Collaboration, K.Ackerstaff *et al.*, Z. Phys. **C75** (1997) 385.

[45] ALEPH Collaboration, R. Barate *et al.*, Phys. Lett. **B434** (1998) 415.

[46] DELPHI Collaboration, P.Abreu *et al.*, E. Phys. J. **C10** (1999) 219.

[47] OPAL Collaboration, G. Alexander *et al.*, Z. Phys. **C73** (1996) 379.

[48] SLD Collaboration, *Direct measurement of* $\mathcal{A}_b$ *at the* Z^0 *Pole using a lepton tag*, SLAC-PUB-8516, Contributed Paper to ICHEP2000 , **#741**.

[49] SLD Collaboration, SLAC–PUB–7637, contributed paper to EPS-HEP-97, Jerusalem, **EPS-124**;
S. Fahey, *Measurements of Quark Coupling Asymmetries at the SLD* , talk presented at ICHEP 98 Vancouver.

[50] SLD Collaboration, *Measurement of* $\mathcal{A}_c$ *with charmed mesons at SLD*, Contributed Paper to ICHEP2000 , **#744**.

[51] SLD Collaboration, *Measurement of* $\mathcal{A}_{\rm b}$ *at the Z resonance using a Jet-Charge Technique* SLAC–PUB–7886, contributed paper to ICHEP 98 Vancouver **ICHEP'98 #179** ;
N. de Groot, *Electroweak results from SLD*, talk prsented at XXXIVth Rencontres de Moriond, Electroweak Interactions and Unified Theories, Les Arcs, March 13-20 1999.

[52] SLD Collaboration, *Direct measurement of* $\mathcal{A}_b$ *using charged kaons at the SLD detector*, SLAC-PUB-8200, contributed paper to EPS 99 Tampere **HEP'99 #6_473** .

[53] SLD Collaboration, *Direct measurement of Ab using charged vertices*, SLAC-PUB-8542, Contributed Paper to ICHEP2000 , **#743**.

[54] SLD Collaboration, *Direct measurement of $\mathcal{A}_c$ using inclusive charm tagging at the SLD detector*, SLAC-PUB-8199, contributed paper to EPS 99 Tampere **HEP'99 #6_474** .

[55] ALEPH Collaboration. , *Inclusive semileptonic branching ratios of b hadrons produced in Z decays*, ALEPH 2000-069 CONF 2000-047, Contributed Paper to ICHEP2000 , **#182**.

[56] DELPHI Collaboration, *Measurement of the semileptonic b branching ratios in Z decays* DELPHI 99-111 CONF 298, contributed paper to EPS 99 Tampere **HEP'99 #5_522** .

[57] L3 Collaboration, M. Acciarri *et al.*, Z Phys. **C71** 379 (1996).

[58] OPAL Collaboration, G. Abbiendi *et al.*, Eur. Phys. J. **C13** (2000) 225.

[59] OPAL Collaboration, G. Abbiendi *et al.*, Eur. Phys. J. **C8** (1999) 573.

[60] ALEPH Collaboration, D. Decamp *et al.*, Phys. Lett. **B259** (1991) 377.

[61] ALEPH Collaboration, ALEPH-Note 93-041 PHYSIC 93-032 (1993);
ALEPH Collaboration, ALEPH-Note 93-042 PHYSIC 93-033 (1993);
ALEPH Collaboration, ALEPH-Note 93-044 PHYSIC 93-035 (1993).

[62] ALEPH Collaboration, D. Buskulic *et al.*, Z. Phys. **C71** (1996) 357.

[63] DELPHI Collaboration, P. Abreu *et al.*, Phys. Lett. **B277** (1992) 371.

[64] DELPHI Collaboration, *Measurement of the Inclusive Charge Flow in Hadronic Z Decays,* DELPHI 96-19 PHYS 594.

[65] OPAL Collaboration, P. D. Acton *et al.*, Phys. Lett. **B294** (1992) 436.

[66] OPAL Collaboration, *A determination of* $\sin^2\theta_W$ *from an inclusive sample of multihadronic events,* OPAL Physics Note PN195 (1995).

[67] T. Sjöstrand, Comp. Phys. Comm. **82** (1994) 74.

[68] G. Marchesini *et al.*, Comp. Phys. Comm. **67** (1992) 465.

[69] LEPEWWG $f\bar{f}$ subgroup: http://www.cern.ch/LEPEWWG/lep2/.

[70] LEPEWWG $f\bar{f}$ Subgroup, D. Bourilkov *et. al.*, LEP2FF/00-03,ALEPH 2000-088 PHYSIC 2000-034, DELPHI 2000-168 PHYS 881, L3 note 2624, OPAL TN673.

[71] The LEP Collaborations ALEPH, DELPHI, L3, OPAL and the LEP Electroweak Working Group, and the SLD Heavy Flavour and Electroweak Groups, *A Combination of Preliminary Electroweak Measurements and Constraints on the Standard Model*, CERN–EP/99-15.

[72] LEP2FF/00-01,ALEPH 2000-026 PHYSIC 2000-005, DELPHI 2000-046 PHYS 855, L3 note 2527, OPAL TN647.

[73] The error quoted is slightly larger than that given in the *Report of the LEP II Monte Carlo Workshop*, M. Kobel *et al.*, *"Two-Fermion Production in Electron Positron Collisions"*, hep-ph/0007180.

[74] D. Bardin *et al.*, CERN-TH 6443/92; http://www.ifh.de/∼riemann/Zfitter/zf.html .
Definition 1 corresponds to the ZFITTER flags FINR=0 and INTF=0; definition 2 corresponds to FINR=0 and INTF=1 for hadrons, FINR=1 and INTF=1 for leptons.

[75] ZFITTER V6.23 is used.
D. Bardin *et al.*, Preprint hep-ph/9908433.
Relevant ZFITTER settings used are FINR=0 and INTF=1.

[76] DELPHI Collaboration, P.Abreu *et al.*, Euro Phys J. **C10**(1999) 415.

[77] P. Langacker, R.W. Robinett and J.L. Rosner, Phys. Rev. **D30** (1984) 1470;
D. London and J.L. Rosner, Phys. Rev. **D34** (1986) 1530;
J.C. Pati and A. Salam, Phys. Rev. **D10** (1974) 275;
R.N. Mohapatra and J.C. Pati, Phys. Rev. **D11** (1975) 566.

[78] G. Altarelli *et al.*, Z. Phys. **C45** (1989) 109;
erratum Z. Phys. **C47** (1990) 676.

[79] DELPHI Collab., P. Abreu *et al.*, Zeit. Phys. **C65** (1995) 603.

[80] E. Eichten, K. Lane and M. Peskin, Phys. Rev. Lett. **50** (1983) 811.

[81] H. Kroha, Phys. Rev. **D46** (1992) 58.

[82] The error quoted is slightly larger than that given in the *Report of the LEP II Monte Carlo Workshop*, M. Kobel *et al.*, *"Two-Fermion Production in Electron Positron Collisions"*, hep-ph/0007180.

[83] A. Leike, T. Riemann, and J. Rose, Phys. Lett. **B 273** (1991) 513;
T. Riemann, Phys. Lett. **B 293** (1992) 451;
S. Kirsch, T. Riemann, Comp. Phys. Comm. **88** (1995) 89.

[84] The 4 LEP experiments : ALEPH, DELPHI, L3 and OPAL, the LEP Electroweak Working Group, and the SLD Heavy Flavour and Electroweak Groups, *"A Combination of Preliminary Electroweak Measurements and Constraints on the Standard Model"*, Note in preparation, summer 2000.

[85] S. Kirsch and T. Riemann, *"SMATASY – A program for the model independent description of the Z resonance"*, DESY 94-125 (1994).
SMATASY version 6.23 is used together with ZFITTER version 6.23.

[86] ALEPH Collaboration, R. Barate *et al.*, Phys. Lett. **B484** (2000) 205.

[87] DELPHI Collaboration, P. Abreu *et al.*, Phys. Lett. **B479** (2000) 89.

[88] L3 Collaboration, M. Acciarri *et al.*, CERN–EP/2000-104, submitted to Phys. Lett. **B**.

[89] OPAL Collaboration, G. Abbiendi *et al.*, CERN–EP/2000-101, submitted to Phys. Lett. **B**.

[90] L3 Collaboration, L3 Note 2376.

[91] ALEPH Collaboration, ALEPH 2000-005 CONF 2000-002, ICHEP 2000 abstract 288.

[92] DELPHI Collaboration, DELPHI 2000-140 CONF 439, ICHEP 2000 abstract 458.

[93] L3 Collaboration, L3 Note 2514, ICHEP 2000 abstract 512.

[94] OPAL Collaboration, OPAL Physics Note PN437, ICHEP 2000 abstract 168.

[95] OPAL Collaboration, OPAL Physics Note PN420, ICHEP 2000 abstract 184, the W–pair production cross section at $\sqrt{s} = 200$–202 GeV results are updated in [94].

[96] ALEPH Collaboration, ALEPH 2000-071 CONF 2000-049, ICHEP 2000 abstract 188.

[97] DELPHI Collaboration, DELPHI 2000-142 CONF 441, ICHEP 2000 abstract 460.

[98] L3 Collaboration, L3 Note 2599, ICHEP 2000 abstract 411.

[99] L. Lyons, D. Gibaut and P. Clifford, Nucl. Instr. Meth. **A270** (1988) 110.

[100] The LEP WW Working Group, LEPEWWG/WW/00-01, note prepared for the winter conferences 2000, available from: `http://lepewwg.web.cern.ch/LEPEWWG/wmass/ww-0001.ps`.

[101] A. Denner, S. Dittmaier, M. Roth and D. Wackeroth, *"Electroweak radiative corrections to* $e^+e^- \to W^+W^- \to$ *4 fermions in double pole approximation – the RacoonWW approach"*, BI-TP 2000/06, `http://arXiv.org/abs/hep-ph/0006307`, submitted to Nucl. Phys. **B**;
A. Denner, S. Dittmaier, M. Roth and D. Wackeroth, Phys. Lett. **B475** (2000) 127.

[102] S. Jadach, W. Placzek, M. Skrzypek, B.F.L. Ward and Z. Wąs, *"Precision Predictions for (Un)Stable* W^+W^- *Pair Production at and Beyond LEP2 Energies"*, UTHEP-00-0101, `http://arXiv.org/abs/hep-ph/0007012`, submitted to Phys. Lett. **B**;
S. Jadach, W. Placzek, M. Skrzypek, B.F.L. Ward and Z. Wąs, Phys. Rev. **D61** (2000) 113010; Version 1.14 of the program is used.

[103] W. Beenakker, F.A. Berends and A.P. Chapovsky, Nucl. Phys. **B548** (1999) 3, see also [134] for a detailed discussion of different implementations.

[104] Private communication from the authors of [101, 102].

[105] D. Bardin, J. Biebel, D. Lehner, A. Leike, A. Olchevski and T. Riemann, Comp. Phys. Comm. **104** (1997) 161, Version 2.10 of the program, described in [134] is used.

[106] The LEP Collaborations ALEPH, DELPHI, L3, OPAL and the LEP Electroweak Working Group, and the SLD Heavy Flavour Group, *A Combination of Preliminary LEP Electroweak Measurements and Constraints on the Standard Model*, CERN–PPE/97-154.

[107] Particle Data Group (D.E. Groom *et al.*), Eur. Phys. J. **C15** (2000) 1.

[108] The ALEPH Collaboration, Phys. Lett. **B401** (1997) 347.

[109] The DELPHI Collaboration, Phys. Lett. **B397** (158) 1997.

[110] The L3 Collaboration, Phys. Lett. **B398** (1997) 223.

[111] The OPAL Collaboration, Phys. Lett. **B389** (1996) 416.

[112] The ALEPH Collaboration, Phys. Lett. **B453** (1999) 121.

[113] he ALEPH Collaboration, CERN–EP/00-045.

[114] The ALEPH Collaboration, "Measurement of the W Mass and Width in e^+e^- Collisions at $\sqrt{s} \sim 192 - 202$GeV", ALEPH 2000-018, CONF 2000-015.

[115] The DELPHI Collaboration, Eur. Phys. J. **C2** (581) 1998.

[116] The DELPHI Collaboration, Phys. Lett. **B462** (410) 1999.

[117] The DELPHI Collaboration, "Measurement of the mass and width of the W Boson in e^+e^- collisions at $\sqrt{s} = 189$GeV", DELPHI 2000-144 CONF 443, Contributed paper for ICHEP 2000.

[118] The DELPHI Collaboration, "Measurement of the mass and width of the W Boson in e^+e^- collisions at $\sqrt{s} = 192 - 202$GeV", DELPHI 2000-149 CONF 446, Contributed paper for ICHEP 2000.

[119] The L3 Collaboration, Phys. Lett. **B407** (1997) 419.

[120] The L3 Collaboration, Phys. Lett. **B454** (1999) 386.

[121] The L3 Collaboration, "Preliminary Results on the Measurement of the Mass and Width of the W Boson at LEP", L3 Note 2377, March 1999.

[122] The L3 Collaboration, "Preliminary Results on the Measurement of the Mass and Width of the W Boson at LEP", L3 Note 2575, July 2000.

[123] The OPAL Collaboration, Eur. Phys. J. **C1** (1998) 395.

[124] The OPAL Collaboration, Phys. Lett. **B453** (1999) 138.

[125] The OPAL Collaboration, Opal Paper PR320, submitted to Physics Letters.

[126] The OPAL Collaboration, "Measurement of the Mass of the W Boson in e^+e^- annihilations at 192-202 GeV", Opal Physics Note PN422 (updated July 2000).

[127] The OPAL Collaboration, "Determination of the W mass in the fully leptonic channel", Opal Physics Note PN447, July 2000.

[128] LEP Energy Working Group, LEPEWG 00/01, June 2000.

[129] The LEP WW Working Group, LEPEWWG/WW/00–02, note prepared for the winter conferences 2000, available from: `http://lepewwg.web.cern.ch/LEPEWWG/wmass/ww-0002.ps`.

[130] G. Passarino, Nucl. Phys. **B578** (2000) 3.

[131] G. Passarino, Nucl. Phys. **B574** (2000) 451.

[132] E. Accomando and A. Ballestrero, Comp. Phys. Comm. **99** (1999) 270.

[133] J. Fujimoto *et al.*, Comp. Phys. Comm. **100** (1997) 74.

[134] M.W. Grunewald, G. Passarino *et al.*, *"Four fermion production in electron positron collisions"*, Four fermion working group report of the LEP2 Monte Carlo Workshop 1999/2000, in *"Reports of the working groups on precision calculations for LEP2 Physics"* CERN 2000-009, `http://arXiv.org/abs/hep-ph/0005309`.

[135] Y. Kurihara, J. Fujimoto, Y. Shimizu, K. Kato, T. Tobimatsu and T. Munehisa, Prog. Theor. Phys. **103** (2000) 1199.

[136] G. Montagna, M. Moretti, O. Nicrosini, A. Pallavicini, F. Piccinini, *"Higher–order QED corrections to single–W production in electron–positron collisions"*, FNT/T–2000/08, `http://arXiv.org/abs/hep-ph/0006307`.

[137] The LEP TGC Working Group, LEPEWWG/TGC/2000–02, note prepared for the summer conferences 2000, available from: `http://lepewwg.web.cern.ch/LEPEWWG/tgc/o00/note.ps.gz`.

[138] ALEPH Collaboration, R. Barate *et al.*, Phys. Lett. **B469** (1999) 287.

[139] DELPHI Collaboration, P. Abreu *et al.*, CERN–EP/2000-089, submitted to Phys. Lett. **B**.

[140] L3 Collaboration, M. Acciarri *et al.*, Phys. Lett. **B450** (1999) 281,
L3 Collaboration, M. Acciarri *et al.*, Phys. Lett. **B465** (1999) 363.

[141] OPAL Collaboration, G. Abbiendi *et al.*, Phys. Lett. **B476** (2000) 256.

[142] L3 Collaboration, L3 Note 2579, ICHEP 2000 abstract 502.

[143] ALEPH Collaboration, ALEPH 2000-004 CONF 2000-001, ICHEP 2000 abstract 287.

[144] DELPHI Collaboration, DELPHI 2000-145 CONF 444, ICHEP 2000 abstract 659.

[145] OPAL Collaboration, OPAL Physics Note PN423, ICHEP 2000 abstract 154.

[146] S. Jadach, W. Placzek, M. Skrzypek, B.F.L. Ward and Z. Wąs, Phys. Rev. **D56** (1997) 6939.

[147] G. Passarino, in [134].

[148] The LEP WW Working Group, LEPEWWG/ZZ/00-01, note prepared for the winter conferences 2000, available from: `http://lepewwg.web.cern.ch/LEPEWWG/wmass/zz-0001.ps`.

[149] G. Gounaris *et al.*, in *Physics at LEP 2*, Report CERN 96-01 (1996), eds G. Altarelli, T. Sjöstrand, F. Zwirner, Vol. 1, p. 525.

[150] The ALEPH Collaboration, R. Barate *et al.*, Phys. Lett. **B 422** (1998) 369;
The ALEPH Collaboration, *Measurement of Triple Gauge-Boson Couplings at LEP energies up to 189 GeV*, ICHEP 2000 abstract 324;
The ALEPH Collaboration, *Single W Production at Energies up to* $\sqrt{s}$ *= 202 GeV and Search for Anomalous Triple Gauge Boson Couplings*, ICHEP 2000 abstract 304;
The ALEPH Collaboration, *Measurement of Triple Gauge-Boson Couplings at 192-202 GeV*, ICHEP 2000 abstract 302.

[151] The DELPHI Collaboration, P. Abreu *et al.*, Phys. Lett. **B 397** (1997) 158;
The DELPHI Collaboration, P. Abreu *et al.*, Phys. Lett. **B 423** (1998) 194;
The DELPHI Collaboration, *Measurement of Trilinear WWγ and WWZ Gauge Boson Couplings at values of* $\sqrt{s}$ *from 183 to 202 GeV* , ICHEP 2000 abstract 457.

[152] The L3 Collaboration, M. Acciari *et al.*, Phys. Lett. **B 398** (1997) 223;
The L3 Collaboration, M. Acciari *et al.*, Phys. Lett. **B 413** (1998) 176;
The L3 Collaboration, M. Acciari *et al.*, Phys. Lett. **B 467** (1999) 171;
The L3 Collaboration, *Preliminary Results on the Measurement of Triple-Gauge-Boson Couplings of the W Boson at LEP*, L3 Note 2567 (6/2000), ICHEP 2000 abstract 524.

[153] The OPAL Collaboration, K. Ackerstaff *et al.*, Phys. Lett. **B 397** (1997) 147;
The OPAL Collaboration, K. Ackerstaff *et al.*, Eur. Phys. J. **C 2** (1998) 597;
The OPAL Collaboration, G. Abbiendi *et al.*, Eur. Phys. J. C9 (1999) 191;
The OPAL Collaboration, G. Abbiendi *et al.*, CERN–EP/2000-114, submitted to Eur. Phys. J. **C**;
The OPAL Collaboration, *Triple gauge boson couplings in* W^+W^- *production at LEP energies up to 202 GeV*, OPAL physics note PN441 (7/2000), ICHEP 2000 abstract 206;
The OPAL Collaboration, *Measurement of Single W production and Triple Gauge Couplings in* e^+e^- *Collisions at* $\sqrt{s}$ *=189 GeV*, OPAL physics note PN427 (3/2000), ICHEP 2000 abstract 148.

[154] The DELPHI Collaboration, *Study of Trilinear Gauge Boson Couplings ZZγ and Zγγ between 189 and 202 GeV*, ICHEP 2000 abstract 456.

[155] The L3 Collaboration, M. Acciari *et al.*, Phys. Lett. **B 436** (1999) 187;
The L3 Collaboration, M. Acciari *et al.*, CERN–EP/2000-057, accepted by Phys. Lett. **B**;
The L3 Collaboration, *Study of anomalous $ZZ\gamma$ and $Z\gamma\gamma$ couplings at LEP*, L3 Note 2552 (6/2000), ICHEP 2000 abstract 504.

[156] The OPAL Collaboration, G. Abbiendi *et al.*, CERN–EP/2000-067, accepted by Eur. Phys. J. **C**.

[157] The DELPHI Collaboration, *Measurement of ZZ production using data between $\sqrt{s}$ =183 and 202 GeV*, ICHEP 2000 abstract 659.

[158] The L3 Collaboration, M. Acciari *et al.*, Phys. Lett. **B 450** (1999) 281;
The L3 Collaboration, M. Acciari *et al.*, Phys. Lett. **B 465** (1999) 363;
The L3 Collaboration, *Study of Z Boson Pair Production at LEP*, L3 Note 2579 (7/2000), ICHEP 2000 abstract 502.

[159] The OPAL Collaboration, G. Abbiendi *et al.*, Phys. Lett. **B476** (2000) 256;
The OPAL Collaboration, *Z boson pair production in e^+e^- collisions at $\sqrt{s} > 190$ GeV*, OPAL physics note PN423 (3/2000), ICHEP 2000 abstract 154;
The OPAL Collaboration, *Measurement of Standard Model Processes in e^+e^- collisions at $\sqrt{s} >$202 GeV*, OPAL physics note PN437 (7/2000), ICHEP 2000 abstract 168.

[160] The ALEPH Collaboration, *Constraints on Anomalous Quartic Gauge Boson Couplings from $e^+e^- \to \nu\bar{\nu}\gamma\gamma(\gamma)$ at 189-202 GeV*, ICHEP 2000 abstract 286.

[161] The L3 Collaboration, M. Acciari *et al.*, Phys. Lett. **B 478** (2000) 39;
The L3 Collaboration, *Measurement of the $e^+e^- \to Z\gamma\gamma$ Cross Section and Study of Anomalous Quartic Gauge Couplings*, L3 Note 2578 (7/2000), ICHEP 2000 abstract 505;
The L3 Collaboration, *Preliminary Measurement of the $W^+W^-\gamma$ Cross Section and direct Limits on Anomalous Quartic Gauge Boson Couplings at LEP*, (includes $\nu\bar{\nu}\gamma\gamma(\gamma)$), L3 Note 2569 (7/2000), ICHEP 2000 abstract 520.

[162] The OPAL Collaboration, G. Abbiendi *et al.*, Phys. Lett. **B 471** (1999) 293;
The OPAL Collaboration, *Constraints on anomalous quartic gauge boson couplings from acoplanar photon pair events*, OPAL physics note PN410 (7/1999), EPS 1999 abstract 6-353;
The OPAL Collaboration, *Measurement of the $e^+e^- \to q\bar{q}\gamma\gamma$ cross section and limits on anomalous electroweak quartic gauge couplings*, OPAL physics note PN452 (7/2000), ICHEP 2000 abstract 572.

[163] K. Gaemers and G. Gounaris, Z. Phys. **C 1** (1979) 259.

[164] K. Hagiwara, K. Hikasa, R.D. Peccei and D. Zeppenfeld, Nucl. Phys. **B 282** (1987) 253.

[165] K. Hagiwara, S. Ishihara, R. Szalapski, and D. Zeppenfeld, Phys. Lett. **B 283** (1992) 353;
K. Hagiwara, S. Ishihara, R. Szalapski, and D. Zeppenfeld, Phys. Rev. **D 48** (1993) 2182;
K. Hagiwara, T. Hatsukano, S. Ishihara and R. Szalapski, Nucl. Phys. **B 496** (1997) 66.

[166] M. Bilenky, J.L. Kneur, F.M. Renard and D. Schildknecht, Nucl. Phys. **B 409** (1993) 22;
M. Bilenky, J.L. Kneur, F.M. Renard and D. Schildknecht, Nucl. Phys. **B 419** (1994) 240.

[167] I. Kuss and D. Schildknecht, Phys. Lett. **B 383** (1996) 470.

[168] G. Gounaris and C.G. Papadopoulos, Eur. Phys. J. **C 2** (1998) 365.

[169] G. J. Gounaris, J. Layssac and F. M. Renard, Phys. Rev. **D 61** (2000) 073013.

[170] G. Bélanger and F. Boudjema, Phys. Lett. **B 288** (1992) 201.

[171] W. J. Stirling and A. Werthenbach, Eur. Phys. J. **C 14** (2000) 103.

[172] W. J. Stirling and A. Werthenbach, Phys. Lett. **B 466** (1999) 369.

[173] G. Bélanger *et al.*, Eur. Phys. J. **C 13** (2000) 283.

[174] The LEP-TGC combination group, LEPEWWG/TGC/2000-01, March 2000.

[175] O.Klein, *On the Theory of Charged Fields*, New Theories in Physics, Proceedings, Warsaw, 1938; reprinted in: Surveys of High Energ. Phys. **5** (1986) 269.

[176] L.Maiani and P.M.Zerwas, *W Static ELM Parameters*, Memorandum to the TGC Combination Group (1998).

[177] SLD Collaboration, J. Brau, *Electroweak Precision Measurements with Leptons*, talk presented at EPS-HEP-99, Tampere, Finland, 15-21 July 1999.

[178] CHARM II Collaboration, P. Vilain *et al.*, Phys. Lett. **B335** (1994) 246.

[179] UA2 Collaboration, J. Alitti *et al.*, Phys. Lett. **B276** (1992) 354.

[180] CDF Collaboration, F. Abe *et al.*, Phys. Rev. Lett. **65** (1990) 2243;
CDF Collaboration, F. Abe *et al.*, Phys. Rev. **D43** (1991) 2070.

[181] CDF Collaboration, F. Abe *et al.*, Phys. Rev. Lett. **75** (1995) 11;
CDF Collaboration, F. Abe *et al.*, Phys. Rev. **D52** (1995) 4784.
A. Gordon, talk presented at XXXIInd Rencontres de Moriond, Les Arcs, 16-22 March 1997, to appear in the proceedings.

[182] DØ Collaboration, S. Abachi *et al.*, Phys. Rev. Lett. **84** (2000) 222.

[183] `http://www-cdf.fnal.gov/physics/ewk/wmass_new.htm`.

[184] CDF Collaboration, W. Yao, *t Mass at CDF*, talk presented at ICHEP 98, Vancouver, B.C., Canada, 23-29 July, 1998.

[185] DØ Collaboration, B. Abbott *et al.*, Phys. Rev. Lett. **84** (2000) 222.

[186] The Top Averaging Group, L. Demortier *et al.*, for the CDF and DØ Collaborations, FERMILAB-TM-2084 (1999).

[187] CCFR/NuTeV Collaboration, K. McFarland *et al.*, Eur. Phys. Jour. **C1** (1998) 509.

[188] NuTeV Collaboration, K. McFarland, talk presented at the XXXIIIth Rencontres de Moriond, Les Arcs, France, 15-21 March, 1998, hep-ex/9806013. The result quoted is a combination of the NuTeV and CCFR results.

[189] T. van Ritbergen and R.G. Stuart, Phys. Rev. Lett. **82** (1999) 488.

[190] S. Eidelmann and F. Jegerlehner, Z. Phys. **C67** (1995) 585.

[191] M. Steinhauser, Phys. Lett. **B429** (1998) 158.

[192] *Reports of the working group on precision calculations for the Z resonance*, eds. D. Bardin, W. Hollik and G. Passarino, CERN Yellow Report 95-03, Geneva, 31 March 1995.

[193] G. Degrassi, S. Fanchiotti and A. Sirlin, Nucl. Phys. **B351** (1991) 49;
G. Degrassi and A. Sirlin, Nucl. Phys. **B352** (1991) 342;
G. Degrassi, P. Gambino and A. Vicini, Phys. Lett. **B383** (1996) 219;
G. Degrassi, P. Gambino and A. Sirlin, Phys. Lett. **B394** (1997) 188.

[194] A. Czarnecki and J. Kühn, Phys. Rev. Lett. **77** (1996) 3955;
R. Harlander, T. Seidensticker and M. Steinhauser, Phys. Lett. **B426** (1998) 125.

[195] Electroweak libraries:
ZFITTER: see Reference 36;
BHM (G. Burgers, W. Hollik and M. Martinez): W. Hollik, Fortschr. Phys. **38** (1990) 3, 165; M. Consoli, W. Hollik and F. Jegerlehner: Proceedings of the Workshop on Z physics at LEP I, CERN Report 89-08 Vol.I,7 and G. Burgers, F. Jegerlehner, B. Kniehl and J. Kühn: the same proceedings, CERN Report 89-08 Vol.I, 55;
TOPAZ0 Version 4.0i: G. Montagna, O. Nicrosini, G. Passarino, F. Piccinni and R. Pittau, Nucl. Phys. **B401** (1993) 3; Comp. Phys. Comm. **76** (1993) 328.
These computer codes have upgraded by including the results of [192] and references therein. ZFITTER and TOPAZ0 have been further updated using the results of references 193 and 194. See, D. Bardin and G. Passarino, *Upgrading of Precision Calculations for Electroweak Observables*, CERN-TH/98-92, hep-ph/9803425.

[196] T. Hebbeker, M. Martinez, G. Passarino and G. Quast, Phys. Lett. **B331** (1994) 165;
P.A. Raczka and A. Szymacha, Phys. Rev. **D54** (1996) 3073;
D.E. Soper and L.R. Surguladze, Phys. Rev. **D54** (1996) 4566.

[197] BES Collaboration, Z.G. Zhao, *New R values in 2-5 GeVfrom BES*, talk presented at ICHEP2000, Osaka, July 27 - August 2,2000, to appear in the proceedings (URL: `http://pony2.ihep.ac.cn/~besr/ps/ichep2k_proc.ps`).

[198] B. Pietrzyk, *The global fit to electroweak data*, talk presented at ICHEP2000, Osaka, July 27 - August 2,2000, to appear in the proceedings. Preprint LAP-EXP-00.06.

[199] M. L. Swartz, Phys. Rev. **D53** (1996) 5268.

[200] A.D. Martin and D. Zeppenfeld, Phys. Lett. **B345** (1994) 558.

[201] H. Burkhardt and B. Pietrzyk, Phys. Lett. **B356** (1995) 398.

[202] R. Alemany, *et al.*, Eur. Phys. J. **C2** (1998) 123.

[203] M. Davier and A. Höcker, Phys. Lett. **B419** (1998) 419.

[204] J.H. Kühn and M. Steinhauser, Phys. Lett. **B437** (1998) 425.

[205] J. Erler, Phys. Rev. **D59**, (1999) 054008.

[206] A. D. Martin, J. Outhwaite, and M. G. Ryskin. A new determination of the qed coupling alpha(m(z)**2) lets the higgs off the hook. *Phys. Lett.*, B492:69–73, 2000.

[207] F. Jegerlehner, *Hadronic Effects in (g-2) and $\alpha_{QED}(M_Z)$: Status and Perspectives*, Proc. of Int. Symp. on Radiative Corrections, Barcelona, Sept. 1998, page 75.

[208] K.Hoffman, *Year 2000 update for OPAL and LEP HIGGSWG results"*, talk presented at ICHEP2000, Osaka, July 27 - August 2,2000, to appear in the proceedings.